

**PROPOSAL FOR A BOTTOM
COLLIDER DETECTOR**

**University of Pennsylvania
R. Van Berg, R. Hughes, N. S. Lockyer**

**Yale University
P. Karchin**

March 1987

Bottom Collider Detector

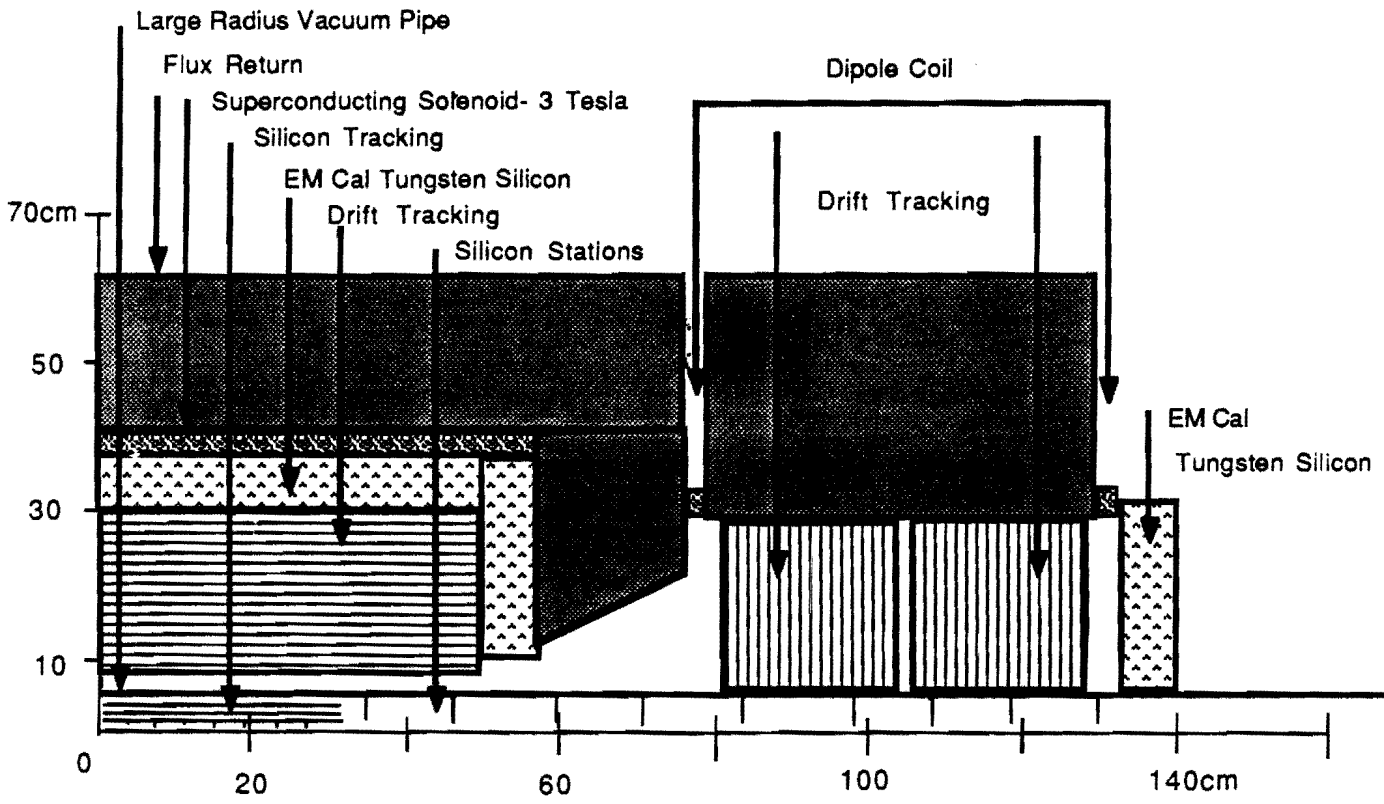


Figure 1a

- Note. 1. Double pipe starts at 4 meters
 2. Main Ring must move up a few inches
 3. Tev Pipe 81cm from Tunnel Wall (to right)
 4. 6 Meter Diameter Tunnel

C0 Hall

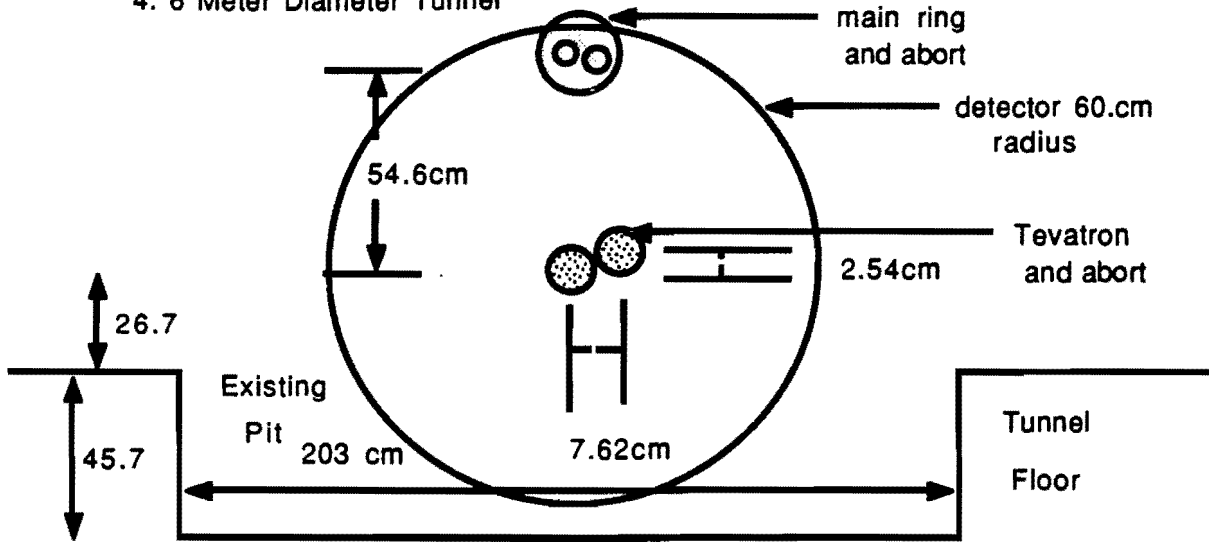


Figure 1b

C0 Hall

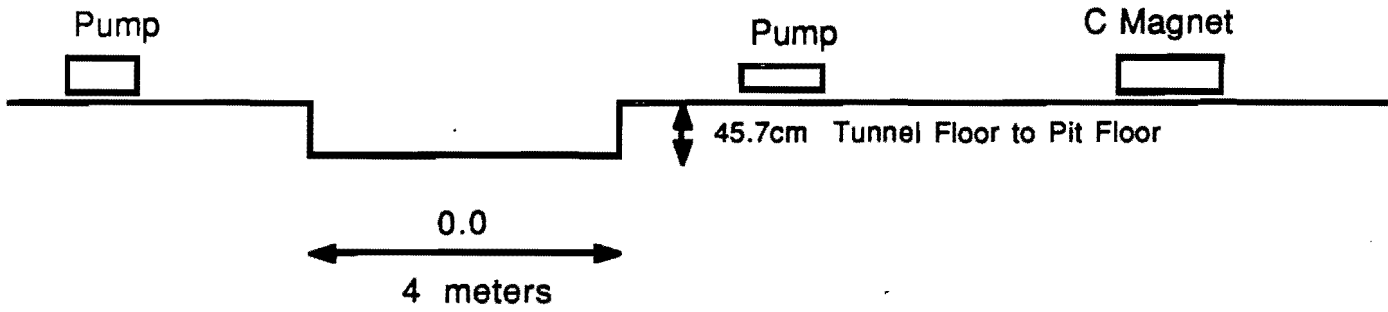


Figure 1c

Contents

1	Physics Goals	3
2	Introduction	5
2.1	Mixing/CP Violation	5
2.2	Measurement of $b \rightarrow u$	7
3	CP/Mixing Experimental Estimates	8
3.1	Mixing with Like Sign Dileptons	8
3.2	CP Violation with Dileptons	8
3.3	CP Violation with Exclusive Modes	9
3.3.1	$B \rightarrow \psi K_s^0$	9
3.3.2	$B_s \rightarrow D^0 \phi$	10
4	The $B \rightarrow \rho\pi$ and $B \rightarrow \rho^0 e\nu$ Estimates	10
4.1	$B \rightarrow \rho e\nu$	10
4.2	$B \rightarrow \rho\pi$	11
5	General Description of the Detector	12
5.1	Introduction	12
5.1.1	Central Region Overview	13
5.1.2	Forward Backward Detectors Overview	14
5.1.3	Detector Acceptance	15
5.2	Microvertex Detector	16
5.2.1	Introduction - Philosophy of Design	16
5.2.2	Microvertex Detector Design and Performance	17
5.3	Charged Particle Tracking - Radial Drift Chamber	19
5.3.1	Momentum and Mass Resolution	22
5.4	Electromagnetic Calorimeter	23
5.4.1	Introduction	23
5.4.2	Electronics	24
5.4.3	Reasons for Choosing Si/W	24
5.4.4	General Design Parameters and Performance	25
5.5	Trigger	26

5.5.1	Level One	27
5.5.2	Level Two	27
5.5.3	Level Three	29
5.6	Buffering - Electronics	29
6	Comparison to Other Experiments	30
6.1	Introduction	30
6.2	D-Zero Experiment	31
6.3	CDF Experiment	32
6.4	Comparison to High Energy e^+e^- Machines	33
6.4.1	Slac-Linear-Collider and LEP	33
6.4.2	TPC at PEP	34
6.5	CESR	34
6.6	UA1	35
6.7	Fixed Target	35
6.7.1	NA32	35
6.7.2	E-691	36
7	Acknowledgements	36
8	Budget	37
A	Appendix	38
B	Appendix	38

PROPOSAL FOR A BOTTOM COLLIDER DETECTOR

1 Physics Goals

The ultimate goal of this experiment is to record about 100 million bottom events tagged with a lepton trigger. It is only with a sample of this size that CP violation and very rare decays from bottom can be studied. In order to produce 10^9 bottom events an integrated luminosity of $500 pb^{-1}$ is needed, which could be accomplished in a one year run of 10^7 sec at a luminosity of $5 \times 10^{31} cm^{-2} sec^{-1}$, assuming a total bottom cross section of 10μ barns. With a trigger efficiency of about 10 percent, the goal of about 10^8 bottom events recorded seems attainable. Having produced and recorded this large data set, the task of reconstructing these events and extracting physics will be a tremendous challenge to the detector design and physicists involved.

This experiment begins the process of how to best tag a very large sample of bottom events in a high energy hadron collider environment. The most challenging aspects concern studying the secondary vertices when multiple scattering effects are large and detecting very soft leptons in a busy tracking environment. This will lead to a better exploitation of the high luminosity Tevatron as well as eventually preparing for the SSC.

The interim goal of this experiment is to build a compact yet easily upgradable detector that will be installed in the C0 collision hall as soon as the detector can be designed and built, approximately three to four years from now. The detector has been designed to be physically small, 2 meters long and 1 meter in diameter, so that no construction is necessary for the C0 Tunnel. It is the general philosophy of this proposal that experience is needed in reconstructing bottom mesons at the Tevatron and that a C0 sized effort is an excellent way to start this process. The luminosity in the C0 region is naively expected to be 1/75th of that in B0 or D0, since C0 is not a low beta region. It is hoped that the luminosity can be upgraded by about a factor of ten in C0 with a modest change to the beamline quadrupoles. The minimal amount of useful luminosity in C0 is $5-50 pb^{-1}$, since this would give optimistically a sample of about 10,000-100,000 reconstructed bottom events.

A successful program at C0 would be hopefully followed with a high luminosity run in either B0 or D0 for about a year while those detectors are undergoing major upgrades or simply analysing their large data sets.

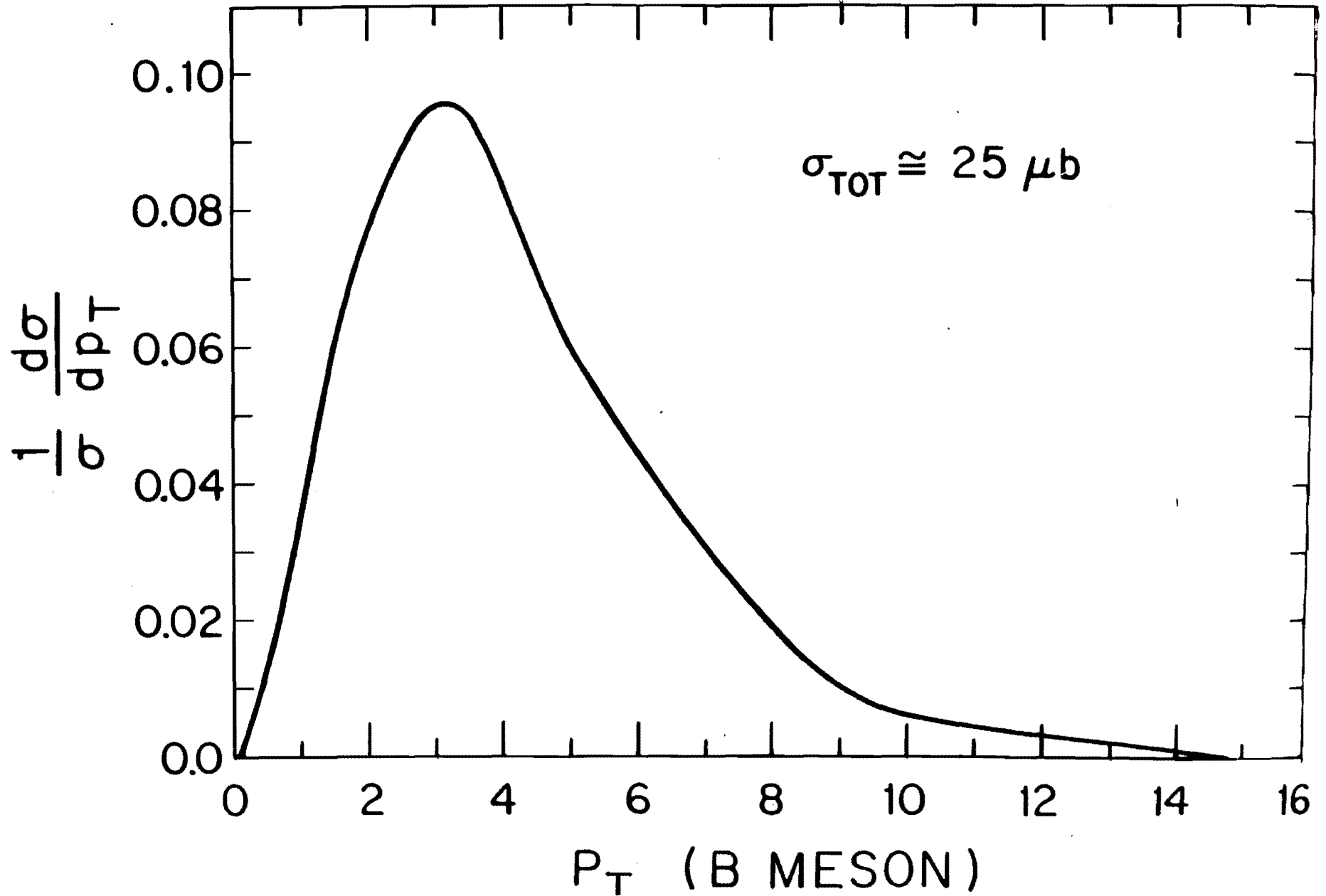
The following are the main areas of study this experiment will address initially.

1. Observe and study $B^0 \bar{B}^0$ mixing/CP violation by measuring the dilepton signal, exclusive decay modes and inclusive rates from a sample of tagged bottom mesons. Ultimately this leads to a better understanding on how to test CP violation in the bottom system at a high rate, high luminosity hadron collider.
2. Observe the decay of the bottom quark to up quark by identifying the decay $B \rightarrow \rho^0 e \nu$ and $B \rightarrow \rho \pi$. There are of course many other decay modes. Measure the rate.
3. Search for rare B decays which are all charged and have low multiplicities.
4. Measure the $B^0 B^+$ lifetimes.
5. Measure the bottom cross section using 2 different methods.
6. By assuming a fragmentation function for bottom measure the produced p_t distribution of bottom and compare to charm from D^0 tagging of charm jets and secondary vertex tagging of charm.
7. Identify the decay $W \rightarrow tb$ by tagging the two bottom jets and the high p_t electron from top. Measure the low p_t part of the lepton spectrum from top. This type of tagging experience would be important for a high energy, high luminosity collider.
8. The decay of Z^0 's to Majorana neutrinos can have measureable lifetimes in some models. In addition heavy neutral leptons can also be long lived. The study of these processes or limits on them are possible with this detector because of the high efficiency relative to other detectors for tagging bottom and the tendency of new physics signatures to be cascades to bottom.

These physics topics can be studied either uniquely or better in this dedicated detector as compared to the present general purpose collider detectors at the Tevatron.

The cost of this detector is estimated to be about \$5.9M. The technical design report will take about 6 months to a year to compile. The construction of the detector will require two to three years. The disruption to the Tevatron program is discussed in Appendix A. It is believed this detector can add substantially to the breadth of physics being addressed at the Tevatron.

Figure 2



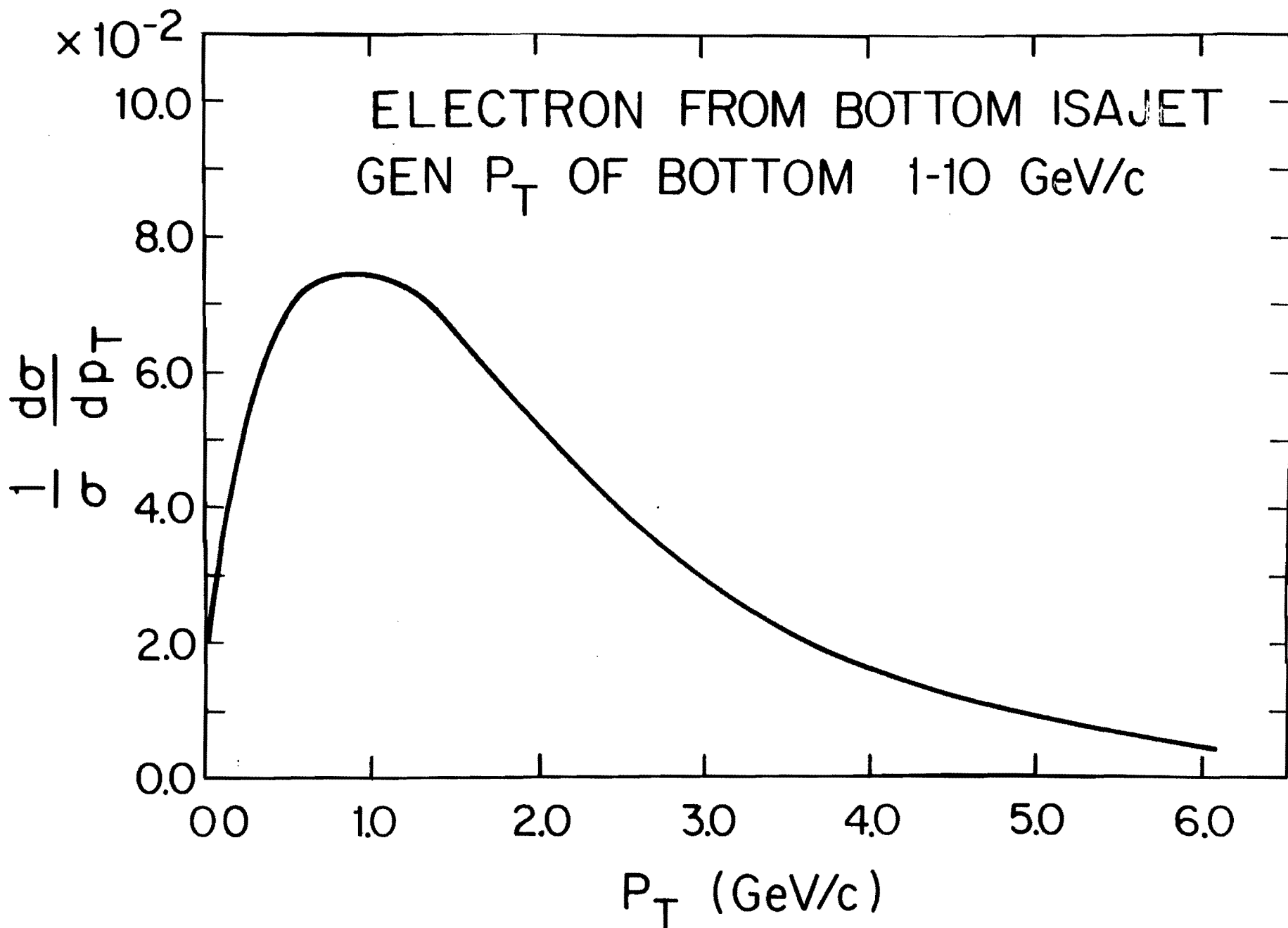


Figure 3

2 Introduction

We propose to build a small, $\sim 4\pi$ special purpose magnetic detector for the Tevatron. See Fig. 1. The detector design has been optimized to identify prompt electrons and secondary vertices coming from bottom quark decays. It has very good mass resolution for charged decay modes which is necessary in discriminating bottom from combinatorial backgrounds. It has no hadron calorimetry. Only modest particle identification comes from dE/dX measurements. The main emphasis of this detector is to:

- (a) Detect the large bottom cross section at the Tevatron which in general is isotropically produced and quite soft. See Fig. 2.
- (b) Provide complete electron coverage down to $p_t \sim 1 \text{ GeV}/c$ over ± 4 units of pseudo-rapidity. The lepton spectrum is soft and peaks at $p_t \sim 1 \text{ GeV}/c$. See Fig. 3.
- (c) Provide complete efficient triggering on electrons over the full solid angle of the detector.
- (d) Demonstrate the principle of tagging a large sample of bottom mesons in a hadron collider environment using a vertex detector.
- (e) Demonstrate the ability to count charged prongs from a secondary vertex. This permits the reconstruction of charged exclusive decay modes with very little background. Investigate the ability to identify tertiary vertices (i.e. the vertex from bottom cascade to charm).
- (f) Provide excellent rejection of pairs from gamma conversions.

2.1 Mixing/CP Violation

In the standard six-quark electroweak theory, the particle states to which the weak intermediate vector bosons couple are mixtures of the physical particle states. The charged weak current is given by

$$J^\mu = (u, c, t)\gamma^\mu(1 + \gamma^5)U \begin{pmatrix} d \\ s \\ b \end{pmatrix}$$

where u, c, t are charge $2/3$ quark fields and d, s, b are the $-1/3$ fields. The 3×3 unitary matrix U is characterized by 3 Cabibbo-like mixing angles and a phase factor. This parametrization is due to Kobayashi and Maskawa and is given by

$$U = \begin{pmatrix} V_{ud} & V_{us} & V_{ub} \\ V_{cd} & V_{cs} & V_{cb} \\ V_{td} & V_{ts} & V_{tb} \end{pmatrix} = \begin{pmatrix} c_1 & s_1 c_3 & s_1 s_3 \\ -s_1 c_2 & c_1 c_2 c_3 - s_2 s_3 e^{i\delta} & c_1 c_2 c_3 + s_2 c_3 e^i \\ -s_1 s_2 & c_1 s_2 c_3 + c_2 s_3 e^{i\delta} & c_1 s_2 c_3 - c_2 c_3 e^{i\delta} \end{pmatrix}$$

where $s_i = \sin \theta_i$ and $c_i = \cos \theta_i$ for $i = 1, 2, 3$. The V_{ij} 's denote the coupling of the quarks $q_i q_j$'s to the W^{+-} intermediate vector bosons. The unitarity of the matrix prevents flavor changing neutral currents. The precise measurement of $s_1 = 0.2270 \pm 0.011$ comes from comparing $O^+ \rightarrow O^+$, nuclear β decay of O^{14} and AL^{26m} with μ decay. However, until recently, values of the K-M angles s_2 and s_3 could be as large as 0.5. New knowledge of the angles s_2 and s_3 comes from measurements of the long B meson lifetime and the improved limit on $R = \Gamma(b \rightarrow u)/\Gamma(b \rightarrow c)$. The value of $\tau_b = (1.11 \pm 0.16) \times 10^{-12}$ s is longer than charmed hadron lifetimes despite the enhancement expected in the rate of b decay from $(m_b/m_c)^5$. This implies a very small mixing angle to the second quark generation. The limits on R are presently best determined from the shapes of lepton spectra from CLEO and CUSB groups. They find R less than about 5% which says the b quark is almost completely decoupled from the first generation of quarks. Together these measurements determine s_2 to be very small and s_3 to be consistent with zero. The contour plot in the $s_2 - s_3$ plane is shown in Fig. 4 for various top quark masses and B parameter values. (The latter parametrizes the matrix element of the $\Delta S = 2$ operator. $B = 1$ for vacuum insertion. Most estimates of B are included in the range 0.2 to 1.5). In addition, further constraints arise from a study of the CP-violating mixing parameter ϵ_m . The box diagram of Fig. 5 gives the main short distance contribution to ϵ_m and is thought to be reliable. This leads to a contour in the $s_2 - s_3$ plane for given B, m_t , and τ_b and is seen in Fig. 4. Ginsparg et al argue the small $s_2 s_3$ determined from the τ_b require the top mass to be large. However uncertainties in the B parameter calculations weaken this statement. This point is illustrated in Fig. 6. Experimental information from UA1 regarding the top quark seems unclear and therefore does not provide a mass window around the top quark.

The box diagram in Fig. 5 leads to $B^0 \bar{B}^0$ mixing from either B_d or B_s . The amount of mixing depends on the ratio of the $B\bar{B}$ mixing amplitude ΔM and the

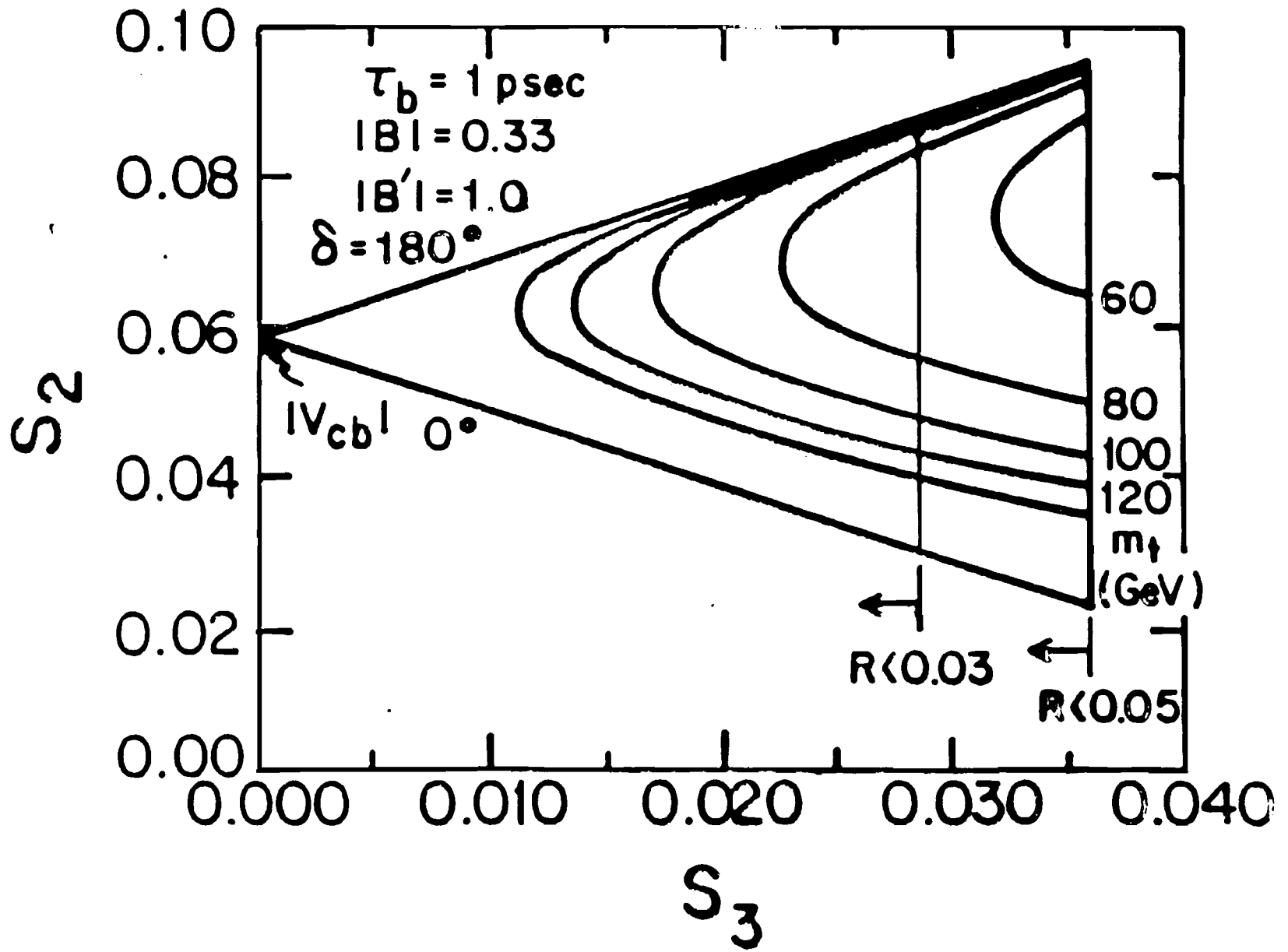


Figure 4

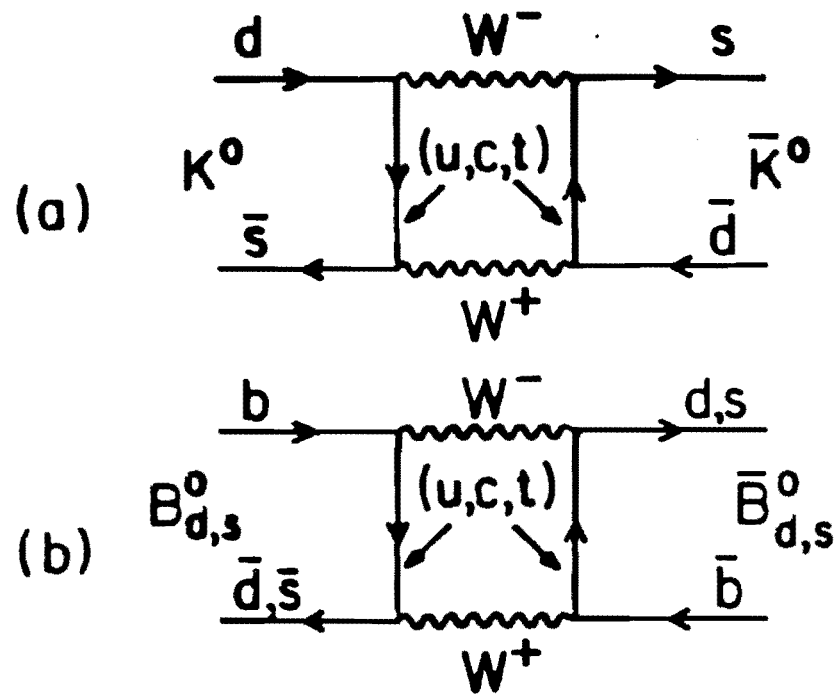


Figure 5

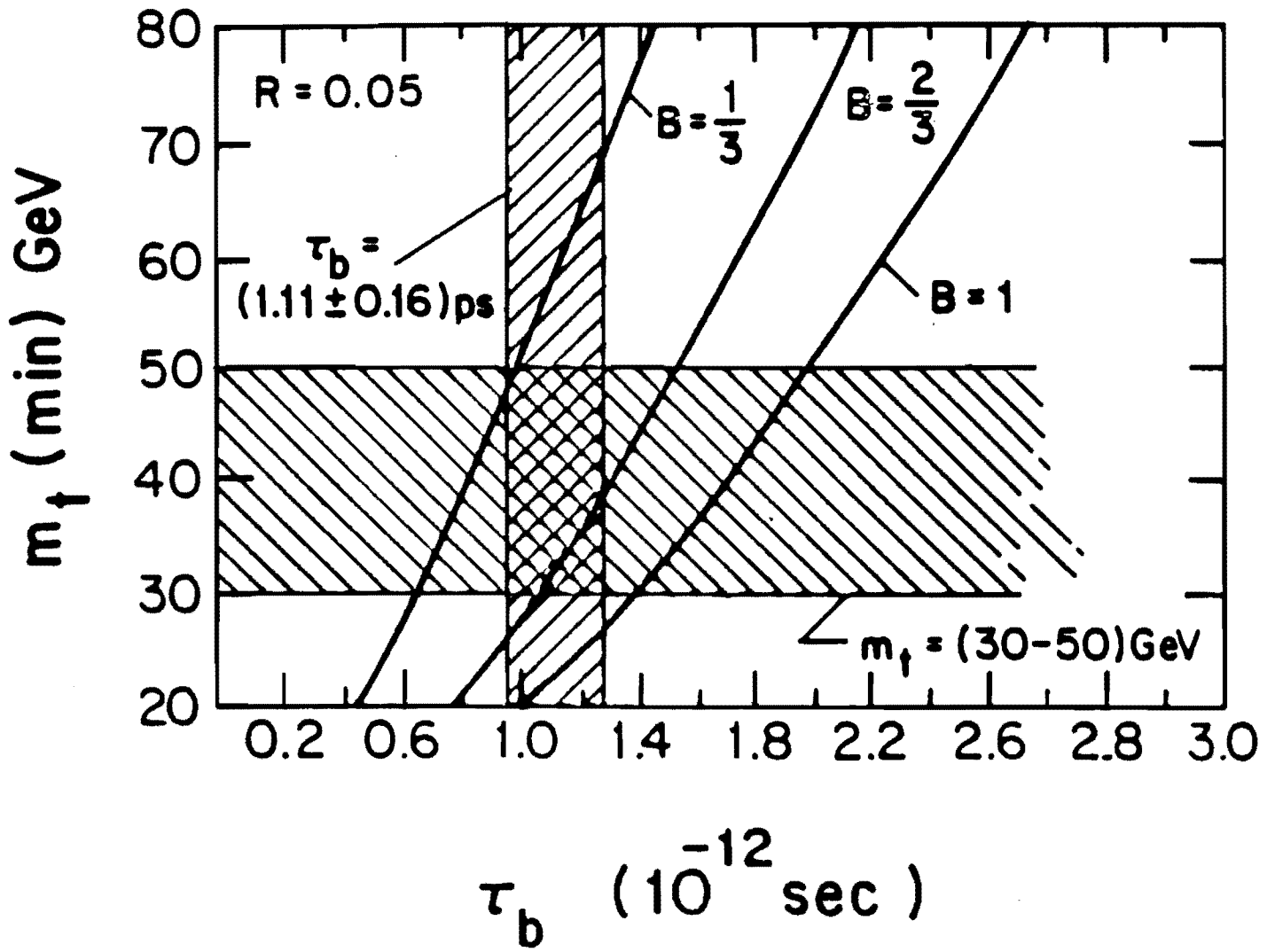


Figure 6

total b decay width Γ_b . The decay widths $\Gamma(B_s^0)$ and $\Gamma(B_d^0)$ are similar but the mass differences differ by a factor of $(\sin \theta_c \sim 0.23)^2$. The mass mixing in the B_d system is expected to be at most a few percent while in the B_s system substantial mixing is possible. For a given top quark mass and τ_b fixed, *the range of s_2 allowed is quite narrow*. As a measure of mixing we define

$$r(B_s) = \Gamma(B_s^0 \rightarrow l^+ \nu x) / \Gamma(B_s^0 \rightarrow l^- \nu x)$$

The value of $r(B_s)$ could be as large as one. From the Mark-II a limit on this ratio at PEP gives $r_{\text{continuum}} < 0.12$. This excludes full mixing in B_s , and by including the amount of B_s expected in the continuum at PEP energies, typically 0.15, the theoretical value becomes $r(B_s) < 0.08$, lower than the Mark-II limit. Mixing leads to like sign dileptons and a convenient measure is

$$R_{ll}(bb) = N^{++} + N^{--} / N^{+-}$$

Estimates of $R_{ll}(bb)$ range from $10^{-3} - 0.02$ for B_d to $0.12 - 0.75$ for B_s . The stated range represents the uncertainties from the B parameter, where a larger B gives a larger $R_{ll}(bb)$. The prospects for observing mixing look good.

2.2 Measurement of $b \rightarrow u$

In the standard six quark model the bottom quark can decay to either a charm or up quark and a W^- . The best determination of the K-M matrix element $|V_{bu}|$ has come from the study of the leptonic decay of the virtual W^- . The CLEO group has studied the momentum spectrum of leptons from $B \rightarrow Xl\nu$. The CUSB group studied just the electrons. The mass of the charm quark is $m_c = 1.8 \text{ GeV}/c^2$ and that of the up quark is $m_u = 0.33 \text{ GeV}/c^2$. Therefore the shape of the electron momentum spectrum from $B \rightarrow ce\nu$ is softer than the $B \rightarrow ue\nu$. The end-points are 2.35 and 2.55 GeV respectively. Experimentally the decay spectrum is completely consistent with only $B \rightarrow ce\nu$. The published 90%-confidence-level upper limit on $\Gamma(b \rightarrow ul\nu) / \Gamma(b \rightarrow cl\nu)$ of 4% by CLEO and 5.5% by CUSB. When combined with the b lifetime expression

$$\tau_b^{-1} \sim G_F^2 m_b^5 / 192 \tau^3 [2.95 |V_{cb}|^2 + 6.33 |V_{ub}|^2]$$

this gives $|V_{ub}| < 0.0051$ and $|V_{cb}| = 0.044 \pm .005$. This says the b quark decouples from the first two generations with the coupling to the first being extremely small

though still consistent with other measurements and constraints on the K-M mixing angles.

Recently, the model of Altarelli et al. being used to describe the end-point behaviour has encountered some problems. It has been suggested that the limits are too stringent. The more reasonable limits are probably around 8%.

It has been pointed out that calculations of partial rates to the exclusive mode $B \rightarrow \rho^0 e^- \nu_\mu$ permit the determination of $|V_{ub}|$. This mode is about 1% of the total $b \rightarrow u$ rate and is thought to be reliably calculated. It is this mode and $B \rightarrow \rho\pi$ which we seek to measure in this experiment being proposed.

3 CP/Mixing Experimental Estimates

3.1 Mixing with Like Sign Dileptons

In the semileptonic decay of the b quark, $b \rightarrow e$ and $\bar{b} \rightarrow \bar{e}$, the sign of the lepton determines whether the parent is particle or antiparticle. The signal for mixing will be the presence of like sign pairs. The mixing parameter is defined as

$$r \equiv \frac{N^{++} + N^{--}}{N^{+-} + N^{-+} + N^{++} + N^{--}}$$

Consider the experimental situation. We take the bottom cross section to be $25 \mu b$ at 2 Tev. The acceptance times p_t cut is $\sim .9$ per B meson. So the useable cross section $\sigma_{b\bar{b}}$ is $25 \times .81 \sim 20 \mu b$. For the electron trigger we fold in the branching ratio, 12%, the probability the p_t of electron is > 2 GeV/c, and the impact parameter requirement of $\frac{b}{\sigma} > 3$ cuts $\sim 50\%$. Therefore, the cross section for useable dielectrons is about 8 nb. The track acceptance reduces this to about 5 nb assuming a possible worst case of 10% loss on each track.

The running period of two weeks at a luminosity of $5 \times 10^{31} cm^{-2} sec^{-1}$ gives $80 pb^{-1}$ total integrated luminosity. This gives 4×10^5 di-electrons. The 2σ limit is then simply $\frac{2}{\sqrt{N}}$ or ~ 0.003 . The standard model prediction for the range of r is 0.01 - 0.2.

3.2 CP Violation with Dileptons

If CP is violated a slight preponderance of one species is expected. The asymmetry

parameter is

$$a = \frac{N^{++} - N^{--}}{N^{++} + N^{--}}$$

Using the number of di-electrons calculated in the mixing section, and assuming a standard model value of r between 0.01 – .2, we obtain a like sign sample of 6400 – 128,000 events. At the 2σ level, this gives a best limit of .025 – .006. The standard model is at the 10^{-3} – 10^{-4} level, but “new physics” scenarios do allow a $\sim 10^{-2}$. If we assume a high luminosity run of $5 \times 10^{31} cm^{-2} sec^{-1}$ for 10^7 sec, then limits are between .01 – .002, and this does begin to exclude the larger nonstandard model predictions.

3.3 CP Violation with Exclusive Modes

The basic idea is to look for a difference between $\Gamma(B^0 \rightarrow f)$ and $\Gamma(\bar{B}^0 \rightarrow \bar{f})$. The exclusive decay asymmetry turns out to be

$$|A| = \frac{\Gamma(B^0 \rightarrow f) - \Gamma(\bar{B}^0 \rightarrow \bar{f})}{\Gamma(B^0 \rightarrow f) + \Gamma(\bar{B}^0 \rightarrow \bar{f})}$$

The experiment must discriminate between B^0 and \bar{B}^0 . This means tagging the bottom system on the other side with a lepton.

3.3.1 $B \rightarrow \psi K_s^0$

This mode is popular because the signature is clean, and the B meson is completely reconstructable. The expected value of the asymmetry $A \sim 4 - 12\%$. Other factors to fold in are the branching ratios of $B \rightarrow \psi K_s^0 \sim 5 \times 10^{-4}$, $\psi \rightarrow \mu\mu = 0.074$ and $K_s \rightarrow \pi^+\pi^- = .68$. A conservative estimate of the trigger efficiency reduces this rate by a factor of 0.02. Including a 50% efficiency for K_s and 70% for ψ , the useful cross section is $2 \times 10^{-36} cm^2$, and gives about 160 events in $80 pb^{-1}$ of integrated luminosity. At the 2σ level, the minimal A measurable is $\sim 15\%$.

The transverse momentum spectrum of the μ pairs from the ψ and the π 's from the K_s^0 averages about a few GeV/c. This is hard enough that a small sample of these events would be reconstructed. A longer run, of $10^7 sec$ would give ~ 960 events and lower the minimal A measurable to 6%.

3.3.2 $B_s \rightarrow D^0 \phi$

This is an interesting mode that has a large asymmetry, $\sim 60\%$, which does not suffer from competing modes from B_s with the opposite sign asymmetry. Consider $B_s \rightarrow D^0 \phi$ where $D \rightarrow K\pi$, 2% and $\phi \rightarrow KK \sim 50\%$ of the time. The B_s is produced $\sim 15\%$ of the time and $B_s \rightarrow D\phi$ has a branching ratio of about 2×10^{-4} . Including the electron tag of 0.02 and a reasonable K identification probability of 50%, a useful cross section of about 10^{-38}cm^2 gives about 1 event. It is clear a higher luminosity run would be required to see this decay mode. The momentum versus rapidity is shown in Figure 7 for kaons coming from $D \rightarrow K$ and $\phi \rightarrow KK$.

4 The $B \rightarrow \rho\pi$ and $B \rightarrow \rho^0 e\nu$ Estimates

4.1 $B \rightarrow \rho e\nu$

The $B \rightarrow \rho e\nu$ decay mode has the advantage that it is large relative to the overall $b \rightarrow u$ rate and that it is a mode this detector will trigger on. The obvious disadvantage is that it does not reconstruct to the B meson mass and the ρ is a wide resonance. The background and signal was studied in detail by Monte Carlo. The events were generated using Isajet in the p_t range 5-10 GeV/c. The branching ratio of the exclusive mode $B \rightarrow \rho e\nu X$ is about 10^{-4} .

In the analysis chain, the event is first tagged with an electron of $p_t > 2$ GeV/c and an impact parameter significance of $\delta/\sigma > 3$. The two charged prongs were assumed to be identified cleanly. Both prongs were kept within ± 3 units of rapidity to enable a momentum measurement and each must have a momentum > 1 GeV/c so as to reduce multiple scattering effects. The major background comes from $B \rightarrow De\nu$ and $\bar{D} \rightarrow K\pi\pi$ and the $K \rightarrow K_L$ for example. The sum of the 2 prong decay modes have a branching ratio of about 5.5%. Some additional cuts were:

- reject an event if $K_s \rightarrow \pi\pi$ is present.
- reject an event if detectable 3rd vertex is present.

Additional cuts required the mass of the two charged prongs to be consistent with a ρ mass and if one prong was assumed to be a K, inconsistent with a D mass. The above cuts result in a signal to noise of about 1:20. A simple kinematic cut requiring the angle of one of the charged prongs relative to the B meson direction enhances

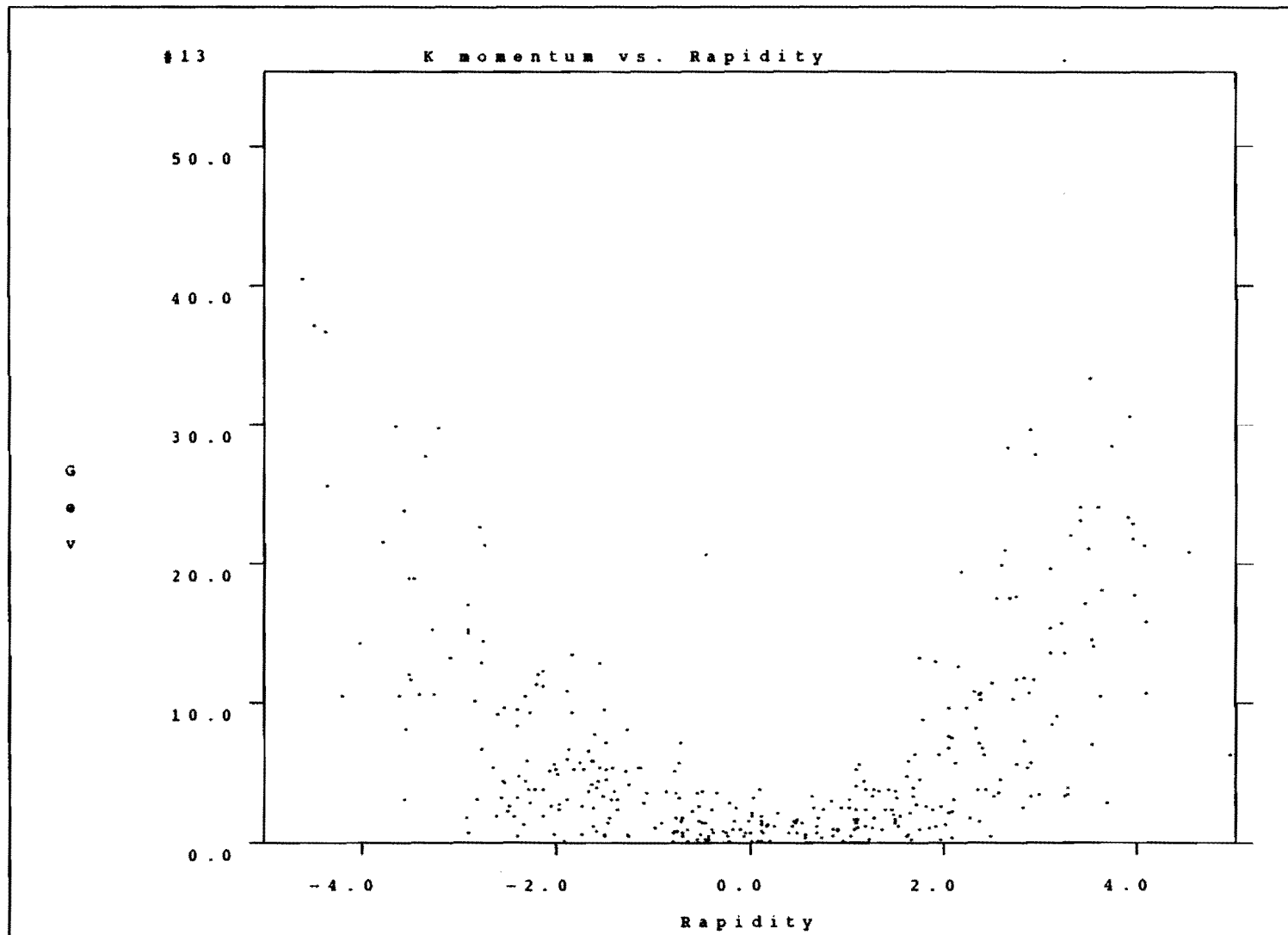


Figure 7

the signal by 10:1. It is concluded that the noise to signal ratio is about 2-3:1. From a data set taken in two weeks, 3000 events will be produced and 50 should survive the analysis cuts. A longer run of 3 months would make the signal quite evident.

The above estimates demonstrate that interesting physics with bottom requires many millions of events and collecting such a large sample is difficult to imagine at any other accelerator than the Tevatron. It is important to note that a more powerful detector would have trouble improving upon the above backgrounds the detection of π^0 's coming from the B meson is very difficult at the Tevatron.

4.2 $B \rightarrow \rho\pi$

In $B \rightarrow \rho\pi$, the decay of interest is the 3 charged prong mode that reconstructs to the bottom mass. Unfortunately the branching ratio is the product of roughly 10^{-2} for the KM matrix elements and $\sim 10^{-3}$ for the rate relative to $b \rightarrow u$. This must now be combined with the trigger efficiency based on the single electron trigger. The effective branching ratio is then less or equal to 3×10^{-7} . For the 3 month run at a luminosity of 5×10^{31} , this is about 60 events produced and recorded. This rate should be measurable.

The background for this decay mode has been studied briefly using a small sample of Monte Carlo events. Bottom was generated with a p_t between 1 and 20 GeV/c and a rapidity between ± 6 units. First, a momentum cut of 0.5 GeV/c is applied to all charged tracks to reduce background effects from large multiple scatters. The ± 3 rapidity cuts have been applied to all charged decay products. In addition a track is assumed to be reconstructable only if its momentum is greater than 100 MeV/c. Now the remaining events with 3 charged prongs are analysed to see if they produce a rho mass, which is defined to be 770 ± 300 MeV/c. If a ρ mass is found, the remaining prong is added to make a B meson mass. All tracks are assumed pions. The momentum resolution is $\delta p/p \sim \sqrt{(.001p)^2 + (.008)^2}$. Effects due to dip angle are included in the mass calculation. A candidate B meson must fall within 400 MeV/c of the average B meson mass. These cuts leave about 77% of the $B \rightarrow \rho\pi$ events.

The background comes from sources of 3 charged prongs at the vertex. The fraction of bottom decay modes which produce 3 charged prongs was estimated to be 4%. From a sample of 468 events produced, 149 pass the cuts up to the rho mass requirement on 2 of the prongs. One event out in the tail falls into the B mass region.

Taking into account the 4% for the branching ratios, this implies 0.04 events in the B meson mass region. Since the ratio of production is 10^5 , the noise to signal ratio is about 10:1. After including the kaon identification from dE/dX measurements, and some kinematic constraints, a signal to noise of 1:1 seems attainable. The reconstruction probabilities not mentioned above are assumed to effect noise and signal equally. In addition the branching ratios for 3 prongs are just estimates and a more detailed analysis would not change the general conclusion.

Therefore it is concluded that this decay mode could be identified with a detector of this design.

5 General Description of the Detector

5.1 Introduction

The experimental design is driven by the need for a highly efficient detector which triggers on bottom events and provides sufficient information to reconstruct them in the complex environment of the Tevatron collider. The principle behind the design of this detector is to maximize the ability to reconstruct primary and secondary vertices as well as tag soft electrons from bottom decay over the full rapidity range in which bottom is produced. In addition, the size of the detector is kept small so as to minimize the cost and to allow easy installation into an existing intersection region.

This goal is achieved by a solenoidal spectrometer located between two dipole spectrometers. The chosen magnet geometry momentum analyses the charged tracks optimally, minimizes the size of the overall detector by matching the geometry of the detector volume to the laboratory angles of the tracks it is to encompass and provides uniform tracking over the full rapidity range.

A critical design feature involves the design of the silicon vertex detectors. Here it is believed that the combining of a central and forward piece, so necessary for utilizing the full luminosity, does not reduce the effectiveness of either system. In other words, the impact parameter resolution over the forward rapidity range is not reduced by the presence of the central silicon barrels. Clearly a major design feature is that the entire silicon vertex detector is inside the Tevatron vacuum vessel. This is absolutely necessary for tracing the low momentum charged decay products of the bottom mesons.

The principle for charged particle tracking is the same for both large and small

angle tracks: pattern recognition and momentum analysis is accomplished with very high resolution radial drift chambers immersed in a magnetic field while the intercept and angle measurement is made with silicon microstrip detectors located inside the beam pipe. Since a given track pierces only a few silicon planes, and because these planes are close to the beam line, the effect of multiple scattering on vertex resolution is minimized. However, the momentum measurement is *completely unaffected* by the multiple scattering in the silicon and beam pipe since only the drift chamber information need be used in the momentum measurement.

Silicon/Tungsten electromagnetic calorimetry provides the necessary lepton detection and triggering while keeping the overall size small. A projected 1cm^2 tower geometry is used to maximize low momentum identification. The small tower allows a fast readout before the next beam crossing.

This experiment has been designed to a 200 nsec beam collision rate. By anticipating the high rate crossing of an upgraded Tevatron in this design, the luminosity can be readily used.

The detector divides logically into a central region and forward backward region. It is felt the natural boundary is $\tan\theta(\text{lab}) = 0.25$. The central region is typically ± 2 units of rapidity while the forward backward region covers down to 4 units of rapidity. There is thought to be little bottom produced beyond 4 units of rapidity.

The detector is shown in Figure 1.

5.1.1 Central Region Overview

The central detector consists of 3 approximately cylindrical layers of double sided silicon microstrip detectors placed with the first layer about 2.0 cm from the beam collision point inside of the 7 cm radius Beryllium Tevatron vacuum pipe. Subsequent layers are located at radii 3.0 cm and 4.0 cm. In addition, the inner layer is segmented every 4.0 cm, at which point a silicon detector arranged radially occurs. This piece extends to within 1 cm of the beam axis. This unit cell is repeated 16 times. The assembly of 4 unit cells is retractable out to the wall of the beam pipe remotely. The strip to strip pitch is 25 microns in the first barrel layer and radial pieces. The outer barrels have a pitch of 50 microns. Our studies have shown that to unambiguously define the bottom vertex, a 3-D reconstruction is necessary in the central region and that the resolution needed is 10-20 microns. Centroid finding software will utilize the information from the strips maximally. An intrinsic impact parameter resolution of 5

microns seems attainable with present signal to noise ratios from integrated amplifiers in the range 15:1. The multiple scattering contribution to the impact parameter is larger, for 1 GeV/c tracks about 15 microns error is expected.

The silicon is encompassed by a 1 meter long high resolution radial drift chamber, the inner radius beginning at about 7 cm and extending out to 30 cm. This provides about 100 ionization measurements, useful for dE/dX , and good pattern recognition. The resolution per point needs to be about 30 microns and a double track separation of 1 millimeter is adequate. The limitations to this device appear to be the ability to control systematics, but potentially it can provide a large step forward in the accuracy of drift chamber measurements since all of the information from the track is being used.

The tracking system is followed by a 16 radiation length tungsten-silicon sampling electromagnetic calorimeter for electron identification. The resolution of this system is expected to be about $25\%/\sqrt{E}$. It has a projected tower geometry with four longitudinal measurements and a total of about 18,850 towers, the size of each tower being matched to the Moliere Radius. The integrated electronics needed for this design require development but with techniques already familiar for analog amplifiers used with the microstrip detectors. A prototype integrated circuit is given in section 5.5.2.

The tracking system and calorimeter are immersed in a 3.0 Tesla solenoidal magnetic field, 1 meter in length and 40cm in radius. The field permits the effects of multiple coulomb scattering to be studied and the reconstruction of exclusive charged decay modes of bottom. In addition, it provides useful information in studying electron backgrounds, as well as the charged track sign determination. The expected resolution is about $\delta p_t/p_t < 0.1\%p_t + 0.8\%$, the latter term coming from multiple scattering.

5.1.2 Forward Backward Detectors Overview

The forward backward detectors are symmetric about the $Z=0$ plane. They cover the rapidity range 2 to 4 units for an event produced at $Z=0$, and in fact cover down to 4 units for events produced out at $Z=30$ cm. Due to the left right symmetry about the Z axis, the following discussion refers only to the forward detector.

The forward detector utilizes the silicon barrel in conjunction with silicon annuli located inside the inner barrel. The planar silicon annuli have inner radius 1 cm,

outer radius 2 cm, and are interspersed every 4 cm along the barrel. Because small angle tracks pierce the annuli nearly perpendicular to their surface, there is minimal multiple scattering for the first measurement point. The vertex design is based on the principle that a good angle measurement is needed before the first large scatter, either the silicon barrel or the beam pipe, in order to extrapolate accurately to the vertex. Beyond the barrel region (after $Z = 28\text{cm}$) there are planar silicon annuli of inner radius 1 cm and outer radius 4 cm. They are spaced every 12 cm along the Z-axis out to about $Z = 140\text{ cm}$.

The vertex resolution for tracks in the forward region (2 degrees to 15 degrees) is given by

$$\sigma^2 \sim \left(\frac{16\mu\text{m}}{P_t}\right)^2 + (10\mu\text{m})^2$$

where P_t is in GeV/c. A typical track pierces 1 or 2 silicon detectors before passing at a large angle through either the silicon barrel or the beam pipe. Thus, the intercept and angle measurements are made with 4 or 6 silicon detectors.

Inside the dipole magnet are 3 assemblies of very high resolution planar radial drift chambers, immersed in a 1 Tesla field. The momentum resolution is

$$\left(\frac{\delta p}{p}\right)^2 \sim [(.08\%)p]^2 + (.25\%)^2$$

The above assumes .25% of a radiation length of material in the drift chamber hodoscope and a resolution of $30\ \mu\text{m}$ over 50 cm providing a total of 100 measurement points.

The momentum resolution of the forward spectrometer is well matched to that of the central detector. Each plane provides either X-Y or U-V tracking.

A tungsten silicon sampling electromagnetic calorimeter follows, 20 radiation lengths in depth. The calorimeter has projective tower geometry, about 3600 towers per end, and four longitudinal measurements of the shower development.

Upgrades to the forward region envisioned are possibly Ring imaging Cherenkov counters for Kaon identification. The CRID system could fit in the CO collision hall.

5.1.3 Detector Acceptance

The acceptance for $\bar{p}p \rightarrow B\bar{B}X$ where $B \rightarrow eX$ and $\bar{B} \rightarrow 5$ charged prongs has been studied. The results are summarized in Figs. 8. A comparison has been made of

the two forward 20° cones versus the full solid angle. Losses due to cracks, efficiency, etc. are assumed similar in both the forward and central regions. The study merely asks whether the track points into the angular range 2-20 degrees. The probability of detecting an electron in either of the cones is $192/447=.43$. The probability of getting all of the other charged prongs from the semileptonic decay is $115/192$. The subsequent bins are events where 1 prong, 2 prong etc. are missed. The probability of getting all the decay products from the hadronic side is $42/192$. The overall probability, having triggered already in one of the cones, of seeing all charged prongs from both bottom is $25/192$. It is concluded that about a factor of 18 is gained by covering the full solid angle.

5.2 Microvertex Detector

5.2.1 Introduction - Philosophy of Design

Charged particles from bottom hadrons are identified by measuring a significant miss of their impact parameters from the beam collision point. The factors that determine the tagging efficiency are; intrinsic detector resolution, multiple scattering, δ -electrons, and the two track separation distance near the bottom decay vertex. The intrinsic resolution and multiple scattering effects contribute to the impact parameter resolution. In addition, the impact parameter resolution is maximized if the high resolution points are obtained closest to the decay vertex and by having a reasonable lever arm over which the trajectory is determined. This can be seen from the expression

$$\sigma_{intrinsic}^2 = \left(\frac{\sigma_1 r_2}{r_2 - r_1} \right)^2 + \left(\frac{\sigma_2 r_1}{r_2 - r_1} \right)^2$$

where the track measurement has been made at radii r_1 and r_2 with resolution σ_1 and σ_2 . As stated above, a second contributing factor to the impact parameter resolution comes from multiple coulomb scattering which we call σ_{mcs} . This is determined by the expression

$$\sigma_{mcs} = \sum (r_i \times \Delta\theta)^2$$

where $\Delta\theta$ is the multiple scattering valid for small angles. This is given by the particle data book expression

$$\Delta\theta = 0.014/p \times \beta(\sqrt{(\Delta X/X)} \times (1 + \log(\Delta X/X)/9))$$

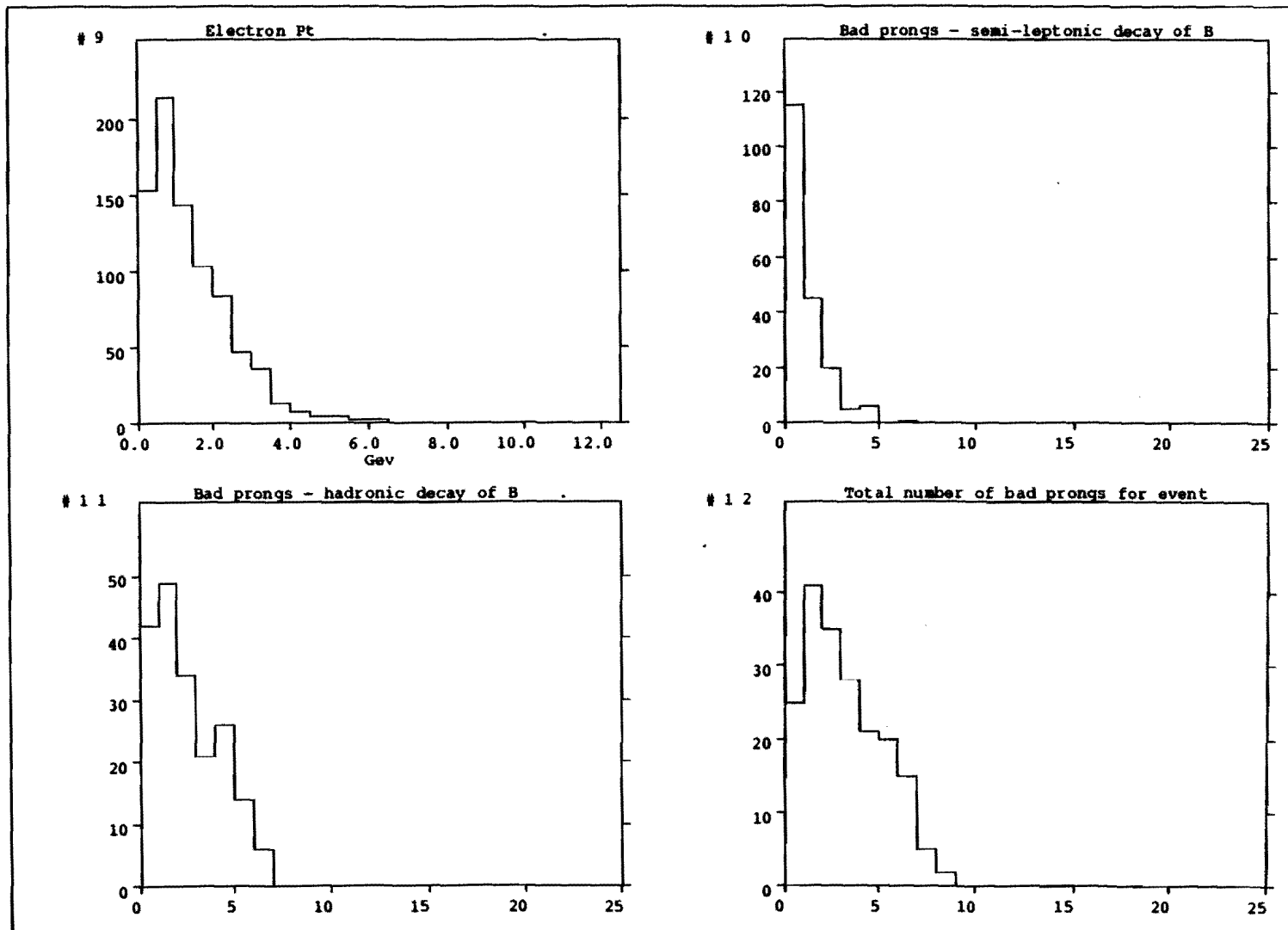


Figure 8

where p is in units of GeV/c. Two factors are important in the above expression for the σ_{mcs} . First the amount of material must be minimized and secondly the material must be placed as close to the decay vertex as possible. The latter effects the impact parameter linearly in the distance while the amount of material goes as a square root. This experiment attempts to maximize the impact resolution by considering the above effects in the design and placement of the microvertex detector and the drift chambers. The possibility of using 100 micron thick wafers, rather than the standard 300 micron thick wafer is very important for reducing the effects of multiple scattering. This is possible due to recent progress in integrated microamplifiers.

Finally, the confusion associated with many tracks from the underlying event extrapolating to the region of the bottom decay vertex is of greater concern at the Tevatron than at Lepton Colliders. Due to finite resolution in extrapolating a charged track to a decay vertex, tracks not coming directly from the bottom decay can appear to do so. This effect has been studied by Monte Carlo. The results are given in Figs. 9a and 9b. All charged tracks not coming from the bottom decay are checked to see whether they pass within 3 sigma of the known bottom vertex. The sigma accounts for the finite track resolution and the multiple scattering effects expected at that momentum. The results indicate that a 2-D measurement of the impact parameter would give only a few percent of the events completely without confusion. Next the plots indicate the separation in the z coordinate of the prongs causing confusion at the vertex. The results are divided into the resolution needed in the central region and forward backward region. The central region needs about 20 microns in z to remove 90 per cent of the confused tracks while the forward region requires about 200 microns. Therefore with the stated resolutions in 3-D, the ability to reconstruct bottom vertices is possible without too much confusion caused by the underlying event.

5.2.2 Microvertex Detector Design and Performance

The detailed layout of the silicon microvertex detector is shown in Fig. 10a and 10b. Consider the detector for $Z > 0$ and $Z < 32$ cm. The detector is symmetric about $Z = 0$. This is designated the silicon comb structure. There are three approximately cylindrical barrels in the vertex detector at radii 2, 3, and 4 cm from the beam line. The departure from a pure cylindrical geometry makes tracking and triggering more difficult due to the loss of symmetry. Therefore the geometry we choose will be at

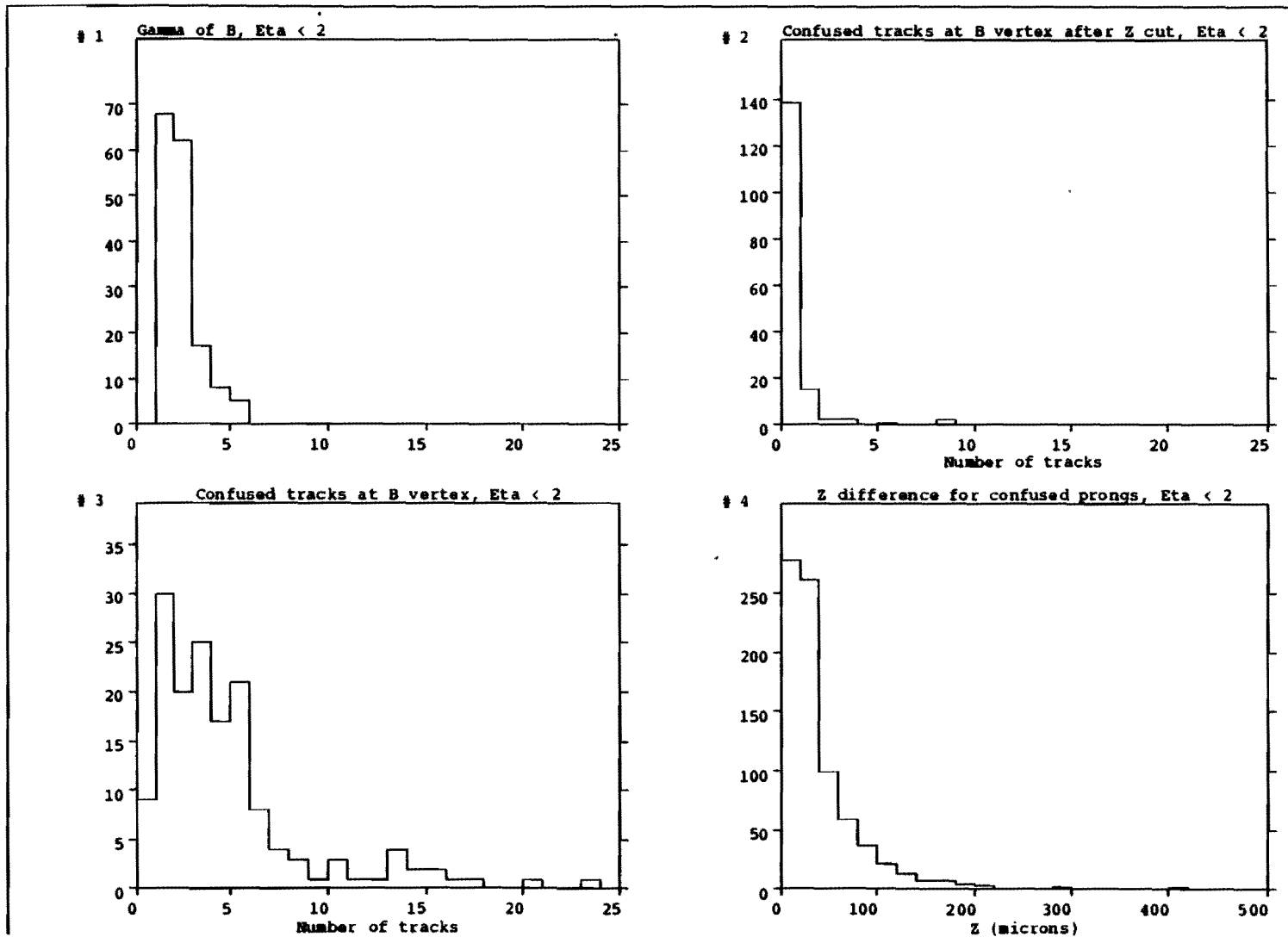


Figure 9a

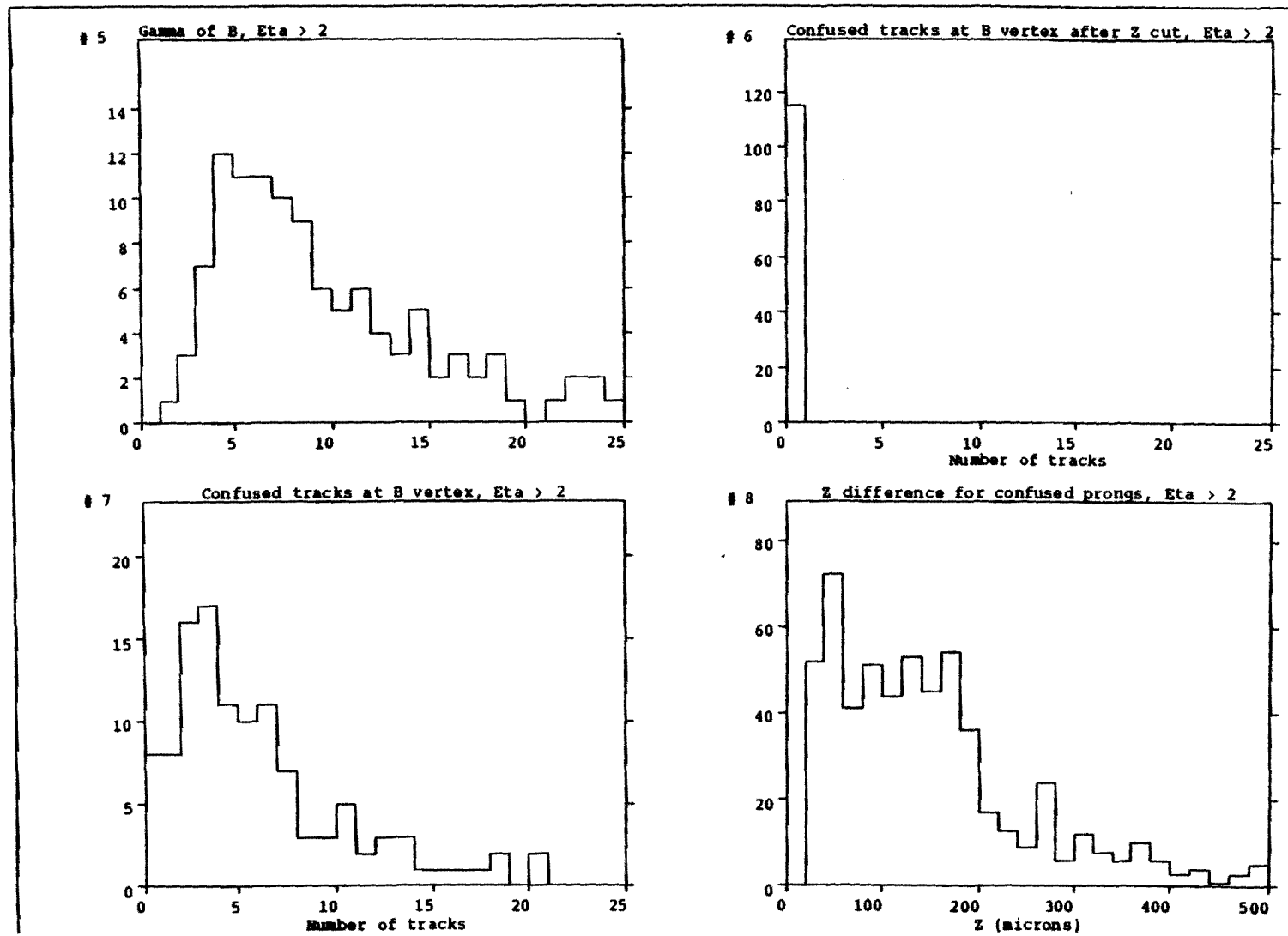


Figure 9b

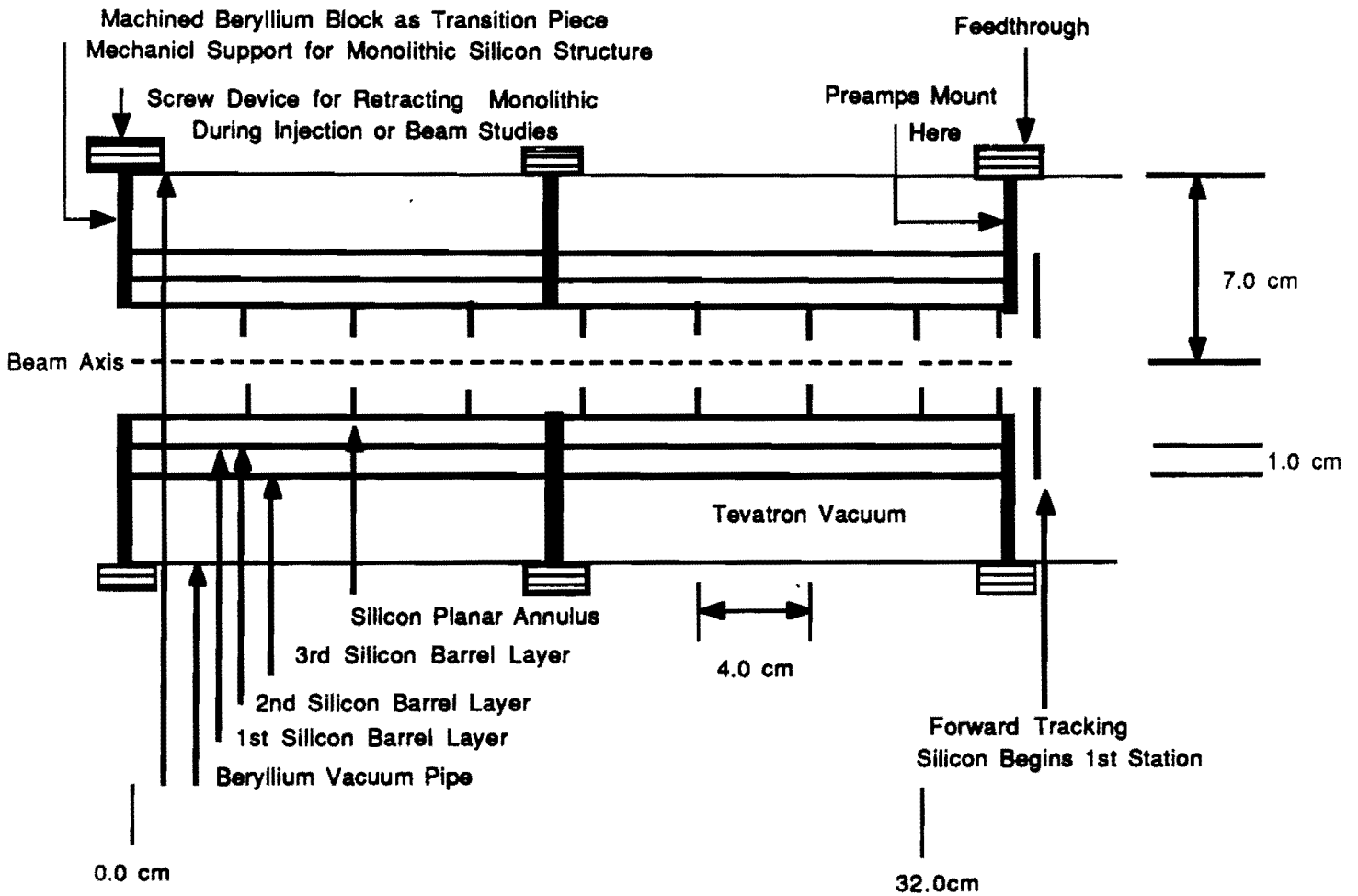
least octagonal. The final mechanical design will obviously influence this decision. There are planar silicon annuli of inner radius 1cm and outer radius 2cm spaced every 4 cm. This spacing is chosen to optimize the impact parameter resolution.

The forward section, located between $Z > 32$ and $Z < 140$, contains 9 stations of double sided silicon annuli. The inner radius being 1 cm and the outer radius being 4cm. The stations are spaced by 12 cm.

This entire configuration is enclosed inside of a beryllium vacuum pipe of radius 7 cm. This includes the integrated circuits. Consider the physical mounts for the comb structure. There are three beryllium mounts placed at $Z=0,16$, and 32 cm. These mounts are machined from solid beryllium and act as the transition piece between the 16cm long section of the beryllium beam pipe. These short pieces of 16cm, a total of 4 pieces are needed, are cheaper and easier to construct than one long piece. This segmenting accomplishes two things. First it allows the comb structure to be supported in 3 places, permitting greater mechanical rigidity. Secondly, the preamplifiers need to be connected to a metal surface to help dissipate the heat load. This implies that the chips are mounted at 16cm intervals. The thermal conductivity of beryllium is about 1/2 of that of silver and is therefore an excellent heat conductor. In addition, the mechanical procedure for retracting the silicon comb structure, 4 monolithic pieces total, is controlled at this point. The forward sections are built from 12 cm pieces of beryllium pipe and are individually retractable. Table I summarizes the material and expected impact parameter resolutions.

The heat dissipation from the preamplifiers is of concern for both mechanical stability and the effects on signal to noise. Signal to noise scales as $1/\sqrt{T}$ where T is temperature. In order to reduce the thermal gradient across the comb structure it is divided into 4 equal pieces of 16 cm in length, starting at $Z=-32$ to $Z=+32$ cm. The majority of heat comes from the large number of high capacitance channels in the barrel detector. Given the anticipated detector capacitance of 32pf per channel, the power per channel from an integrated amplifier built using CMOS technology should dissipate about 1.0 mwatt per channel. The barrel channel count is about 40,000, giving roughly 40 watts of power. The mounting of the chips directly onto the beryllium transition piece and hence to the beam pipe provides an excellent heat sink. If necessary, the beam pipe could be liquid cooled at the transition piece. Chips would be mounted only at $Z = \pm 32$ cm except for the first layer where with present technology there would be chips at $Z=0$ to handle the 25 micron pitch first layer. It should be noted however that MICRON Semiconductor is experimenting

Silicon Comb Structure Design



Forward section- 3 of 9 Stations Shown

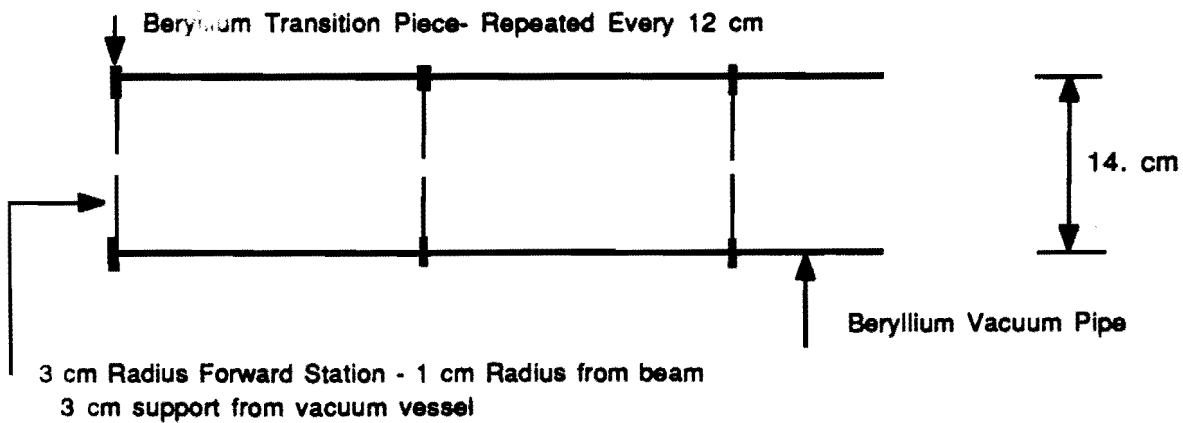
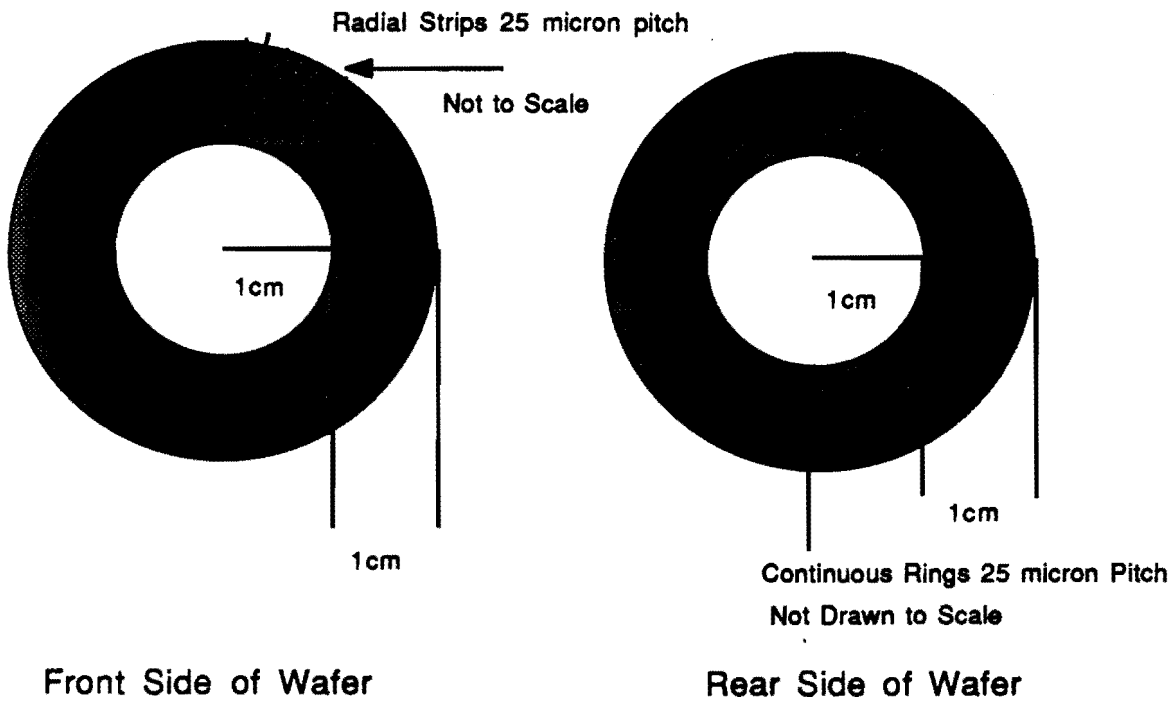


Figure 10a

View of Comb Section Annulus



Note: Downstream Annuli have inner radius 1cm outer radius 4cm

Figure 10b

Table I - Material Traversed at 90°

Central Detector Component	%R.L.	Radius (cm)	$\delta_{m.c.s.}$ 1 Gev/c (microns)	$\delta_{intrinsic}$ (microns)
Beam Pipe	.10	7.0		
Silicon 1st Layer	.50	2.0	20.	
Silicon 2nd Layer	.50	3.0		
Inner Carbon Tube	.24	7.1		
Cathode Pads	.32			
Wires	.12			
Outer Tubes	.24	28.775		8.0
Coil	1.5	30.		

with much smaller microbonding wire, 17 microns in diameter, and smaller pad sizes. This would allow denser packing of the electronics readout. The radial annuli are thermally connected to the silicon barrel. However the lower detector capacitance of the radial strips, about 1 pf , suggests the power for these channels will be much reduced since the power scales as detector capacitance squared. Each station has about 3300 channels, assuming 25 micron pitch, and this leads to an estimated 3.3 watts per annuli.

Type	Channel Count Per Layer for $Z > 0$ detector	Pitch	Layer	Radius
Barrel	5026 (1 side)	25	1	1cm
	2512	50	2	2cm
	3768	50	3	3cm

Total Channels 2 sided, 2 detectors is $2 \times 2 \times 11,306 = 45,224$

Annuli				
Strips	2512	25	1 of 15	1cm
Rings	800	25	1 of 15	1cm

Total number is $15 \times 2512 + 15 \times 800 = 49680$ Add 18 downstream planar stations
 $= 59,616$

Total channels for experiment is 154,520 or 1,207 preamplifier chips

5.3 Charged Particle Tracking - Radial Drift Chamber

The tracking requirements of this experiment are severe. A tracking chamber in the region between 5 and 30 cm must achieve the primary goals of momentum measurement with the precision of $\frac{\Delta p_t}{p_t} \sim 0.1\%$ p_t in a 3.0 Tesla magnetic field. In addition to this, the chamber should be capable of resolving separated electron positron pairs.

Some secondary goals of such a device are the resolution of tracks in the $r - z$ plane along with $\langle dE/dX \rangle$. The Z resolution should aid in pattern recognition, decays in flight and vertex recognition. The $\langle dE/dX \rangle$ information should aid in pion/kaon separation as well.

At a luminosity of $5 \times 10^{31} \text{cm}^{-2} \text{sec}^{-1}$, the bunch crossing frequency will be 5 MHz. By taking a typical drift velocity for proportional chamber gases at ~ 50 microns/nanosecond, the largest drift length possible is 1 cm without confusion resulting from events in subsequent crossings.

Conventional drift chambers, although well understood, use the track ionization from essentially the first electron arriving at the sense wire. With ~ 100 ionization electrons per cm of track length, much available information is not being used. Because of the constraints on the tracking device we have decided to adopt an approach which uses the information from nearly all the electrons arriving at the sense wire.

The tracking chamber we have chosen is based on the radial drift chamber (NIM A241 (1985)p 375). See the cell schematic in Fig. 11. In the radial drift chamber, track ionization formed in a linear drift region is drifted radially to a sense wire flanked by a pair of pickup wires. In certain gases, such as dimethyl ether, the avalanche (Fig. 12) will be very localized around the field line an ionization electron followed. Because of this localization there will be an asymmetry in the response of the pickup wires, L-R/L+R, depending on the location of the avalanche coordinates azimuthally around the sense wire.

By knowing the mapping of the field lines from the linear to the radial drift region, it is possible to determine to a high precision the location of the original ionization cluster from the quantity L-R/L+R. In a real configuration the left and right pickup wires will be read out by a pair of flash ADC's or using GaAs CCD's as sample and hold devices. See Fig. 13. From the time bucket of an arriving signal, the isochrone in the drift cell is determined and from the value of L-R/L+R, the field line is determined. By plotting the intersection of the isochrone with L-R/L+R an $r - \phi$ coordinate for each time bucket is determined. For each cell, it is possible to achieve many $r - \phi$ measurements to a high precision.

The design of the chamber features ten layers of 1 cm drift cells. Each cell contains 2 pickup wires, 2 field shaping wires and 1 sense wire with a pitch of 1.5 mm. Neighboring pairs of wire planes share a common central cathode grid consisting of aluminum wires. In this configuration pairs of drift regions drift inward and outward radially.

By running at a value of E/P of ~ 10 V/cm-torr, in the linear drift region (7600 V on the center grid) in DME the chamber can be read out in 200 nsec. The left and right pickup wires are to be sampled at 50 MHz giving 10 samples/layer, with each sample consisting of the signal from 12 ionization electrons on average.

From the Huth and Nygren NIM paper cited above it is possible to calculate that each measurement can be made to a precision of 30 microns, limited by the diffusion of the electrons. Using these parameters as a guide, the chamber should provide about 100 measurements, each with a 30 micron accuracy. This coupled with a 3.0 Tesla magnetic field should give a momentum resolution of $\delta p/p \sim 0.1\%p$ in the central region.

It should be pointed out that DME, in addition to being a low diffusion gas with very narrow avalanches has a small Lorentz angle (2°) and is favorable with respect to ageing (J. Kadyk, Proc. of Berkeley Conf. on wire chamber ageing).

In addition to tracking accuracy, the summed left and right pickup wire signals allows a determination of $\langle dE/dX \rangle$ in the chamber. Using the formula

$$\frac{\delta \langle dE/dX \rangle}{\langle dE/dX \rangle} (FWHM) = 96\% \times (N)^{-.46} (tp)^{-.32}$$

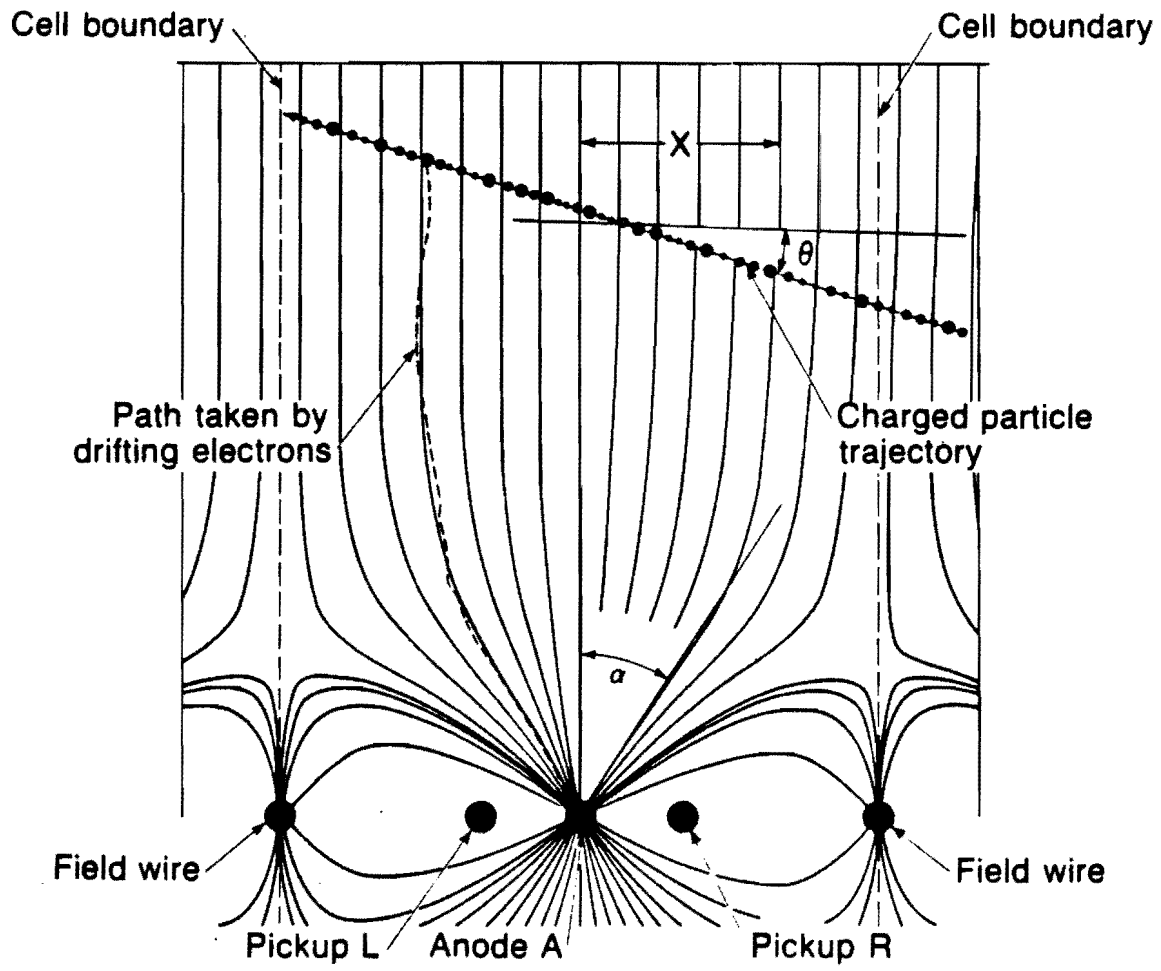
we can predict the resolution. This is appropriate to Argon (Rev. Particle Properties) where

- (a) N = No. of samples
- (b) t = thickness of sample (cm)
- (c) p = pressure (atm).

The predicted $\langle dE/dX \rangle$ resolution is $\sim 10\%$ rms. The relativistic rise in DME is unknown and is a crucial parameter in the determination of $K - \pi$ separation. However if the relativistic rise is assumed to be ~ 1.5 , then a $K - \pi$ separation of $\sim 1.5\sigma$ is possible. At higher pressure, better resolution is possible.

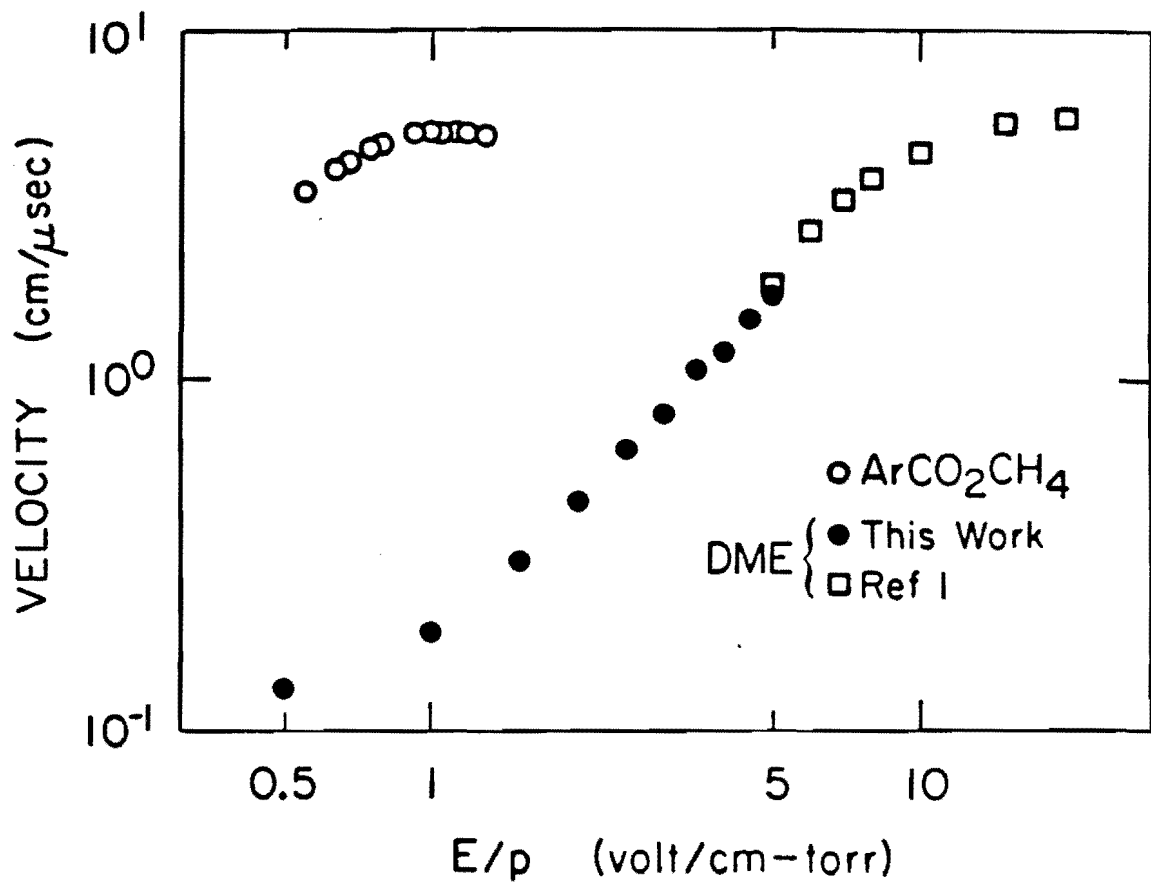
With the addition of cathode pads, covering 1/8th of the azimuth and ~ 5 mm in Z, a measurement of the Z coordinate of tracks is possible with an accuracy of 500 microns/hit. The design for each layer of pads is that used in the CLEO vertex detector (H. Kagen, R. Cass et al., to be published NIM) with only one sample collected per bunch crossing. It consists of a single pulse height of charge integrated over 200 nsec. of drift. With 10 layers instrumented this gives 10 Z measurements to a precision of 500 microns/hit.

The total axial wire force (~ 3 tons) is to be supported via a pair of carbon fiber composites at the inner radius (~ 10 mil) and the outer radius (~ 50 mil) to reduce the overall mass. Details are found in Table II. Figure 14 shows the layout of the forward radial drift chambers in the dipole magnet.



XBL 854-11065

Figure 11



XBL 854-2114

Figure 12

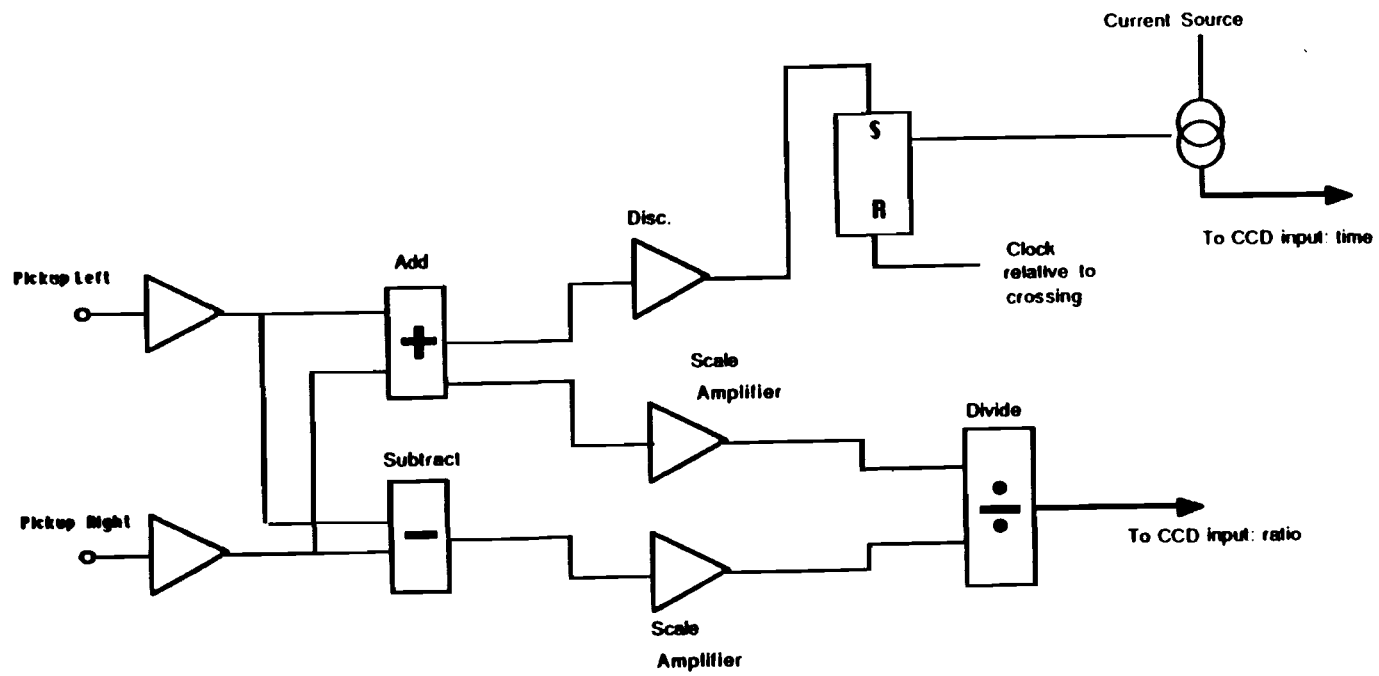


Figure 13

Table II

Chamber Parameters

Drift Length	= 1 cm
Max Drift Time	= 200 nsec
Sampling Speed	= 50 MHZ
Resolution/Hit	= 30 mm
No. Layers	= 10
No. Pickup Wires	= 14,139
Cell Pitch	= 1.5 mm
Lorentz Angle	= 2°
B Field	= 1.0 T
Drift Field	= 10 V/cm-torr
No. Pad Channels	= 24,000
No. Samples	= 100/30 μ m/hit
No. Z Hits	= 10/500 μ m/hit
Radiation length before last tube = 0.675%	
Contributions:	Inner Carbon Fiber Tube = .24%
	Alum. - Mylar Pad Cathodes = .15%
	Wires = .12%

Layer Parameters¹

Layer	R_{inner} (cm)	R_{outer} (cm)	Circ. (cm)	No. Cells	No. Channels (wires)
1a	<u>5.0</u>	6.25	31.42	209	418
1b	7.5	<u>8.75</u>	54.98	367	734
2a	<u>10.0</u>	11.25	62.83	419	838
2b	12.5	<u>13.75</u>	86.39	576	1152
3a	<u>15</u>	16.75	94.25	629	1258
3b	17.5	<u>18.75</u>	117.81	785	1570
4a	<u>20.0</u>	21.25	125.66	838	1676
4b	27.5	<u>23.75</u>	149.23	995	1990
5a	<u>25.0</u>	26.75	157.08	1047	2095
5b	27.5	<u>28.75</u>	180.64	1204	<u>2408</u>
					14,139

Note: Since this design was made, the chamber has been moved out in radius to about 7 cm.

¹underlined = Radius for Wire Plane

Forward Radial Drift Chambers

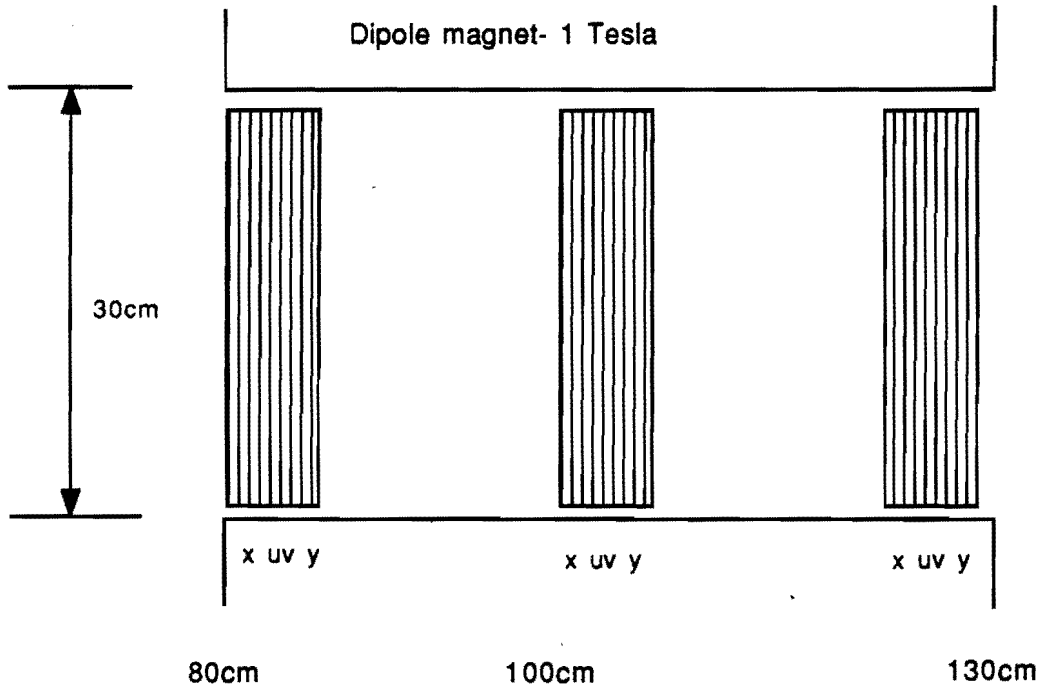


Figure 14

5.3.1 Momentum and Mass Resolution

The momentum resolution at 90° comes from evaluation

$$\left(\frac{\delta P_t}{P_t}\right)_m^2 = \frac{(\delta c)_m^2}{\left(\frac{.03H}{P_t}\right)^2}$$

where

$$(\delta c)_m^2 = \frac{\epsilon^2}{L^4} \left[\frac{720N^3}{(N-1)(N+1)(N+2)(N+3)} \right]$$

where the subscript m denotes measurement error, whereas, ms will denote multiple scattering. The quantities c , ϵ , L , N and H are curvature, uncorrelated rms position error, projected path length, number of uniformly spaced measurements along the track and the magnetic field. The units are meters, kilogauss, and GeV. Assuming a tracking length of 0.26m, a resolution of 30 microns/measurement, 100 measurements, and a field of 30 kilogauss, the transverse momentum resolutions is

$$\frac{\delta P_t}{P_t} = .1\% P_t$$

The contribution from multiple scattering to the uncertainty in curvature is given by

$$(\delta c)_{ms}^2 = \frac{\phi^2}{L^2} C_N$$

where $C_N = 1.43$ for $N \geq 15$ measurement points and

$$\phi^2 = \left(\frac{.015}{p\beta c}\right)^2 \frac{L}{L_R}$$

Taking L as .26m and L/L_R as 1.2% where the radiation length includes 1 plane of silicon plus supports, $\sim 0.5\%$ r.l., the beam pipe at $\sim 0.15\%$, and the drift chamber inner support, wires and gas. The multiple scattering contribution to the momentum resolution is

$$\left(\frac{\delta P_t}{P_t}\right)_{ms} = 0.8\%$$

and the overall expression is $\frac{\delta P_t}{P_t} = \sqrt{(0.1\% P_t)^2 + (0.8\%)^2}$

The worst case mass resolution calculated from the momentum resolution comes from a two body decay at rest. Taking the momentum of each track to be 2.5 GeV/c, this leads to a mass resolution of about 30 MeV which is dominated by multiple scattering. Silicon tracking, with its very high radiation length will make this mass resolution much worse. The above quoted mass resolution is adequate to separate B_d from B_s , which is one of the goals of this experiment.

5.4 Electromagnetic Calorimeter

5.4.1 Introduction

Electron identification is strongly desired as a tag for bottom mesons. The presence of a prompt electron is a clear signal for heavy quark production. When this is coupled with additional constraints placed on the electrons transverse momentum an enhanced data sample of bottom particles is obtained.

The choice of electron versus muon systems has been made for several reasons. The strongest physics motivation is that low energy rejection factors, applied in the 1-10 GeV range, are higher for electrons than muons. It is our belief that the best possible muon system will allow muon identification down to 2 GeV/c at best, and this may be in practice 3 or 4 GeV/c. It is hoped that with dE/dX samples along the track in the drift chamber, a good momentum measurement and a finely segmented calorimeter that electrons down to less than 1 GeV/c may be cleanly identified. This is very important since the electron spectrum from bottom is peaked around 1 GeV/c.

Another motivation for building an electromagnetic calorimeter is the fact that any upgrades to the detector, for example a muon system, can simply be added to the existing detector. If the muon system is built first, then adding calorimetry of course forces the muon system to be replaced.

The ability to detect neutral pions is of great interest when reconstructing bottom mesons since it opens many more decay modes to study. However, the ideal neutral energy resolution should match the charged particle momentum resolution to give equal contributions to the error in the invariant mass calculation. The cost and size of a total absorption calorimeter like BGO is beyond the scope and basic goals of this experiment, ie. easily fit into the CO collision hall. A sampling calorimeter in the hadronic environment can only be useful if it has excellent segmentation. If it is known the shower was initiated by a neutral pion, the pion energy can be determined from the angle between the prongs and the energy of one prong. This is a very useful

constraint in some circumstances. The energy measurement may be useful for some physics but is insufficient for separating the B_s and B_d variety of bottom mesons, the mass difference being about 100 to 200 Mev.

Finally, a very practical reason for choosing to build an electromagnetic calorimeter is that the detector can be made extremely small. This permits the detector to be installed in C0 intersection region without major construction, and therefore any disruption to the laboratories overall Tevatron program is minimized. In the following sections we discuss the design of the calorimeters, and the electronics and expected performance.

5.4.2 Electronics

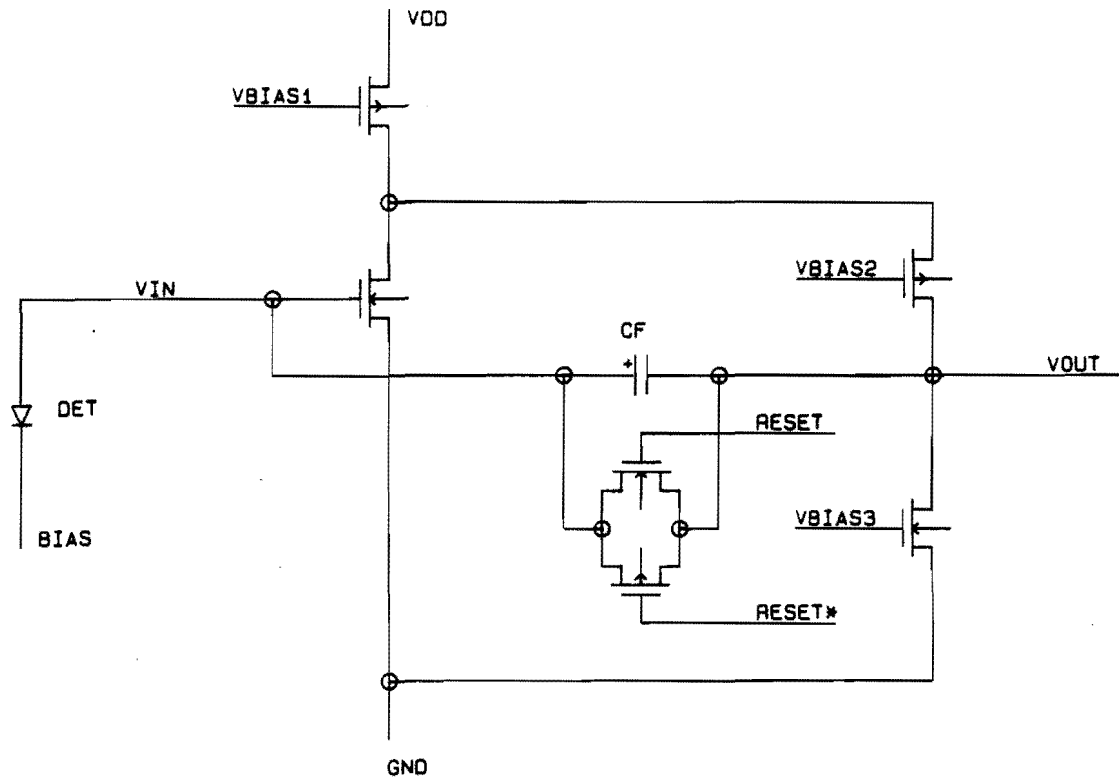
The electronics needed for the calorimeter are necessarily integrated due to the limited space available. An important parameter in the noise to signal considerations is the detector capacitance. In this design the relatively small capacitance expected from 300 micron thick, 200 micron depletion region, about $90\text{pf}/\text{cm}^2$, and the small leakage current of about 0.5 micro amps allows an amplifier design that should give a signal to noise of about 10-15:1.

Shown in Fig. 15 is a FOLDED CASCODE charge sensitive preamplifier suitable for use with the both silicon silicon strip and the calorimetry detectors. The expected signal to noise is estimated to be 10:1 and the power requirements are of order 1 milliwatt per channel. The expected risetimes are of order 100nsecs. The circuit is intended to be located close to the detector. The circuit will probably be built in CMOS technology so as to reduce the power consumption. Furthermore it may be necessary to study new processes which replace the silicon dioxide layer with silicon nitride to minimize the effects of radiation. This study is continuing.

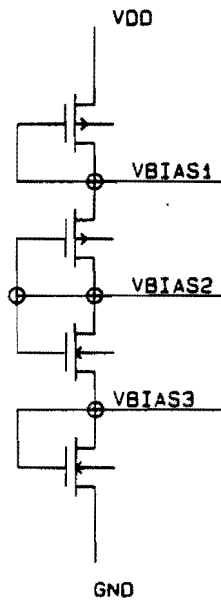
5.4.3 Reasons for Choosing Si/W

A projection tower geometry sampling calorimeter using tungsten as the absorber and silicon as the detection medium has been chosen. This choice is motivated by several reasons.

The fake electron signal from π^+/γ overlap decreases inversely as the area of the tower. In addition the matching of charge tracks in the tracking chamber to the small tower size further reduces the background from interaction pions, and multiple π^0 's overlaps.



Folded Cascode Charge Sensitive Preamp
(a)



Bias Circuitry for the above Preamp
(b)

Figure 15

	UNIVERSITY OF PENNSYLVANIA HIGH ENERGY PHYSICS	
	TITLE: CHARGE SENSITIVE PREAMP	DATE: FEB 87
	ENGINEER: T. TROJAK	PAGE: 1/1

Tungsten has been chosen since it permits the use of a material with the density of uranium to be employed without the problems normally associated with machining and obtaining uranium. The reduction in size of the overall detector as well as the solenoid magnet, and the fact it can be easily located in the CO collision hall more than offsets the additional cost of tungsten. In addition, future upgrades to the detector would permit easy integration of a hadron calorimeter with equal pion electron response.

Low energy electrons are difficult to identify cleanly if the first radiation length of material is not instrumented. This means the calorimeter should sit inside the magnetic volume, before the magnet coil. The need for a finely segmented calorimeter with the concomitant large number of channels immersed in a magnetic field of one tesla, precludes the use of phototubes. Even with waveshifter techniques, the number of channels, about 140,000 still makes a phototube design impractical.

Gas calorimetry can be operated in a magnetic field and is fairly inexpensive. However, it would force the detector size to grow, and therefore preclude easy installation into the CO collision hall. This is the main reason for not choosing gas calorimetry. In addition, the problems with gas gain monitoring are most unattractive for an experiment hoping to reconstruct a large number of bottom mesons.

The need for small radial extent, stability, and the ability to operate inside of a large magnetic field with large numbers of channels has made silicon the choice for the active device in this calorimeter. The work of G. Barbiellini et. al. has encouraged several groups to adopt or investigate the use of W/Si electromagnetic calorimeters. For example the SLD group has decided to build a W/Si luminosity monitor for many of the above reasons.

5.4.4 General Design Parameters and Performance

Inside the solenoid, the drift chamber extends radially from about 5 cm to 30 cm. radius, at which point the calorimeter begins. The solenoid is about 1 meter in length. To estimate the number of towers, we use the transverse shower size as a preferred tower radius. The transverse shower size is usually described in terms of the "Molière Radius", the average lateral deflection of electrons of energy E after traversing one radiation length. The Molière Radius can be approximated by this simple expression

$$\rho_m = 7A/Z(\text{gcm}^{-2}),$$

which for tungsten gives $7(184)/74$. For a density of $18g/cm^3$, the Molière Radius is about 1 cm. About 95% of the energy is deposited in a cylinder of $2\rho_m$ radius. This quantity has now been measured and we choose our tower size to be $1cm^2$. The shower size is shown in Fig 16. This translates readily to 35,000 towers if we use $1cm^2$ towers and 140,000 channels with 4 longitudinal segmentations. A detailed optimization of the tower size and longitudinal segmentation is underway with emphasis on electrons in the 1-10 GeV/c range in the busy hadron collider environment.

The present design estimates for the central region call for 16 radiation lengths of tungsten or 5.6 cm. The plates are 2 radiation lengths thick and silicon is present after each layer, giving 8 samples. This gives about 16 square meters of silicon for the central region. The forward backward detectors require another 7.0 square meters for a 20 radiation length detector, segmented every 2 radiation lengths.

The energy resolution of a silicon tungsten calorimeter of 20 radiation lengths, ten samples, 1 after every 2 radiation lengths has been measured by G. Barbiellini *et al.*, and they found

$$\frac{\sigma(E)}{E} = (17.6 \pm .3)\% \sqrt{\tau/E}$$

where in this experiment $\tau = 2$, the number of radiation lengths of passive material interspaced between two active layers of silicon. For this experiment, the energy resolution would be about

$$\frac{\sigma(E)}{E} \sim \frac{25\%}{\sqrt{E}}$$

Further study is needed to see whether this is adequate for identifying and triggering on the soft electrons.

5.5 Trigger

The trigger design is influenced by the experience of the detectors at the CERN Collider and the work of the CDF collaboration. The trigger is of the multi-leveled design, assumes a beam crossing \sim every 200nsec and requires at least one electron candidate with a $P_t > 1GeV/c$. Recall the electron spectrum from bottom semi-leptonic decays peaks at 1 GeV/c. The operations performed at each level are summarized below.

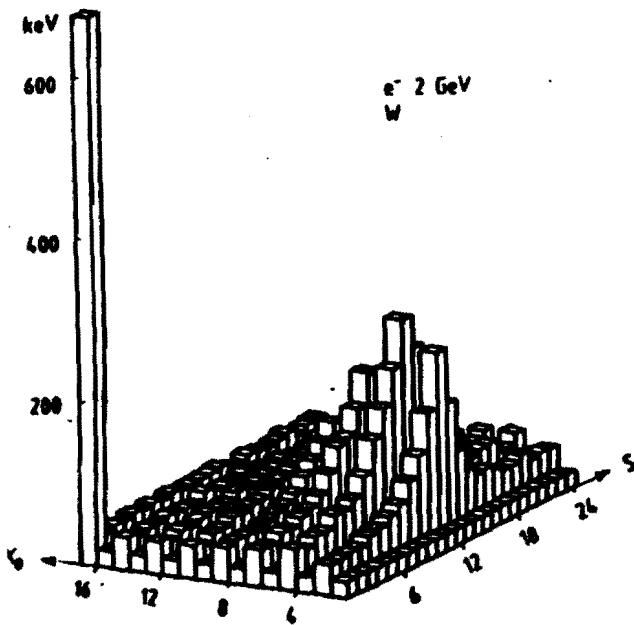


Fig. 2: Lateral shower distribution at 2, 4, 6, 8, 10, 12, 14 and 16 radiation lengths (X_0) of tungsten; S is the 1 mm pitch strip number; (a) for 2 GeV electrons.

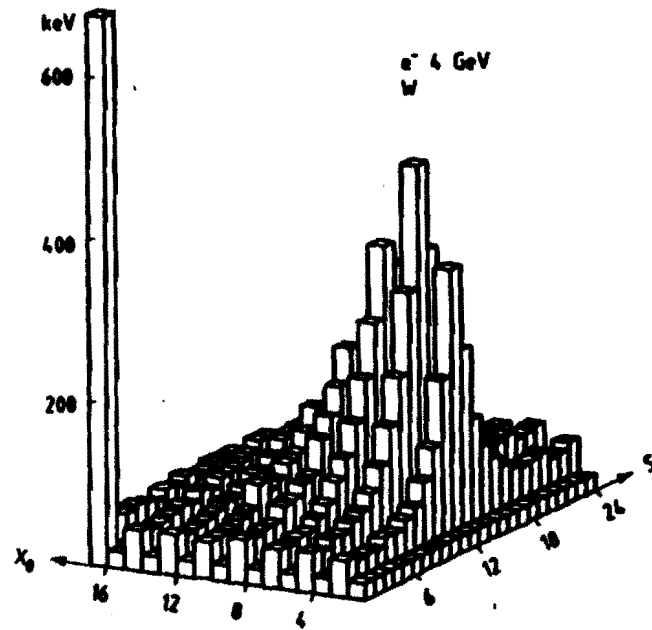


Fig. 2: Lateral shower distribution at 2, 4, 6, 8, 10, 12, 14 and 16 radiation lengths (X_0) of tungsten; S is the 1 mm pitch strip number; (b) for 4 GeV electrons.

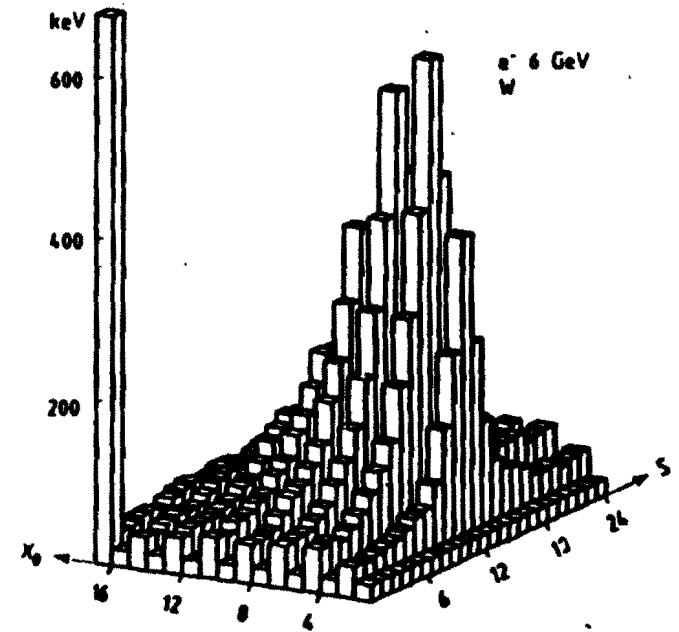


Fig. 2: Lateral shower distribution at 2, 4, 6, 8, 10, 12, 14 and 16 radiation lengths (X_0) of tungsten; S is the 1 mm pitch strip number; (c) for 6 GeV electrons.

Figure 16

5.5.1 Level One

The level one trigger adds no deadtime to the detector. A simple yet fast track processor using the radial drift information will find, with a resolution of $\frac{\delta P_t}{P_t} \sim 2\% P_t$ in the range 1 - 10 GeV/c, the number of tracks above 1 GeV/c in momentum and the sum of the charged P_t in the event. Fig. 17a shows the number of events with tracks above 1 GeV/c P_t and Fig. 17b shows the sum P_t for a sample of minimum bias events and Fig. 17c shows the sum P_t for a sample of bottom events generated with P_t 5 - 10 GeV/c.

This can be compared to the sum P_t for a bottom event, which is typically about 34 GeV/c, since the average P_t of tracks from bottom is about 500 MeV/c, and is about 300 MeV/c for minimum bias tracks. A fast track processor, similar in conceptual design to the level two CDF TRACK PROCESSOR (being built by U. of P, see Fig. 18), will find stiff tracks in the tracking chambers in a few microseconds. The monte carlo indicates that a level one trigger requiring at least one track above 1 GeV/c P_t and a sum P_t of greater than 10 GeV/c will reduce the 50 kHz primary rate by a factor of 20.

5.5.2 Level Two

This trigger decision will be completed in a few μsec , leading to a negligible deadtime. It is designed to reduce the incoming rate of about 2 kHz down to 50 Hz.

The major source of unwanted triggers comes from pions interacting in the tungsten, π^0 's overlapping with charged tracks, Dalitz decays of π^0 and conversions. All estimates are done using kinematics of minimum bias events since these will clearly dominate the trigger rate when looking for soft bottom events. The following is a rough estimate of the trigger rate.

Consider first the effects from interacting pions, ie. charge exchange. The interaction length of tungsten is 9.5 cm and the radiation length is 0.35 cm. This means the probability of a pion interacting in one radiation length is about 2%. Each unit of rapidity contains on average 4 charged tracks, giving about an 8% probability on an interaction per unit of rapidity or 64% probability in the whole detector. It is estimated that 1 in 25 tracks in a minimum bias event has a momentum above 1 GeV/c. Since the pion shower probability is not uniform through the depth of the calorimeter, the longitudinal shower profile is expected to yield a factor of 10 rejection. This gives a rate of about 12hz at a luminosity of 10^{30} .

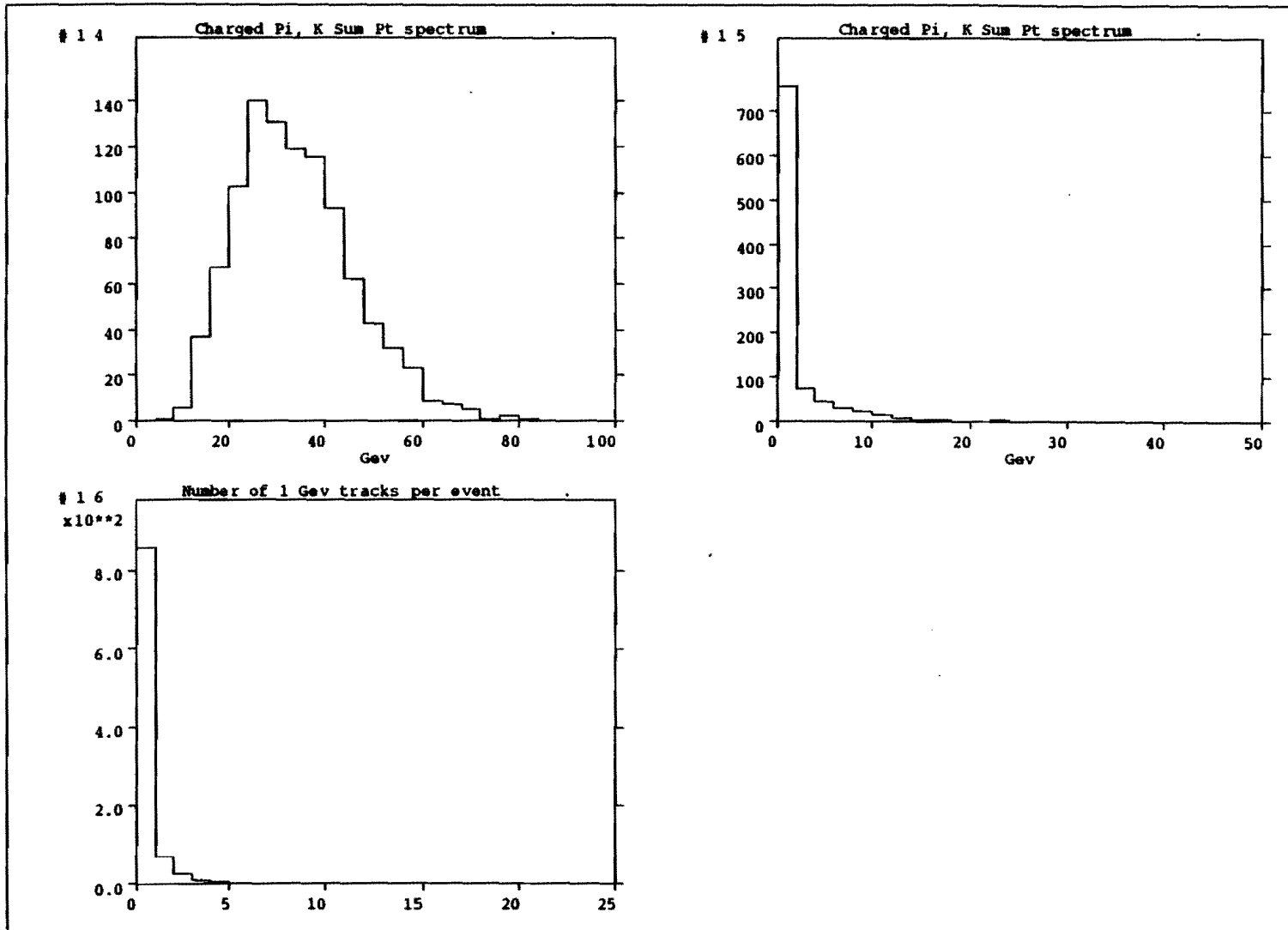


Figure 17a, b, and c

Now consider the problem of overlap between charged tracks and neutral pions. In the central region, the unit of rapidity extending from 0-1 covers from about 90 to 45 degrees. If we take the number of particles per unit of rapidity to be 4, and distribute then evenly in ϕ this implies 1 particle for each roughly $188/4\text{cm}$ in ϕ . This defines a box of area 47cm by 30cm or 1410cm^2 which on average contains one charged and one neutral particle. In order to fake an electron, they must overlap in space and the momentum of the track and the π^0 must match. A factor of $1/16$ from requiring the momentum to match gives a overall probability per track of about 4.0×10^{-5} . This gives an $\sim .1\text{Hz}$ rate, assumming 50 charged tracks per event and a rate of 3 kHz into level two. The overlap in the forward section is increased by the ratio of the track densities measured at the calorimeter, which is a factor of ten, or about a 1 Hz rate.

The final source of fake electrons comes from γ conversions in material and Dalitz decays which give a topology of $\pi^0 \rightarrow e^+e^-\gamma$. The branching ratio for the Dalitz decays is $\sim 1.2\%$. Since each non-Dalitz π^0 decay produces two photons and since the pair production rate per unit distance is $\sim 0.8/L_R$, the number of e^+e^- pairs expected from Dalitz decays is about the same as expected from pair conversions in $0.7\% X_0$ of material. At 90° there is about $2.7\% X_0$ implying that Dalitz pairs account for at most 25% of the produced pairs. This can be expressed simply by the expression for the probability of producing a pair.

$$P_{rob} = (\text{Dalitz Decay Branching Ratio} + 1.6 \frac{t}{X_0 \sin \theta})$$

where t is the thickness of the material, X_0 the radiation length and θ the polar angle. The appropriate radiation length to use in the above expression is that of the first silicon layer. Taking the above probability to be about 1%, the trigger rate expected is about 20 Hz.

The principle of the trigger is simply to require the ratio of energy in the front of the calorimeter relative to the drift chamber momentum measurement to be about 30%. In addition the track and shower position and momentum must match. The use of dE/dX measurments in the trigger for tagging low energy electrons has yet to be considered. The present design would probably amplify each pad separately by running short, low inductance cables to the end of the calorimeter, where an amplifier is mounted, quite likely with attached cooling. Multiplexing and zero suppression at the detector would be desirable. The signal would then be buffered, either in an AMU or CCD device. These signals would then be driven to the small number of ADC's in

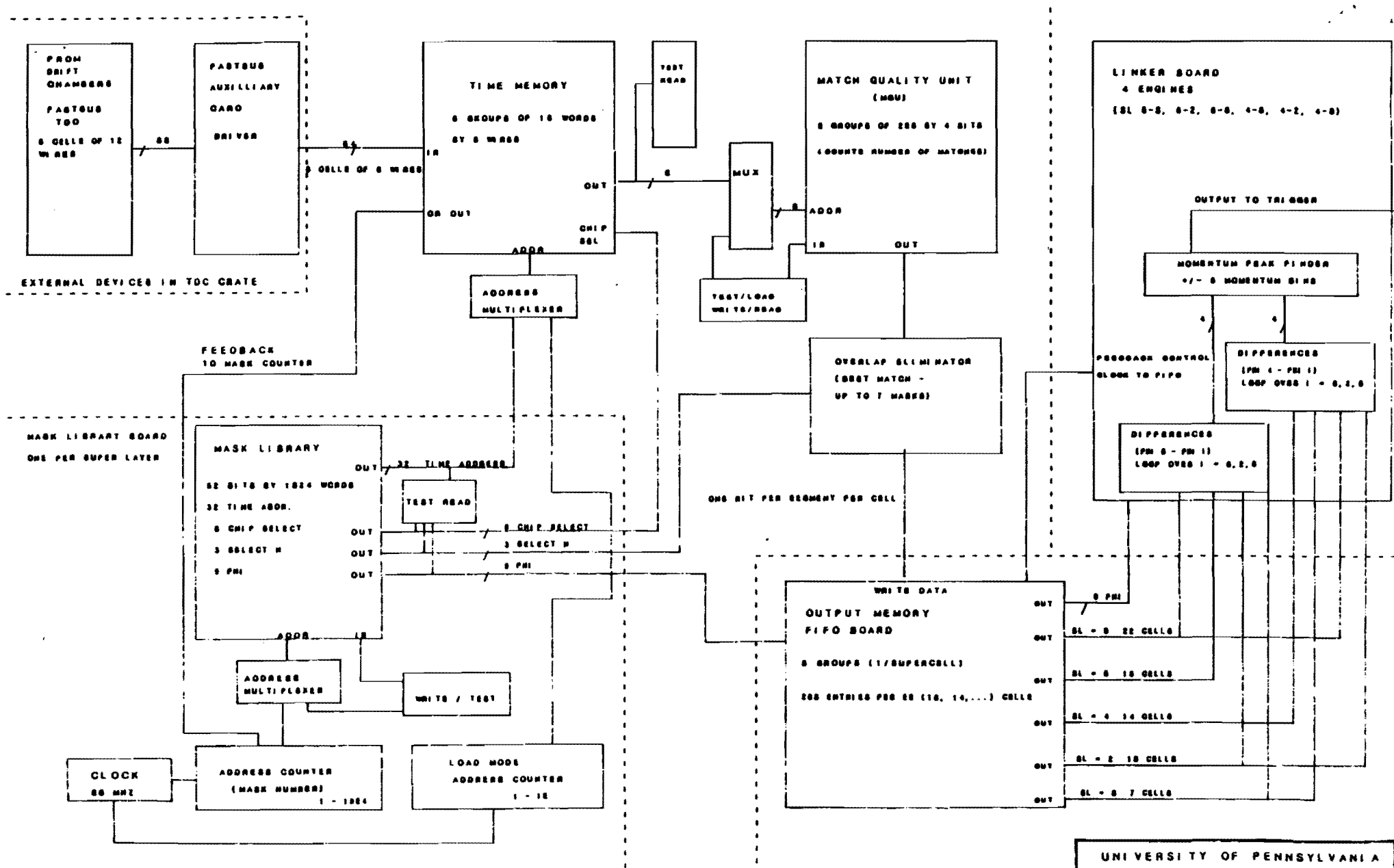


Figure 18

the counting room. After digitization, the information would be dumped into memory where majority operations and centroid finding could be used to maximize rejection against the above backgrounds. Notice this procedure does not involve analog sums. Options which minimize the cost would have to be evaluated by simulation and prototyping since much progress has been made in this field in the last year and many groups are considering similar problems. Detailed simulations of the trigger are underway.

5.5.3 Level Three

An array of processors such as the FERMILAB ACP could add significant filtering power to the data analysis stream. Higher resolution matching of drift chamber tracks and the track segments from the electron system where multiple scattering effects are taken into account would give a cleaner sample of events for tape storage. In addition, an algorithm that has the ability to track pair conversions can reduce the electron rate by about a factor of 20.

5.6 Buffering - Electronics

The upgrade of the TEVATRON will have a crossing rate of 5 MHz. Since the trigger decision from the electromagnetic calorimeter system will take roughly one to two microseconds, the data in the tracking systems must be buffered. The approach that is being proposed is based on a system of CCD's. The hope is that by using the Gallium Arsenide CCD's developed at TRIUMF we can store charge (clock through the CCD) for the amount of time needed to make a trigger decision, at which point the charge is transferred to a high quality low noise amplifier. This design differs from the present scheme being pursued by CDF (and most other experiments). CDF employs a NMOS MICROPLEXOR chip which has 128 amplifiers on a single chip. There is a sample and hold and multiplexing capabilities as well. This was developed by the MARKII group for SLC, and is being redesigned by the CDF LBL group using CMOS technology so as to reduce power consumption and hence avoid the heating problems. The CCD approach is well suited to the buffering scheme and holds the possibility of good signal to noise and much less sensitivity to radiation damage. Shown in Fig. 19 is a schematic representation of the buffering for the silicon strip detector. This can be generalized for use with the drift chamber also.

Viewing Fig. 19, the charge from the silicon strip enters from the left. A before

and after sample is made to reduce noise. Charge injection from the strip to the first CCD bucket is being presently studied by us and others (for example T. Kondo). In our present design, an FET on the same CCD wafer assists in charge injection from the strip to the bucket. The trigger decision time of about one microsecond then sets the clock speed and length of the CCD to be roughly 10 MHz and 16 buckets. Clearly a silicon CCD works well at these clock speeds. Next the trigger decision, if positive, loads the charge into another CCD which acts as a buffer until it can be read out and digitized. Shown in the schematic is a ring buffer which takes into account the small probability that events close together in time may trigger. Depending on the storage time capabilities of the CCD (early numbers are implying that a microsecond per bucket is possible without much charge loss) the ability to make further trigger decisions may be possible and this is shown in the schematic also.

The amount of electronics to digitize the data is actually very small. The rate into the Level Two trigger is assumed to be a couple of kHz. Again, using the silicon strip detector as an example, at 4 tracks per unit of pseudo-rapidity, coverage of roughly 8 units of pseudo-rapidity, 2 strips per track, there are roughly 10,000 channels/layer with charge per second. Even at 100,000 digitizations per second, and assuming a few microseconds to digitize, this implies only a few ADC's are required for this system.

6 Comparison to Other Experiments

6.1 Introduction

The important parameters to remember when designing a bottom detector vary with the physics that one is targeting but in general the following is true. A detector with very good vertex detection is needed to tag the secondary vertex of bottom mesons. At the Tevatron most of the bottom is soft and produced isotropically over ± 4 units of rapidity, therefore low momentum detection of leptons is important and equally as important is the hadron rejection at low momenta, typically momenta between 2-10 GeV/c. A small decay volume reduces the background in a linear fashion from pion and kaon decays. This is the largest background at low momenta and excellent tracking resolution increases the probability of identifying these decays. In addition, a magnetic field is useful for reconstructing exclusive decay modes. Excellent charged particle tracking improves mass resolution and vertex pattern recognition capabilities.

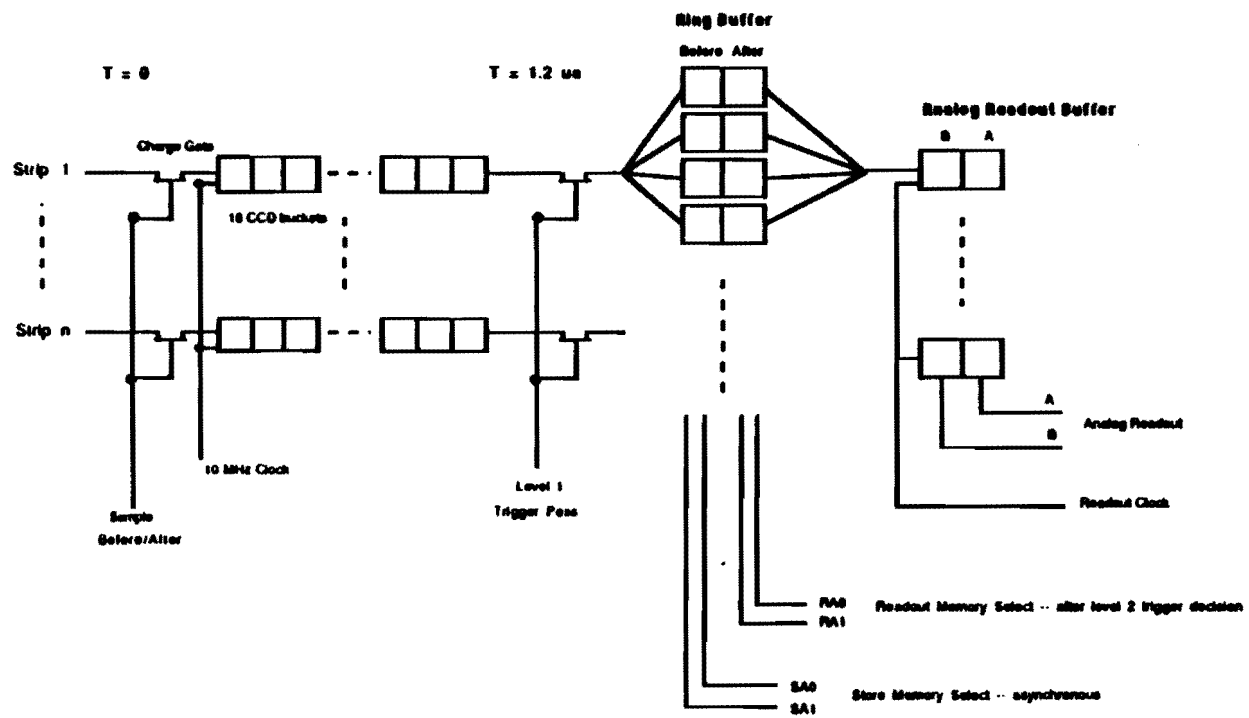


Figure 19

There is much interest in bottom factories throughout the world. At present there are studies in progress at TRISTAN using their accumulator, at CERN with a linear collider, and at SIN using two circular colliders, as well as, a U.S. effort being pursued by a group at U.C.L.A.

In the following, a brief comparison of the essential detector and accelerator features needed to optimally study bottom physics is given to some of the major detectors in the world.

6.2 D-Zero Experiment

The D0 experiment is not well suited to the study of bottom mesons primarily because of the lack of a magnetic field inside the tracking volume. First, the tagging of secondary vertices and the counting of charged prongs at the vertex requires a good knowledge of the effects of multiple coulomb scattering. The number of scattered tracks into an area around the secondary vertex will depend on the distance of the vertex from the primary intersection point (PIP), the number of primary charged tracks originating from the PIP and their momentum distribution. This most important aspect to studying the background rejection to bottom tagging cannot be done in D0. Second, the ability to reconstruct exclusive decay modes is not possible in the D0 experiment. This is necessary in the $b \rightarrow u$ analysis where the invariant mass is needed as a signature.

The muon system of D0 has an appropriate number of interaction lengths of steel absorber based on UA1 stated requirements for non-interacting punch through and leakage. The D0 added absorber thickness relative to CDF aids in reducing leakage and hadron punch through and sets a lower limit on the momentum of muons which pass through the iron. The small decay radius of D0, 70 centimeters at 90 degrees, helps reduce the effects of pion and kaon decays which are the major muon background below 5GeV/c. However it is not optimally instrumented for bottom physics. The D0 experiment instruments only the front and back of their central 100cm steel absorber. This makes the matching of a tracks in the central drift chamber within the limits of multiple scattering with the hits from the muon proportional tubes more difficult. For instance the 3σ scatter search area of a 3GeV/c muon candidate in one plane is a circle of radius roughly 108mm. This is the amount of multiple scattering sustained while traversing the $6.4 \lambda_0$ or 61 radiation lengths at 90° . The overlap of the multiple scattering circles in an event increases with increasing uninstrumented

absorber thickness and causes ambiguous association of drift chamber tracks with muon system tracks. This effectively reduces the statistical sample since these events would be removed as muon candidate events. Furthermore, instrumenting the muon system at several radii allows momenta of exiting tracks to be measured. This is effective in reducing the low momentum tracks from leakage by about a factor of 2. In addition, extrapolating the leakage signal through each layer provides a direct measure of the leakage out the rear of the muon system. Finally, the effects of random noise in the muon system chambers can be troublesome when only an inner and outer measurement are made.

6.3 CDF Experiment

The CDF experiment can be described as it stands in B0 now and how one might imagine the upgraded detector to look in a few years. First, a description of the suitability of CDF as a bottom physics detector is given. Since bottom is detected mostly between ± 4 in pseudo-rapidity, the ability to detect low momentum electrons and muons over this rapidity range is extremely important for detecting the majority of the semileptonic bottom meson decays. It appears to be difficult for CDF to have a rejection of much better than 100:1 for isolated electrons below 10GeV/c and less than 50:1 for electrons inside of a jet below 10GeV/c. Identification of electrons below about 4GeV/c is not possible. The hadron rejection at 30GeV/c is about 3000:1. The muon system suffers from poor acceptance, a large decay volume and not enough absorber. The central muon system covers ± 0.7 units of pseudo-rapidity with $6\lambda^0$ of absorber. There is about a 10% loss in ϕ coverage due to cracks as well. Below 5GeV/c the dominant background comes from pion and kaon decays in flight. The rejection against decays at 10GeV/c is about 150:1 and therefore about 30:1 at 2GeV/c. The ability to reject kinks from decays will improve this rejection factor by a factor of 2 or 3 since the central tracking chamber has about 200 microns resolution per point. The large decay volume of CDF, 1.5 meters in radius, is 5 times that of this experiment. The leakage rejection factor for CDF is underestimated in the design report. Present UA1 information suggests the CDF rejection factor against leakage is about 0.001p or 1% at 10GeV/c. Finally, the CDF experiment has minimal vertex detection, in the $r - \phi$ plane, that is capable of tagging bottom mesons. The VTPC's, optimized for forward tracking, can achieve 300 microns resolution in the $r - \phi$ plane if a single track is detected by the 1cm pads. The multi-track environment at small

radius will reduce this resolution by about a factor of 2.

The upgraded CDF detector will improve upon many of the weaknesses discussed above. An improved muon system would cover 8 units of rapidity. The increased thickness is expected to improve leakage by about a factor of 5-10. The rejection against decays will improve in the upgrade if the steel is magnetized by at most a factor of 2. The proposed super toroids will cover from 4 to 1 in pseudo-rapidity. Together with the central region upgrade, CDF will have very good muon coverage. Improving the central electrons has not been formally proposed at this time but it appears that dE/dX with a factor of ten in rejection is possible from this system. Another major upgrade planned for CDF is a high resolution vertex detector composed of 4 layers of 50 micron pitch silicon strips. It is assumed here that the problems associated with poor signal to noise and high power dissipation presently under discussion within the collaboration will be solved and that questions concerning pattern recognition capabilities of the four layers of silicon will become clear once real data is taken. It may be necessary to add a high resolution drift chamber to aid the pattern recognition capabilities of the silicon. This would give CDF a powerful vertex detector system.

In summary, the planned CDF upgrade will improve the detector greatly. However the necessary low momentum hadron rejection is not adequate to exploit the large bottom cross section below 10GeV/c. Therefore CDF now and in the future cannot address the bottom physics issues requiring high statistics that this experiment is focussing on.

6.4 Comparison to High Energy e^+e^- Machines

6.4.1 Slac-Linear-Collider and LEP

The most important difference between the lepton colliders, SLC and LEP, and the Tevatron is that the number of bottom mesons produced at Fermilab is potentially much larger. Secondly, the lepton colliders have very powerful detectors installed in their intersection regions designed to study bottom physics.

At the SLC, the Mark-II detector will probably record data in the $10^{28} - 10^{29} \text{ cm}^{-2} \text{ sec}^{-1}$ range of luminosities for a couple of years. If we assume a Z^0 cross section of 30nb on the resonance, then 1 pb^{-1} of integrated luminosity gives about 30,000 Z^0 s or about 3900 bottom events. This is a very small bottom data set when compared to what is expected for the other more powerful detectors. The SLC should prove to be a

very powerful bottom laboratory if the luminosity can reach the design average luminosity of $6 \times 10^{30} \text{cm}^{-2} \text{sec}^{-1}$. This would give 1-2 million Z 's per year. The SLD detector has very good particle identification, in particular kaon identification, an excellent vertex detector composed of CCD's placed within 2cm of the beam vertex and good lepton identification over the full solid angle. Of course the SLC is an experimental machine and achieving the design luminosity may not come quickly. Similarly, the LEP detectors at CERN, ALEPH, DELPHI, L3, and OPAL are all well suited to studying bottom physics. They are however weaker in vertex detection capabilities because of the large radius, 8-10cm, of the LEP beam pipe. The LEP machine is more conservative in design and should reach average design luminosity of $\sim 10^{31} \text{cm}^{-2} \text{sec}^{-1}$ by 1991.

6.4.2 TPC at PEP

It is planned to upgrade PEP to a luminosity of $10^{32} \text{cm}^{-2} \text{sec}^{-1}$ to provide a high statistics study of bottom physics. The Time Projection Chamber (H. Aihara et al., PRL 52, 557 (1984)) is being upgraded via the addition of a straw vertex chamber. At high luminosity, a goal of the bottom studies is to accumulate approximately 30,000 tagged bottom events, corresponding to 1fb^{-1} of integrated luminosity at $(\sqrt{s}) = 29 \text{GeV}$. (SLAC Pub. 283 (1985)).

A stated goal of the bottom studies is a measurement of the B lifetime (charged and neutral) to a precision of 0.05 picoseconds. Secondary measurements include a measure of B_c and B_b baryon masses, measurements or limits on the $b \rightarrow u$ rate by observing $B \rightarrow \tau \nu$ and a measurement of mixing in the B_c system. The limitations of this machine arise from the fact that vertex detectors cannot be placed close to the beam collision point. This is a fundamental limitation due to synchrotron radiation.

6.5 CESR

The Cleo detector at CESR is presently undergoing a major upgrade. The new detector will have very good charged particle tracking with dE/dX readout inside a 1.5 meter superconducting coil, and an excellent CsI electromagnetic calorimeter. They expect to reconstruct 1000 charged B's and 1000 neutrals in decay modes in which the signal to noise is better than 3:1. The improved luminosity of CESR is hoped to provide 1fb^{-1} of integrated luminosity in a good year. It is important to note that the ratio of cross sections at CESR relative to the Tevatron is about

2000:1, where the cross section times R on the $\Upsilon(4s)$ is taken as 3nb . An additional advantage at the Tevatron is the ability to separate the bottom meson's secondary vertex from the collision point thereby allowing the counting of charged prongs at the bottom vertex and thus reducing the invariant mass combinatorics. The bottom from the $\Upsilon(4s)$ is produced near threshold and only travels a few microns, a distance too short to tag with present technology.

6.6 UA1

The UA1 experiment, at the CERN Sp \bar{p} S, is also undergoing a major upgrade, it can to a large degree study much the same bottom physics as the experiments at the Tevatron since the production cross section is similar. However the UA1 experiment has decided not to install a high precision vertex detector. This precludes UA1 from doing much of the physics being addressed by this experiment. The hadron rejection for low momentum muons is similar to CDF but is still not optimized for bottom physics. The new electromagnetic calorimeter will improve their electron identification at low momentum. In summary the UA1 experiment will not be able to address the high statistics bottom physics that this experiment is focussing on.

6.7 Fixed Target

6.7.1 NA32

The relative production rate of heavy flavor with respect to light quarks is smallest for hadron interactions, 1000:1 at the SPS, but the absolute rate is the highest. The amount of equivalent luminosity in a fixed target experiment can be very large. For example, with 10^7 interactions/sec from a 1cm target of iron an effective luminosity of a few $\times 10^{33}$ is available. NA32 at CERN has studied for some time the best way of triggering on charm in a fixed target experiment. From their most recent results, based on 4 million triggers, a charm enhancement factor of 15:1 to 30:1 has been achieved when triggering on a high p_t electron. Their trigger had an acceptance of about 10-20%. Triggering on the change in charged multiplicity in a fine-grain active target, using silicon microstrip detectors, gave a small enhancement of 1.3-2. The offline reduced the final sample to a about a hundred D's fully reconstructed. In a different run, the silicon vertex telescope provided very large background rejection factors offline, better than 1:1,000,000, by requiring tracks ($K\pi\pi$) to originate from

the D^+ vertex. Clearly the vertex tag is powerful once the event is on tape. However, when considering bottom production, the cross section is about 1000 times smaller than the $10\mu b$ charm cross section at Fermilab energies. This small cross section combined with the difficult triggering where enhancement factors are at best 30:1, and acceptances are less than one makes the fixed target approach very difficult at this point on the learning curve.

6.7.2 E-691

The charm photoproduction experiment at Fermilab, E-691, has recorded about 10^8 events on tape. These were recorded at a rate of 2000 per spill using a trigger requiring a transverse energy of greater than 2 GeV. This trigger accepts 40% of the cross section and is about 80% efficient for charm. This trigger gave about 25 charm events per spill, with one Tevatron spill per minute. This experiment has demonstrated very convincingly the ability of vertex cuts to extract a clean mass signal which otherwise would be unobservable due to background combinatorics. This approach however would not work well for tagging bottom since the cross section is roughly a factor of 10^3 smaller.

7 Acknowledgements

Many peoples ideas have contributed to this proposal. In particular we would like to thank J. Bjorken and H. H. Williams for many useful suggestions, J. Huth for providing the design for the radial tracking chamber, and D. Amidei for helping with the calculations of the physics rates and M. Nelson for many useful comments. Sebastian White and Georgio Chiarelli have provided useful information concerning the beam pipe design. Special thanks to J. Walsh whose Monte Carlo work has greatly improved our understanding of this experiment. A. Lankford has provided useful comments on the calorimetry. Finally we would like to thank D. Finley and L. Lederman for general advice on use of the Tevatron.

9 Budget

Budget (in thousands)

	System:	
1.0	Superconducting Solenoidal Coil - 3T	1500
	Two Dipole Magnets	100
2.0	Silicon Vertex Detector	
	Central	150
	Forward	150
3.0	Beryllium Pipe	200
	and Transition Pieces	
4.0	Radial Drift - Central	300
	Radial Planar Drift	300
5.0	Electro Magnetic Calorimeter	
	Tungsten \$12/lb	100
	Silicon $23M^2$ at \$ 3/cm ²	700
6.0	Electronics	
	Vertex Detector	
	\$1.50/Channel	
	Barrel 40,000	60
	Annuli 100,000	150
	Buffering	40
	10 ADC	20
	Central Radial drift	
	30,000 at \$2/pickup	60
	Planar Radial drift	
	30,000 channels	60
	Buffering	15
	10 ADC	20
	Calorimeter	
	140,000 channels at \$1.50	210
	Buffering	50
	10 ADC	20
7.0	Trigger System	
	Track Processor	150
	Silicon Trigger	100
	Electron Finder	100
	Level 3 Processor	50
8.0	Computing	
	4 Microvax II	200
	R81 Disk Clustered	
	High Resolution Graphics	100
9.0	Prototyping Costs	300
		4.9 M
	Contingency at 20%	980
	TOTAL	5.9M

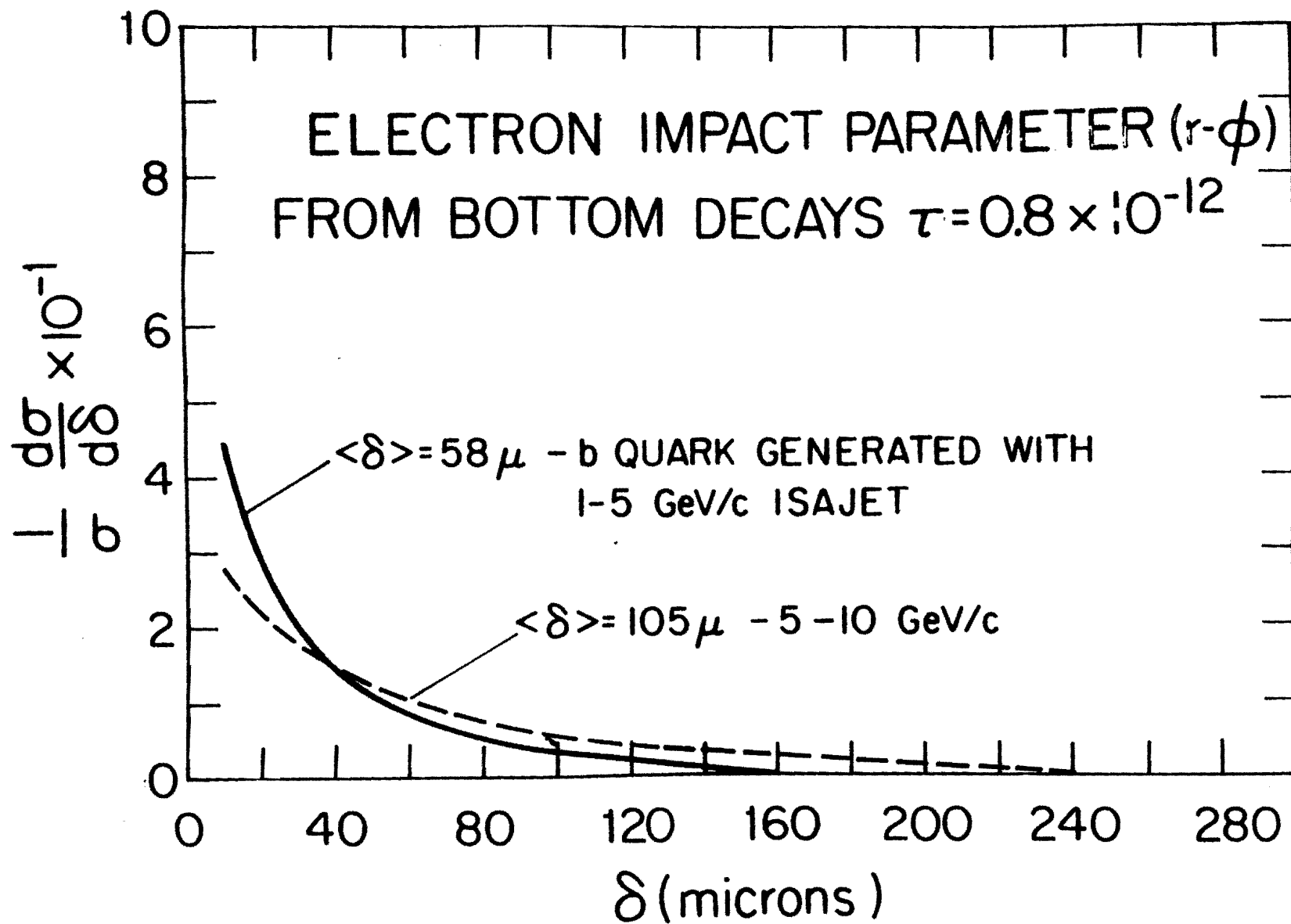


Figure 20

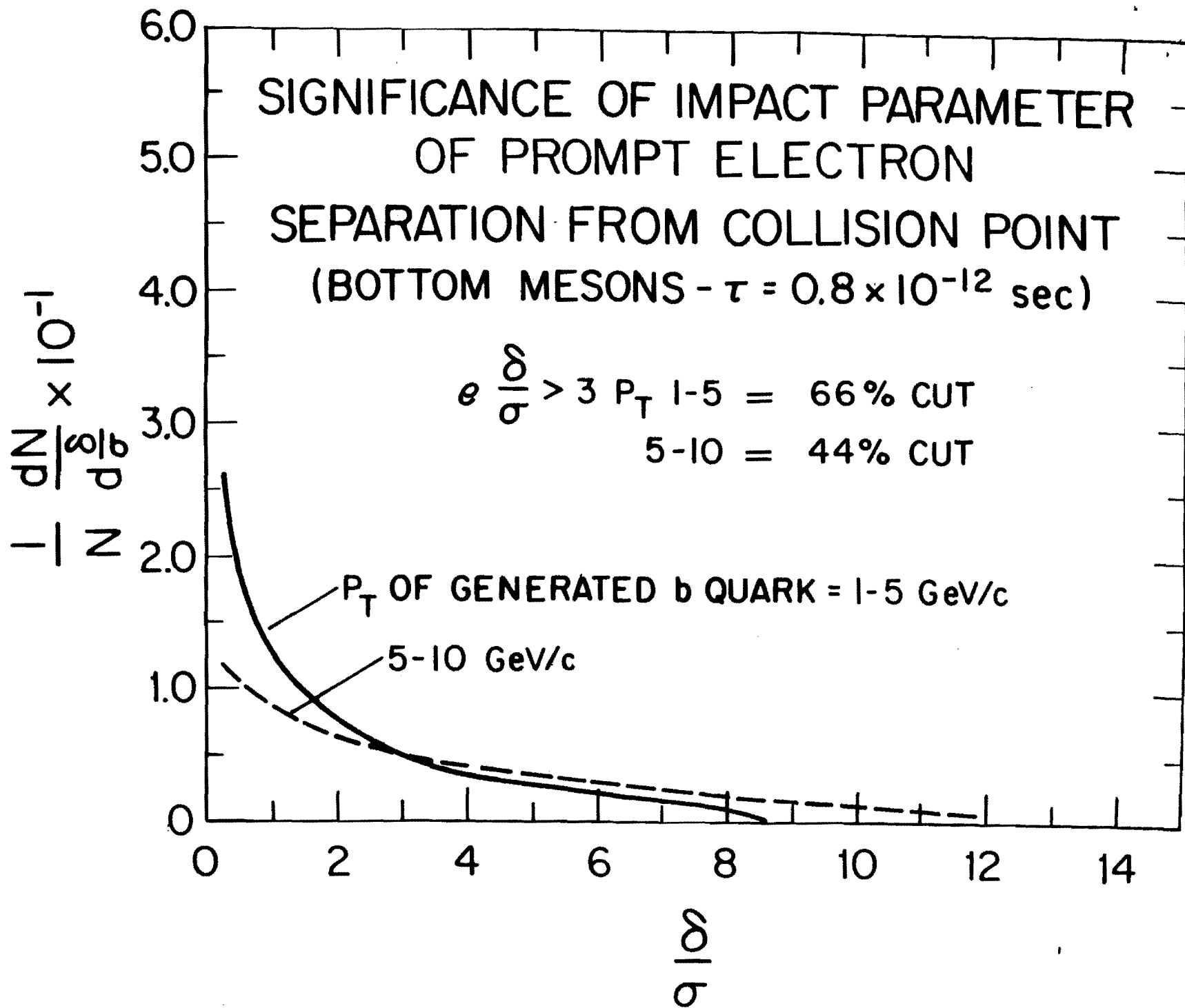


Figure 21

A Appendix

Ideally, a dedicated, new high luminosity region would be requested. However, C0 and E0, the best candidates for being empty in 3-4 years have unique problems. In the case of C0, the tunnel is open only on side, the pit is shallow, and the Tevatron and Main ring abort lines are in the way of any plans for low beta quads. It is estimated that moving the abort would cost several million dollars. The E0 region is where the main ring to Tevatron cross over takes place. Presently there is a quad at $Z = 0$. Even if this one quad could be replaced by 4 further back in Z, the beam pipe would still be much too large for a vertex detector. The losses in transferring might be substantial. In addition, there is not a great deal of room for the low beta quads. Lastly, another low beta intersection region would obviously effect the luminosity in B0 and D0, which is not desirable. The laboratory has invested much into D0 and B0. The physics that this experiment wishes to pursue is complimentary to the big detectors. It is assumed in the next 3-4 years that one of the big detectors will undergo a major upgrade.

This experiment is physically small. The experiment is only 3 meters long and 60 cm in radius. Because this experiment fits into the C0 intersection region it is our plan to take a modest amount of data, prove it is possible to reconstruct bottom in the Tevatron environment and then move to a high luminosity region. It is our suggestion that a push pull arrangement be scheduled. This is the fastest, cheapest method of attaining the goal of several billion bottom events on tape.

B Appendix

The progress in using silicon detectors in high energy physics has been remarkable in the last few years. Perhaps the largest success to date is E-691 at Fermilab. The need for silicon in the colliding beam environment is driven by the desire for high resolution and excellent two track separation. The progress in building electronics to read out 40,000 densely packed channels has also been tremendous. The development of low power, low noise amplifiers on chips will soon be here.

This experiment has been interested in the alternate approach of reading out the detector with CCD's. This has been suggested by several people, such as E. Heijne. Much work has taken place at Triumf Laboratory in Canada on Gallium Arsenide CCD's. GaAs has the property that its electron mobility is about six times that of

silicon and that it is much less sensitive to radiation effects. Triumf would like to collaborate on the electronics R&D ideas surrounding the buffering schematic.

Presently we are setting up to test a silicon strip detector with 500 MHz GaAs CCD's. A number of issues need to be addressed, such as charge injection into the CCD bucket, efficiency at slow clocking speeds, signal to noise etc. In addition, a GaAs strip detector with the CCD integrated onto the same wafer is being discussed. The noise properties of this detector may be very good. The properties of GaAs make it an ideal candidate for the high rate, high radiation environment of the upgraded Tevatron. Since this technology seems to easily meet the present design specifications of 200 nsec crossings, the flexibility of using this for even higher crossing rates seems fairly easy. The feasibility of using GaAs for the buffering can be tested in about 6-8 months. The actual processing R&D should take place at the same time. A working system prototype could be produced on about the same time scale. As part of our overall program of prototyping we intend to test the integrated silicon based preamplifiers presently available. This would allow us to determine the best readout system for this experiment.

Index of Figures

1. (a) View of detector, (b) C0 Hall endview, (c) C0 Hall sideview.
2. B meson p_t distribution at 2 TeV. $\frac{1}{\sigma} \frac{d\sigma}{dp_t}$ vs p_t .
3. Prompt electron from bottom generated between 1-10 GeV/c p_t .
4. Contour plot in $S_2 - S_3$ plane.
5. Box diagram contribution to ϵ_m .
6. Top mass versus bottom lifetime (as function of B parameters).
7. K momentum vs rapidity. $B \rightarrow D0$.
8. Acceptance plots, forward vs 4π design.
9. (a) Track confusion - central region, (b) forward region.
10. (a) Beam pipe and silicon comb structure, (b) view of comb section annulus.
11. Radial drift cell.
12. Velocity versus E/p for D.M.E.
13. Front-end electronics for the radial drift chamber.
14. Forward planar radial drift chambers.
15. Folded cascode schematic
16. Lateral shower sizes in Si/W.
17. (a) Number of tracks above 1 GeV/c P_t in minimum bias events, (b) Sum charged track P_t in minimum bias events, (c) Sum charged track P_t bottom P_t 5 - 10 GeV/c.
18. Block diagram for CDF track processor.
19. Buffering schematic using CCD's.

20. Prompt electron impact parameter in $r - \phi$ plane for b quark generated between 1-5 Gev/c and 5-10 Gev/c.
21. Significance of impact parameter of prompt electron separation from collision point.

References

• Mixing

- A. Ali and C. Jarlskog, Phys. Lett. 44 B (1984) 226.
- A. Ali and F. Barreiro, Z Phys. C. Particles and Fields 30 (1986) 635-642.
- M. Kobayashi and T. Maskawa, Prog. Theor. Phys. 49 (1973) 652.
- F. Paige and S. Protopopescu, A Monte Carlo Event Generator Isajet 5.24, BNL.

• CP

- D. Du, I. Dunietz, D. Wu, A Systematic Study of Large CP Violations in Neutral Beauty Mesons. U. of Chicago, preprint.
- L. Wolfenstein, Present Status of CP Violation, to be published in Annual Review of Nuclear and Particle Science.
- J. S. Hagelin, Nuclear Physics B193 (1981) 123-149.
- A. Pais and S. B. Treiman, Phys. Rev. D. Vol. 12 No. 9 (1975) 2744.
- G. Ecker and W. Grimus, Z. Phys. C. Particles and Fields 30,
- N. Deshpande, Rare Decays of B Mesons, OITS-321.
- B. Stech, Quark Masses, Charged Current Mixing Angles and CP- Violation, TH. 3655 – CERN (1983).
- F. J. Gilman and J. S. Hagelin, Improved Bounds on Some Weak Amplitudes from the b Lifetime, SLAC Pub-3226 (1983).
- Ling-Lie Chau, Physics Reports, Vol. 95, No. 1. April (1983).
- I. I. Bigi, A. I. Sanda, Phys. Rev. D 29, No. 7 (1984).
- I. I. Bigi, CP Violation in B&D Decays, SLAC Pub-4001.
- A. Bean, Limits on $B^0\bar{B}^0$ Mixing and τ_B^0/τ_B^\pm , CLEO-86-11.
- P. Langacker, CP Non-conservation, Invited Talk at the Aspen Winter Conference Series, Aspen, Colorado, 1985.
- A. Ali, Heavy Flavour Production and Decays, CERN.

- $b \rightarrow u$

- A. Chen *et al.*, Phys. Rev. Lett 52 (1984) 1084.
- P. Ginsparg, S. L. Glashow, M. B. Wise, Phys. Rev. Lett 50 (1983) 1415.
- A. Soni, Implications of Non-spectator B Meson Decays, UCLA/83/TEP/24.
- A. Buras, W. Slominski, and H. Steger, B Meson Decay, CP Violation, Mixing Angles, and the Top Quark Mass, MPI-PAE/PTH 77/83.
- B. Grinstein, M. B. Wise and N. Isgur, Phys. Rev. Lett. 56 (1986) 298.

- References

- Design Report for the Fermilab Collider Detector Facility (CDF) August 1981.
- The D0 Experiment, Design Report Nov. 1984.
- Fermilab Proposal 728, D. Green *et al.*
- SLD Design Report, May 1984.
- ALEPH Collaboration, Technical Report 1983.
- Proposal for Mac Detector At PEP, PEP 6 1976.
- Proposal for Mark II at SLAC, April 1983.
- Opal Status Report, Sept. 1984.
- Zeus, A Detector for Hera, Letter of Intent.
- Progress Report on the Upgrade of the CLEO Detector, Dec. 12, 1983.
- Ph. D. Thesis, R. Schindler, Stanford, Univ. 1979.
- R. L. Gluckstern, NIM 24 (1963) 381-389.
- Ph.D. Thesis, M. Nelson, Oct. 1983, LBL-16724.
- G. Barbiellini *et al.*, NIM A235 (1985) 55-60.
- P. Rancoita and A. Seidman NIM 226 (1984) 369-372.
- G. Barbiellini *et al.*, NIM A236 (1985) 316-320.
- F. Lemeilleu, Rancoita, Seidman, IEEE, Vol. NS-34, No. 1, Feb. 1987.
- Linear-Collider $B\bar{B}$ Factory Conceptual Design Workshop, UCLA Jan. 1987.

784
1/27/89

Proposal for Research & Development: Vertexing, Tracking, and Data Acquisition for the Bottom Collider Detector

H. Castro, B. Gomez, F. Rivera, J.-C. Sanabria, *Universidad de los Andes*
P. Yager, *University of California, Davis*
E. Barsotti, M. Bowden, S. Childress, P. Lebrun, J. Morfin, L.A. Roberts, R. Stefanski,
L. Stutte, C. Swoboda, *Fermilab*
P. Avery, J. Yelton, *University of Florida*
K. Lau, *University of Houston*
R. Burnstein, H. Rubin, *Illinois Institute of Technology*
E. McCliment, Y. Onel, *University of Iowa*
G. Alverson, W. Faissler, D. Garelick, M. Glaubman, I. Leedom, S. Reucroft, D. Kaplan,
Northeastern University
S. E. Willis, *Northern Illinois University*
S. Fredricksen, N. W. Reay, C. Rush, R. A. Sidwell, N. Stanton,
Ohio State University
G. R. Kalbfleisch, P. Skubic, J. Snow, *University of Oklahoma*
N. S. Lockyer, R. Van Berg, *University of Pennsylvania*
D. Judd, D. Wagoner, *Prairie View A&M University*
D. R. Marlow, K. T. McDonald, M.V. Purohit, *Princeton University*
A. Lopez, *Universidad de Puerto Rico*
B. Hoeneisen, *Universidad San Francisco de Quito*
S. Dhawan, P. E. Karchin, W. Ross, A. J. Slaughter, *Yale University*

(January 2, 1989)

Abstract

We propose a program of research and development into the detector systems needed for a B -physics experiment at the Fermilab $p\bar{p}$ Collider. The initial emphasis is on the critical issues of vertexing, tracking, and data acquisition in the high-multiplicity, high-rate collider environment. R&D for the particle-identification systems (RICH counters, TRD's, and EM calorimeter) will be covered in a subsequent proposal. To help focus our efforts in a timely manner, we propose the first phase of the R&D should culminate in a system test at the C0 collider intersect during the 1990-1991 run: a small fraction of the eventual vertex detector would be used to demonstrate that secondary-decay vertices can be found at a hadron collider. The proposed budget for the R&D program is \$800k in 1989, \$1.5M in 1990, and \$1.6M in 1991.

Contents

1	Introduction	1
2	Issues for Research and Development	2
2.1	Dipole Magnet	2
2.2	Silicon Vertex Detector	3
2.3	Straw-Tube Tracking System	6
2.4	Ring Imaging Čerenkov Counters	7
2.5	Transition Radiation Detectors	8
2.6	Electromagnetic Calorimeter	9
2.7	Signal-Processing Architecture	10
2.8	Fast Trigger	11
2.9	Front-End Electronics	12
2.9.1	Silicon Strip Front-End Electronics	12
2.9.2	Straw-Tube Electronics	15
2.9.3	RICH-Counter and TRD Electronics	15
2.9.4	Electromagnetic Calorimeter	16
2.10	Data-Acquisition System	17
2.10.1	Local Buffers and Transmitters	17
2.10.2	Barrel-Shifting Event-Builder Switch	17
2.10.3	Numeric Processors and Archival Storage	19
2.11	Accelerator Physics Issues	20
2.11.1	Luminosity	20
2.11.2	Beam Pipe	20
2.11.3	Length of the Interaction Region	20
2.11.4	Bunch Crossing Rate	21
2.11.5	Beam Halo	21
2.11.6	Compensation for the Dipole Field	21
2.11.7	The Detector Hall and Support Facilities	21
2.11.8	System Test at the C0 Intersect	22
3	Research & Development Program	24
3.1	Silicon Vertex Detector	24
3.1.1	Silicon: Mechanical & Electrical Tasks - Phase I	24
3.1.2	Silicon: Costs - Phase I	25
3.1.3	Silicon: Mechanical & Electrical Tasks - Phase II	26
3.1.4	Silicon: Costs - Phase II	27
3.1.5	Silicon: Mechanical & Electrical Tasks - Phase III	27
3.1.6	Silicon: Costs - Phase III	28
3.2	Tracking System	28
3.2.1	Tracking: Mechanical & Electrical Tasks - Phase I	28
3.2.2	Tracking: Costs - Phase I	30
3.2.3	Tracking: Mechanical & Electrical Tasks - Phase II	30

3.2.4	Tracking: Costs - Phase II	31
3.2.5	Tracking: Production R&D - Phase III	32
3.2.6	Tracking: Costs - Phase III	32
3.3	Data-Acquisition System	33
3.3.1	Data Acquisition: Tasks - Phase I	33
3.3.2	Data Acquisition: Costs - Phase I	33
3.3.3	Data Acquisition: Tasks - Phase II	33
3.3.4	Data Acquisition: Costs - Phase II	33
3.3.5	Data Acquisition: Tasks - Phase III	34
3.3.6	Data Acquisition: Costs - Phase III	34
4	Cost Summary	35
5	References	36

List of Figures

1	Detector Overview	2
2	Silicon Vertex Detector	4
3	Model of the Silicon Detector Assembly	5
4	Straw-Tube System	7
5	Signal-Processing Architecture	10
6	Block Diagram of the BVX Readout Chip	13
7	Bonding of Readout Chips to Silicon Detectors	14
8	Block Diagram of Straw-Tube Readout Chip Set	16
9	Local Buffers and Transmitters	18
10	A Simple Barrel Switch	19
11	16-Channel Demonstration Switch	20
12	Collision Hall	22
13	The C0 Intersect	23

List of Tables

1	Momenta Covered in the RICH Counter	8
2	R&D Cost Summary	35

1 Introduction

We have recently submitted a Letter of Intent^[1] to inaugurate a study of B physics at the Tevatron collider with the goal of observing the strongest signals for CP violation in the $B-\bar{B}$ system. This experiment combines a rich physics program for the 1990's with the opportunity for development of detector technology needed in the SSC era. The program is ambitious and is not a direct extension of any existing experiment. We propose here to begin research and development of several critical detector systems as a means of dedicating our efforts towards the B -physics program prior to the approval of the full experiment.

One $B-\bar{B}$ pair is produced in every 1000 interactions at the Tevatron collider,^[2,3] while each interaction produces about 60 'background' particles. To extract the B mesons from this background we will employ two techniques: reconstruction of a secondary decay vertex for the B 's (whose lifetime, $c\tau$, is $360 \mu\text{m}$ ^[4]), and reconstruction of the invariant mass of the products of B decay into all-charged final states. In recent years, the development of silicon vertex detectors has permitted hadronic fixed-target experiments to compete favorably with e^+e^- colliders in the study of charmed mesons. We propose to demonstrate that silicon vertex detectors are also appropriate for a hadron collider.

CP violation is expected to manifest itself prominently only in rare ($\Gamma \sim 10^{-5}$) decay modes of the B mesons; some 10^8 reconstructible B 's will be needed to establish the effect clearly.^[5] Hence the experiment must be performed with a reasonably high collision rate, and we adopt $\mathcal{L} = 6 \times 10^{31} \text{ cm}^{-2}\text{sec}^{-1}$ as the detector-design luminosity. This corresponds to an event rate of 2.5 MHz, and requires the experiment to have a very high rate data-acquisition system by present standards. We propose to develop a data-acquisition architecture based around a 'barrel switch' that can build 10^5 complete events per second, which events are then processed in a large 'farm' of numeric processors before archival storage of at most 10^3 events per second.

The issues of vertex detection and data acquisition are the most critical for B physics at a hadron collider, and are emphasized in the present R&D proposal. A discussion of the technical issues to be studied is given in section 2, which includes a number of secondary items to be covered by the present proposal, as well as important items beyond the scope of the initial effort. Schedules and costs are presented in section 3, with the rough scenario that 1989 is devoted primarily to bench tests with a budget of \$0.8M, leading to tests of individual devices in an external beam in 1990 with a budget of \$1.5M, followed by a system test in 1991 at the C0 intersect with a budget of \$1.6M.

2 Issues for Research and Development

The current vision of the Bottom Collider Detector is shown in fig. 1. The detector is comprised of 5 detector systems, plus the electronics for data acquisition. In this section we outline the technical issues related to these systems that require study, as well as several issues of the impact of the experiment on the accelerator operation.

While some discussion is given of R&D for the particle-identification systems (the RICH counters, the TRD's, and the EM calorimeter), work on this is not part of the initial proposal detailed in section 3. Our plans in this area should become much more well-defined following the upcoming Symposium on Particle Identification at High Luminosity Hadron Colliders, organized by J. Morfin and to be held at Fermilab on April 5-7, 1989.

The present detector design is based on the assumption that the Tevatron collider will operate with 44 bunches with a spacing of 21 rf buckets, so the time between bunch crossings is 400 nsec.

Bottom Collider Detector

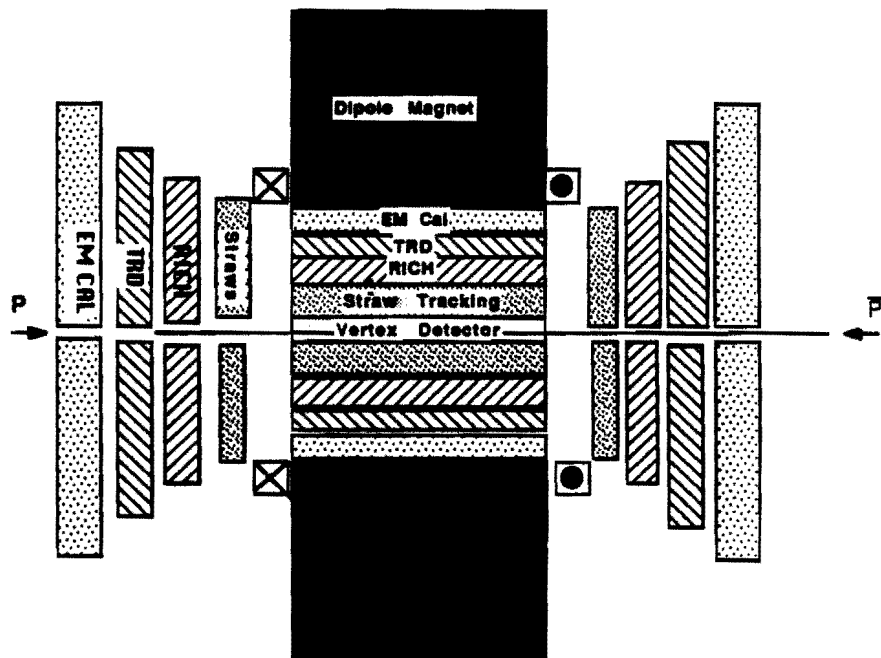


Figure 1: Overview of the Bottom Collider Detector.

2.1 Dipole Magnet

Reconstruction of B -decays requires magnetic analysis. The kinematics of B production and decay at the Tevatron collider indicate the need for coverage for particles primarily

with $P_T < 5$ GeV/c and pseudorapidity $-4 < \eta < 4$ (lab angles $2^\circ < \theta < 178^\circ$). A dipole magnet with field transverse to the colliding beams is the best configuration, and provides good accuracy for high-momentum tracks in the forward and backward directions, at the expense of a small loss in useful solid angle around the direction of the magnetic field. This 'dead' region will be useful for cable paths out from the interior of the detector.

The magnet should have a field integral of $\int Bdl \approx 3$ Tesla-m out from the interaction point along the beam direction, and an integral of 0.6 Tesla-m outwards transversely to the beams. The central-detector systems should be entirely within the magnet (there is no hadron calorimeter), while in the forward/backward directions the particle-identification systems can be outside the field volume.

A magnet with circular pole tips (such as a cyclotron magnet) meets these requirements, while providing a field with circular symmetry to simplify the track-finding algorithm. Such a magnet is relatively open in both the forward and sideways directions, permitting great flexibility in configuring the detectors.

Design studies for such a magnet have been initiated at Fermilab by R. Wands and A. Wehmann, and should be continued. A magnet with pole tips 4 m in diameter and with a 4-m gap would weigh 2500 tons. With a central field of about 1 Tesla the stored energy is 100 mJoule. Superconducting coils are needed to keep the operational cost down, and represent the major design issue. A scenario to recycle the Livermore Magnetic Fusion Test Facility coils could be pursued, but an engineering study is needed to determine whether this option would be cost effective.

2.2 Silicon Vertex Detector

At a hadron collider, the intersection region is typically tens of centimeters long, and tracks of interest emanate in all directions from this line source. Thus the geometry of tracking is much more complicated than in a fixed-target experiment, where most tracks of interest have near-normal incidence on detector planes in the forward direction. Further, to obtain good reliability for finding secondary vertices, the vertex detector must provide all three coordinates of each intercept of a track with a detector plane. In the future this may be best accomplished with pixel detectors, but at present we are exploring the use of silicon strip detectors each with two strip orientations.

Because the collider intersection region is extended, the only practical arrangements of silicon detector planes are those in which some particles must be observed at angles up to 45° incidence. This leads to mechanical and electronic specifications somewhat beyond presently achieved values. The present proposal is to develop the technology to meet these specifications.

Silicon detectors have reduced sensitivity for tracks with large angles of incidence. We currently plan to use silicon strip detectors with $50\text{-}\mu\text{m}$ strip width, $200\text{-}\mu\text{m}$ thickness, and double-sided readout (a.c. coupled). A minimum-ionizing particle creates 80 electron-hole pairs per μm of silicon traversed, so the signal is 16,000 electrons at normal incidence, 5600 electrons per strip at 45° incidence, and only 4000 electrons at grazing incidence. We are setting a goal of an r.m.s. noise level of 600 electrons in the preamplifier, so that tracks

of less than 45° incidence will have better than 9:1 signal-to-noise. The preamplifiers are to be implemented in VLSI technology and bonded directly to the silicon detectors. The R&D program to produce such amplifiers is already underway, and is elaborated upon in section 2.9 below.

The mechanical configuration of the silicon planes is sketched in fig. 2. Tracks with angles less than 45° to the beams are to be observed in detectors oriented perpendicular to the beams, which are called **disks**. Tracks with angles between 45° and 135° to the beams are to be observed in detectors arranged in **barrels** around the beams.

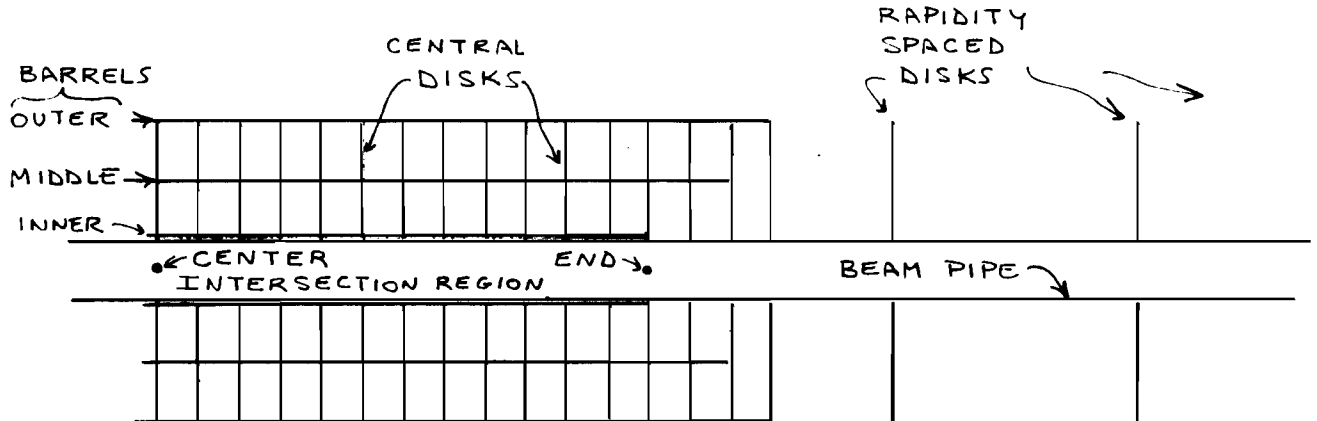


Figure 2: A section through the silicon vertex detector including the beam axis. In this view the disks are vertical and the barrels are horizontal.

If the intersection region were a point, there would be no overlap in the solid angle covered by the **disks** and **barrels**. But for a finite interaction length these two detector types must be interspersed, leading to significant mechanical complexity, especially for the cooling of the preamplifiers mounted on the silicon detectors.

In principle, each particle might pass through so many silicon detectors that the entire task of tracking could be accomplished with the resulting signals (although multiple scattering in the silicon would limit the accuracy). However, the cost of this is deemed prohibitive at present, and we plan for a configuration in which each particle penetrates at least 3 silicon detectors (each providing an x - y - z space point) at an angle of incidence less

than 45° . Even so the number of silicon strips is roughly $2 \times 10^5 + (10^6 \times \text{interaction length in meters})$. The task of pattern recognition of the tracks must be accomplished in the tracking system described in the next section; the silicon detectors provided an accurate measurement of the track segments in the vicinity of the beams.

Double-sided silicon detectors only $200\text{-}\mu\text{m}$ thick are used to reduce the multiple scattering in the detectors. The barrel detectors intermingle with the central disks to form a closed, layered structure. Penetrations must be provided for signal readout, and for cooling of the preamplifiers. This leads to a nontrivial mechanical structure which requires immediate study.

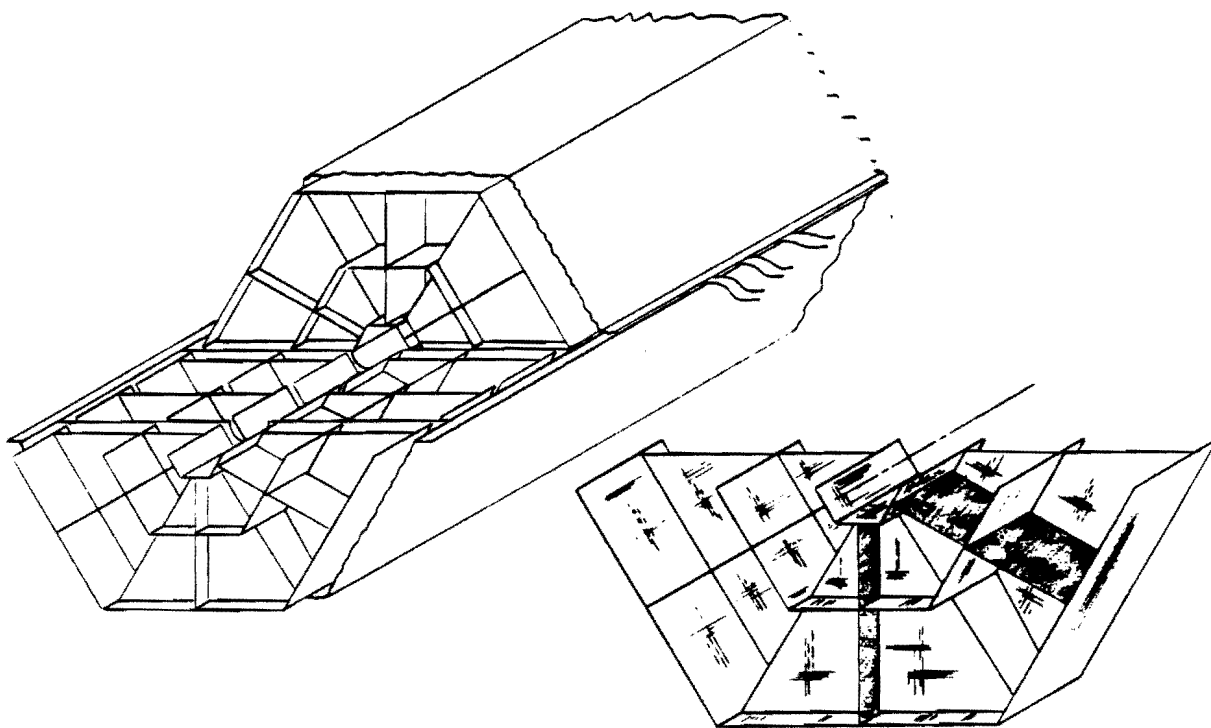


Figure 3: Sketch of a model built to study the assembly of the silicon vertex detector.

Two sets of models have been built to help characterize a suitable arrangement of the detectors into a largely self-supporting structure. These first steps must now be followed by more realistic models, eventually made of silicon, which include heat sources simulating the anticipated load of 2 mWatt per strip (about 2000 Watt for the whole silicon vertex detector).

If the detector is to be gas cooled a flow of order 100 cfm is needed, which flow must be channeled into the inaccessible interior of the detector without inducing vibrations. A scheme in which the disks of the central silicon detector are only partially implemented in azimuth is under study. An alternative scheme involving local cooling of the preamplifiers

by liquid in small tubes is also under consideration.

The individual silicon detectors will be assembled into the overall structure via small channels of beryllium or kevlar, machined to a few μm accuracy, and glued to the silicon at a minimum number of points. The detectors may need to be cradled in an exterior trough to counteract sagging over its 1-m length, and to provide means of alignment of the vertex detector with the exterior tracking system. Figure 3 shows a preliminary conception of the assembly that was the basis for one of the models, and which revealed the need for continued evolution of the design.

The silicon vertex detector will be operated in the 1-Tesla dipole magnetic field. The effect of the Lorentz force on the drift of the signal electrons must be characterized for each of the several orientations of strips relative to the magnetic field.

2.3 Straw-Tube Tracking System

The outer tracking system must reconstruct charged-particle tracks unambiguously in three-dimensional space and extrapolate them into the silicon vertex detector, which functions as a vernier. The tracking system must measure the particles' momenta to $\pm 1\%$ in the dipole field of about 1 Tesla, and cannot have massive support structures such as end plates that would interfere with the particle identification systems which surround it. The tracking system should be configured so that a fast measure of the particles' P_T could be obtained for triggering.

The requirements of low-mass devices with high spatial resolution seem well met with straw-tube technology. A possible layout of some 2×10^6 pressurized straws is shown in fig. 4. The tubes are configured in 'superlayer' modules comprised of 8 layers of tubes each. Each track should pass through at least 8 superlayers, yielding a minimum of 64 measurements per track. With a tube diameter of 3 mm and a gas pressure of 4 atmospheres, a spatial resolution of 50 μm per hit should be achieved. To minimize multiple scattering in the walls of the tubes it is advantageous to use tubes of only 30- μm thickness, half of that achieved to date.

The straw-tube systems will bear the primary burden of pattern recognition for particle tracks. Further study is needed to confirm that our configuration of the straws has sufficient stereo-matching capability. We are exploring the possibility that 'neural-net' hardware processors might be developed which associate vector track segments with the patterns in each superlayer for use in the trigger. The front-end electronics for the straw tubes are relatively modest extrapolations of present designs, as discussed more in section 2.9.2 below.

A hardware R&D program for straw tubes should be initiated in the near future. We must determine whether thin-walled straws can be manufactured, and determine their mechanical stability under pressurized operation. Low-mass end plug must be developed with gas and electrical feed throughs. Spacers may need to be inserted into the longest straws, whose length might be 2 m. The effect of high radiation dose on the chamber gas must be studied along with the more usual aspects of optimizing the gas mixture. Assembly and alignment schemes are to be specified and tested. A lengthy scenario for

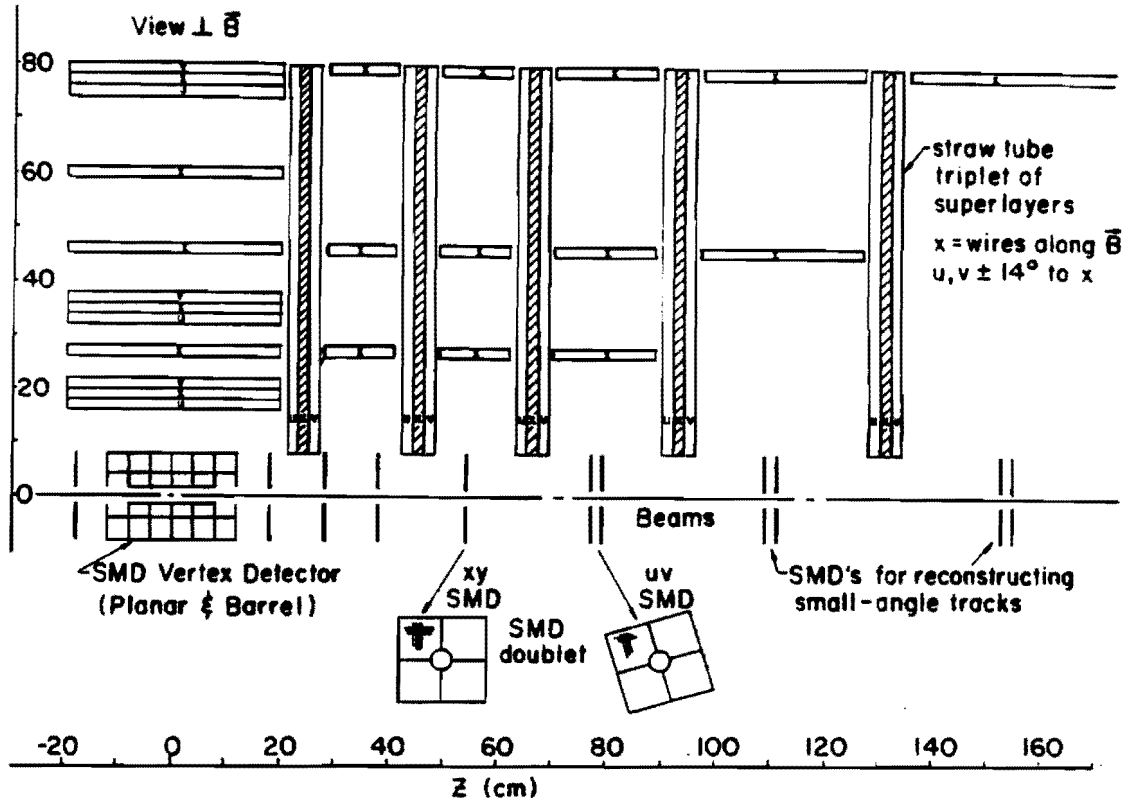


Figure 4: Plan view through the median plane of one quadrant of the tracking system, showing the configuration of the straw-tube 'superlayers' and the silicon strip detectors. The dipole-magnet field and the wires in the z straws are perpendicular to the page.

straw-tube development has been given by DeSalvo.^[6]

2.4 Ring Imaging Čerenkov Counters

Identification of hadrons in the Bottom Collider Detector will be accomplished primarily with RICH counters, supplemented by a time-of-flight system in the central region. The goal is to provide flavor tagging for all hadrons of transverse momenta less than 5 GeV/c. This could be done with RICH counters with a liquid radiator in the central region, and gas + liquid radiators in the forward/backward directions. The desired ranges of momentum coverage are summarized in table 1.

The space available for the RICH counters permits a thickness of approximately 25 cm for the liquid-radiator counters, and 1 m for the gas-radiator counters. Complete coverage of the momentum ranges given in table 1 would require a position resolution of about 1 mm for detection of the Čerenkov photons. This implies the need for about 10^7 detector pixel elements. Readout electronics suitable for such large-scale implementation are currently being designed at the Rutherford Laboratory.^[7]

	P (GeV/c) at $\gamma_t = 2$	γ at $P = 8$ GeV/c	P (GeV/c) at $\gamma_t = 17$	γ at $P = 120$ GeV/c
π	0.3	56	2.5	840
K	1	16	8.5	240
p	2	8	17	120

Table 1: Ranges of momenta and γ which should be covered by the RICH counters. $\gamma_t = 2$ for liquid C_6F_{14} , and $\gamma_t = 17$ for gaseous C_5F_{12} .

The detector for the UV Čerenkov photons needs R&D. The issue is complicated by the use of a liquid radiator, which absorbs photons of energy greater than 7 eV. These photons are to be detected in a photosensitive gas, such as TMAE, and the ionization electrons observed via the signals induced on cathode pads of a multiwire chamber. The drift velocity for the photoelectron is about 15 nsec/mm, so if the signal width is desired to be, say, at most 200 nsec, the active depth of the photodetector must be only 6 mm. However, the absorption depth for TMAE at room temperature is about 2 cm, so only 30% efficiency could be achieved within the desired time window, unless the TMAE is heated. There is a clear need for a ‘designer molecule’ whose photoionization properties are better matched to the experimental requirements. Some progress in this direction has been recently achieved by Ypsilantis in collaboration with a chemist, Alan Katzrik of the U. of Florida.^[8]

Another problem which must be faced in a collider experiment is the large signals due to charged particles passing through the detector gas. The partial pressure of the photosensitive gas is only a few Torr, so operation at atmospheric pressure is obtained by adding a buffer-gas mixture such as argon-isobutane-methane. About ten times as many electrons are ionized directly by a charged particle as are ionized by the Čerenkov photons. With a high gas gain to observe the Čerenkov signal, there is risk of discharges due to the minimum-ionizing ‘background.’ A possible solution is to operate the photodetector at only a few-Torr pressure, which nearly eliminates the signal from minimum-ionizing particles, and actually improves the gas gain. However, considerable development is needed on the mechanical configuration of a large-area, low-pressure detector.

2.5 Transition Radiation Detectors

While evidence for CP violation in B decays will likely come primarily from measurement of asymmetries in all-charged decay modes, it is important to tag semileptonic modes, $B \rightarrow e\nu X$, as well. The best modes for observation of CP violation are those where the final state f is a CP eigenstate, so the particle/antiparticle character of the parent B cannot be determined from measurement of this decay alone; the second B of the produced $B\bar{B}$ pair must be tagged. This leads to the need for electron identification systems, comprised of TRD’s and electromagnetic calorimeter.

Of all the technologies to be used in the BCD, the TRD's are the most well-developed at present.^[9] However, it will be advantageous to use next-generation thin-sampling detectors,^[10] in which some 30 detectors each 1.5-cm thick yield better pion rejection than the 15-cm-thick devices currently in use. An online rejection of 100:1 against pions should be achievable, presuming some processing of the 30 samples per track.

The BCD requires about 60 m² of TRD's. If the size of the cathode readout pad is taken as 1 cm², there are 6×10^5 pads per layer of TRD. Thus a 30 layer system of this granularity has about 2×10^7 readout elements. While the cost of VLSI electronics in such numbers is not excessive, the question of mechanical costs of mounting these chips on a low-density board must be explored.

2.6 Electromagnetic Calorimeter

The calorimeter functions primarily to aid in electron identification, rather than providing a precision energy measurement. As such, position resolution is more critical. We thus have the option to use a sampling calorimeter (as opposed to total absorption in BGO or lead glass, *etc.*).

The calorimeter should have tower geometry, with three longitudinal samplings per tower. This feature should permit an online rejection factor of several hundred for charged π 's. The transverse size of the towers should be sufficient that the energy measurement is of only a single particle with 99% probability, leading to a tower count of 10^4 given an average multiplicity of 100. A position-sensitive detector will be placed between the first and second layers of each tower to reject overlaps of a charged pion with a photon from π^0 decay. For this a two-track resolution of about 1 cm is desirable.

Of the technologies available for calorimetry, liquid argon appears the most satisfactory in terms of performance, but is cumbersome to implement in a 4π experiment. A warm-liquid system could be advantageous if perfected. A calorimeter with scintillator as the sampling medium is adequate, if the difficulty of an optical readout in a magnetic field can be solved.

A speculative option is to read out the scintillating fibers of a 'spaghetti' calorimeter with to-be-developed devices called 'silicon phototubes.' In these, a small photodiode has a silicon pixel detector as its anode, which is bonded to a low-noise amplifier inside the vacuum. About 300 electrons would be liberated per photoelectron per 1000 volts across the diode. For a small pixel size the noise could be held to perhaps 500 electrons, so with a 3-keV voltage, the noise level is 0.5 photoelectrons. The silicon phototubes might have cathode areas of 1 cm², matched to a 2×2 cm² segment of the spaghetti calorimeter, assuming 25% coverage by area with the scintillating fibers. Because they are photodiodes with a small gap, the silicon phototubes are relatively insensitive to magnetic fields. A possible drawback is that the anode is sensitive to charged particles which pass through it, each such giving a signal equivalent to one photoelectron. It would require a large R&D program in cooperation with an interested vendor, perhaps Burle Industries, to develop the silicon phototube.

2.7 Signal-Processing Architecture

Because the *B* experiment is based on reconstruction of all soft charged tracks, a large amount of data is produced by each event. Each of 60 tracks will be sampled approximately 100 times for a total of about 6000 words per event. A word will typically consist of 4 address bytes and one data byte, for a total of 30,000 bytes per event. The detector is to operate at event rates of up to 2.5 MHz, so the potential data rate is 75 gigabytes/sec.

By utilizing the technology of modern telephone switches we can process this high data rate in 3 levels, as illustrated in fig. 5:

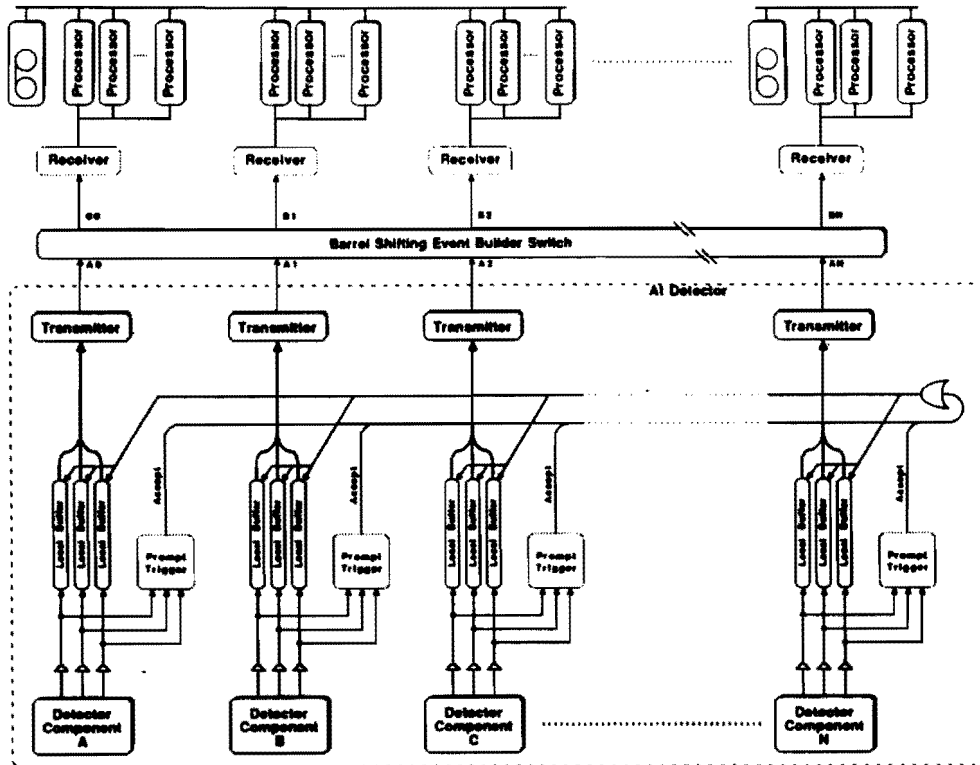


Figure 5: Schematic of the signal-processing architecture.

- A fast trigger reduces the event rate by a factor of 25, for a maximum of 100 kHz of surviving events. The fast trigger is based on analog signal processing; all trigger decisions based on numerical calculations are to be deferred to the second level.
- A 'barrel switch' organizes that data from up to 10^5 events/sec into individual event records, which are fed to a farm of perhaps 10,000 numeric processors. Each processor is about 50 VAX-780 equivalents, and must make a second-level trigger decision in 0.1 sec, with a desired reduction in the event rate of 100.
- The remaining event rate of up to 1 kHz is archived to some storage medium such as video cassette, or perhaps the new technology of 'digital paper.' The archival data

rate is then about 30 Mbytes/sec, which would require 120 present-day Exabyte cassette drives. The archived events would later be analyzed on the processor farm, whose combined processing power is about 0.5 TIPs (0.5×10^{12} instructions per second).

In the next three subsections we discuss issues relating to the fast trigger, the front-end electronics, and the data-acquisition system.

2.8 Fast Trigger

As discussed in our Letter of Intent,^[1] two kinds of fast triggers are under consideration for the Bottom Collider Detector:

- A **topology** trigger which is satisfied whenever n or more tracks in an event have P_T above a cut value. For $n = 1$ the cut might be 3 GeV/c, while for $n = 2$ the cut could be at 2 GeV/c. Either could yield a factor of 25 reduction in the event rate according to preliminary Monte Carlo simulations. This trigger would be based on fast tracking, and could use coarse-grained position information from pad chambers (*i.e.*, the first and last pad layers of the TRD's) as well as signals from the straw-tube tracking system.
 - In addition, the fast-tracking system must have precise ($\sim \pm 1$ cm) z -coordinate information within a few hundred nsec after a collision. This component of the fast trigger would be provided by a scintillating-fiber tracking system located several meters upstream and downstream of the interaction region. One encouraging design consists of 4 identical 9-plane arrays of fibers positioned to cover the rapidity range from 4 to 6. Each detector plane consists of 200 fibers oriented in the nonbend plane.
- An **electron** trigger with a minimum- P_T cut of about 1 GeV/c. Since each event will have about three charged pions with $P_T > 1$ GeV/c, an online pion rejection of greater than 75:1 is needed to reduce the event rate by the desired factor of 25. This should be achievable using signals from the TRD's, and from the longitudinally segmented electromagnetic calorimeter.

Thus the fast trigger will be derived primarily from signals in the outer layers of the detector, but the design should preserve an option to incorporate signals from the inner tracking systems as well. This may be particularly important for rejection of electrons from photon conversions.

Continued study of the trigger scheme is needed, with emphasis in the near term on computer simulations.

2.9 Front-End Electronics

The front-end electronics will be in the form of custom, very-large-scale integrated (VLSI) circuits, permitting low-cost and low-power readout of the large number of detector elements of the Bottom Collider Detector. All of the various chips proposed here are straightforward extrapolations or reconfigurations of presently available devices, although they will necessarily be 'state-of-the-art' devices.

The experience of a number of high-energy-physics groups has shown that such chips can be successfully developed by a small number of people, but that turn-around times with the silicon foundries dictates a time scale of perhaps two years per chip. Resistance to radiation damage is of particular interest to us, and will require additional studies best performed once the chips are electronically operational.

For running of the Bottom Collider Detector at the Tevatron collider we take the bunch crossing time to be 400 nsec (compared to 16 nsec at the SSC). Hence any signals not requiring a fast timing pulse can be shaped to a full width of 400 nsec. This permits the use of low-power CMOS technology for most chips. The notable exception is the preamplifier for the straw tubes, which must use Bipolar technology to provide a time resolution of 0.5 nsec, corresponding to the desired 50- μ m spatial resolution.

While the detector will have a channel count in excess of 10^7 , only about 10^4 channels will be struck during an event of interest. The front-end electronics must include functions to sparsify the data, outputting only addresses and digitized data for the struck channels. Further, the data must be stored at its source until the fast trigger is formed, perhaps as long as 6 μ sec, before passing it on to the data-acquisition system.

The flow of data out of the detector should be on fiber-optic cables whose higher rate capability will minimize the number of physical cables. This requires a class of data-collection chips on the detector which format and buffer the data before transmission off the detector.

The front-end electronics for the various detector systems will be designed with the maximum of commonality. Efforts will begin on chips for the silicon strip detectors. Only the straw-tube chambers will require electronics with considerably different features.

2.9.1 Silicon Strip Front-End Electronics

From the considerations outlined in section 2.2, we have arrived at the following specifications for the front-end chip (designated the BVX) for the silicon strip detectors:

- 1.25- μ m CMOS technology.
- Power consumption: 1 mWatt/channel.
- R.m.s. noise < 600 electrons.
- Signal shaped to 400-nsec full width at base.
- Adjustable discriminator threshold in the range 3000-6000 electrons, with option for a second discriminator threshold.

- On-chip storage of the analog signals for about $6 \mu\text{sec} = 16$ bunch crossings.
- Six-bit ADC for signals above threshold, with digitization beginning only if the fast trigger is satisfied.
- Sparsified readout of the 128 channels which make up a physical BVX chip.
- Individual channel electronics sized for the $50\text{-}\mu\text{m}$ strip pitch of the silicon detectors.
- Radiation hardness to 100 krad, the expected yearly dose at 1 cm from the beam at a luminosity of $10^{31} \text{ cm}^{-2}\text{sec}^{-1}$.

These specifications are slightly beyond those met by the current generation of chips, such as the MPI CAMEX,^[11,12] the LBL SVX^[13] and the RAL MXI.^[14] However, the relatively long bunch crossing time at the Tevatron, 400 nsec, should permit the stringent noise requirement to be met. Also, we plan to use a.c. coupling to the amplifiers, which renders them largely immune to leakage current, and eliminates the need for quadruple-correlated sampling.

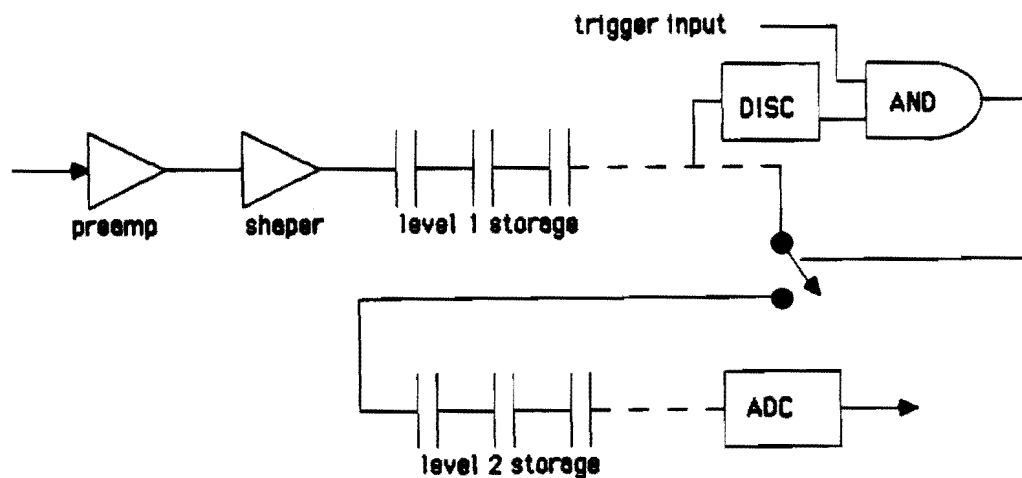


Figure 6: Block diagram of one channel of the BVX readout chip for the silicon strip detectors.

A block diagram of one channel on the BVX chip is shown in fig. 6.

Tracks with angle of incidence greater than 45° present an additional problem for the readout. Such tracks may deposit signals of greater than 4000 electrons into a large number of contiguous strips, called here a cluster. It is not necessary that these signals be processed further, because the silicon is arranged so that all tracks strike at least three detector at angles of incidence less than 45° . However, signals as low as 5600 electrons, due to tracks at exactly 45° incidence, must be kept. Because the r.m.s. noise is a substantial fraction of the difference between 5600 and 4000 electrons, it is dangerous to set a threshold in this region; because of noise fluctuations the cluster of struck strips would be processed as a number of isolated hits, filling the event records with useless data.

It would be preferable if there were an on-chip capability to sense the number of contiguous struck strips above a threshold of, say, 4000 electrons, and suppress the readout of the entire cluster (or entire chip!) if more than 6 contiguous strips were struck.

The BVX chips are to be bonded directly to the silicon wafers, without requiring a dead space near the readout end of the wafer. Figure 7 sketches how this might be accomplished with a tab-bonding technique.

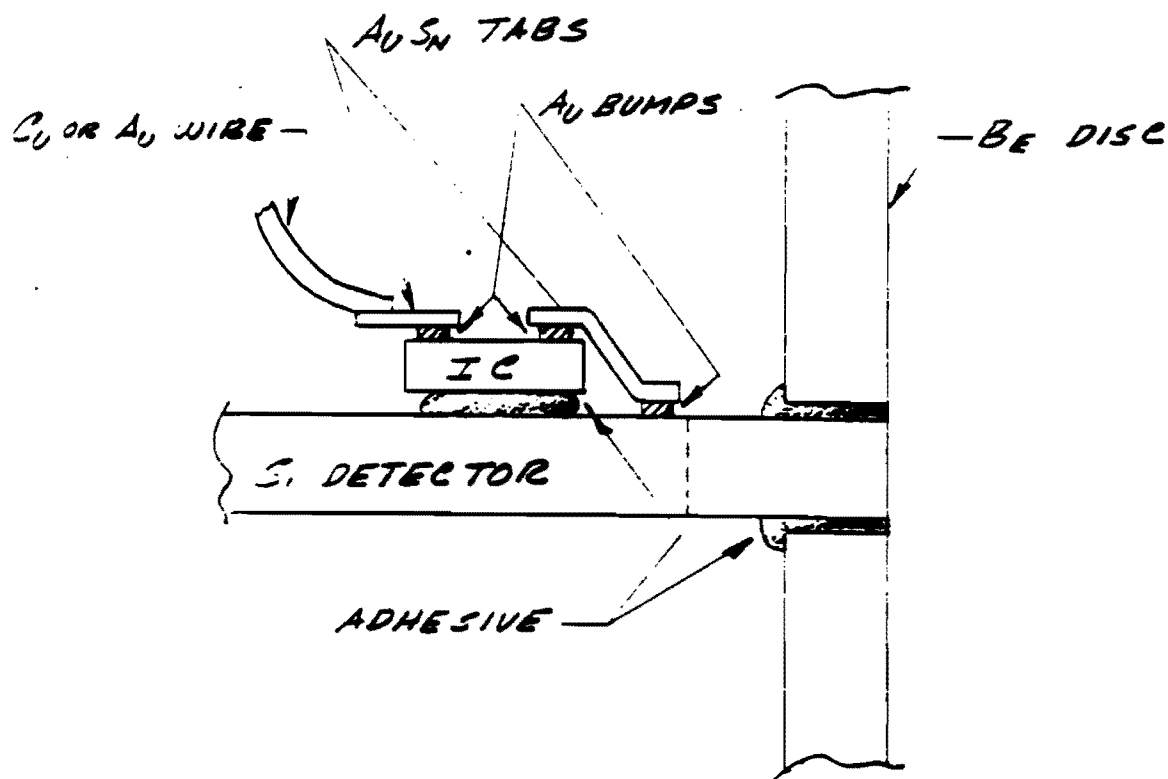


Figure 7: Possible scheme for bonding the BVX readout chips to the silicon strip detectors.

If there are 10^6 silicon strips serviced by the 128-channel BVX chips, then about 10^4 of the latter are required. If separate data lines emerge to the outside world from each BVX chip the cabling problem would be severe. However, the average occupancy of a BVX

chip should be less than one channel per event (if clusters of greater than six strips can be suppressed). It will be advantageous to route the signals from 10 to 100 neighboring BVX chips into a 'data collection' chip, which further buffers the data until the data-acquisition system is ready to receive it. Details of the data-collection architecture need further specification; this architecture should be suitable for collection of signals from all systems of the Bottom Collider Detector.

2.9.2 Straw-Tube Electronics

The high spatial resolution of the straw tubes is obtained by measuring the time of arrival of the first ionization electron. A resolution of $50 \mu\text{m}$ requires a timing accuracy of 0.5 nsec. Hence the preamplifiers for the straw tubes must be fast devices even though the event rate is at most 2.5 MHz. The speed requirement dictates the use of Bipolar technology for the integrated circuits, at the expense of a heat load of about 15 mWatt per channel. Cooling the low density of straw-tube preamps is, however, a straightforward matter. Once the electron-arrival time has been converted to a voltage, the rest of the signal processing (trigger delay and digitization) can be performed in CMOS circuitry very similar to that on the BVX chip

The block diagram of the proposed Bipolar/CMOS chip is shown in fig. 8, which closely follows the so-called TVC chip set developed at U. Penn for the SSC.^[15] The Bipolar amplifier/shaper/discriminator of the TVC could be used directly, and the CMOS analog store could be used but with a slower clock, typically 5-10 MHz.

The system would consist of the Bipolar preamp/shaper/discriminator followed by the CMOS analog-store/ADC/readout-control chip. The Bipolar chip will have four channels and the CMOS chip will have 8 channels. In addition the system would need a data-collection chip (digital CMOS), similar to that for the silicon strip electronics, for every 8-32 front-end chips. Total power costs would be about 20 mW per channel.

A possible arrangement would have a thin printed-circuit board mounted on the ends of a group of 128 straws, with 32 Bipolar chips, 16 CMOS TVC chips, and one data-collection chip, in addition to discharge protection and bypass and coupling capacitors for the straws. The cost would be about \$2-3 for the Bipolar chip/channel, \$1-2 for CMOS, \$0.25 for the data chip and \$0.50 for mounting, for a total of < \$6/channel.

It will be useful to include segment-finding electronics for some of the straw-tube superlayers. This should be possible by adding a CMOS digital-logic chip in parallel to the CMOS TVC chip. Found segments would then be shipped to the trigger system. The increase in power cost should be only about 10% assuming a high level of multiplexing. An intriguing alternative possibility for the segment-finding chip is an analog processor based on 'neural-net' concepts. This option is currently being explored for the Bottom Collider Detector by Bruce Denby.^[16]

2.9.3 RICH-Counter and TRD Electronics

Both the RICH counters and the TRD's will have pad sensors whose signals will be similar in magnitude and shape to the signals from silicon strips. Thus we have the option that

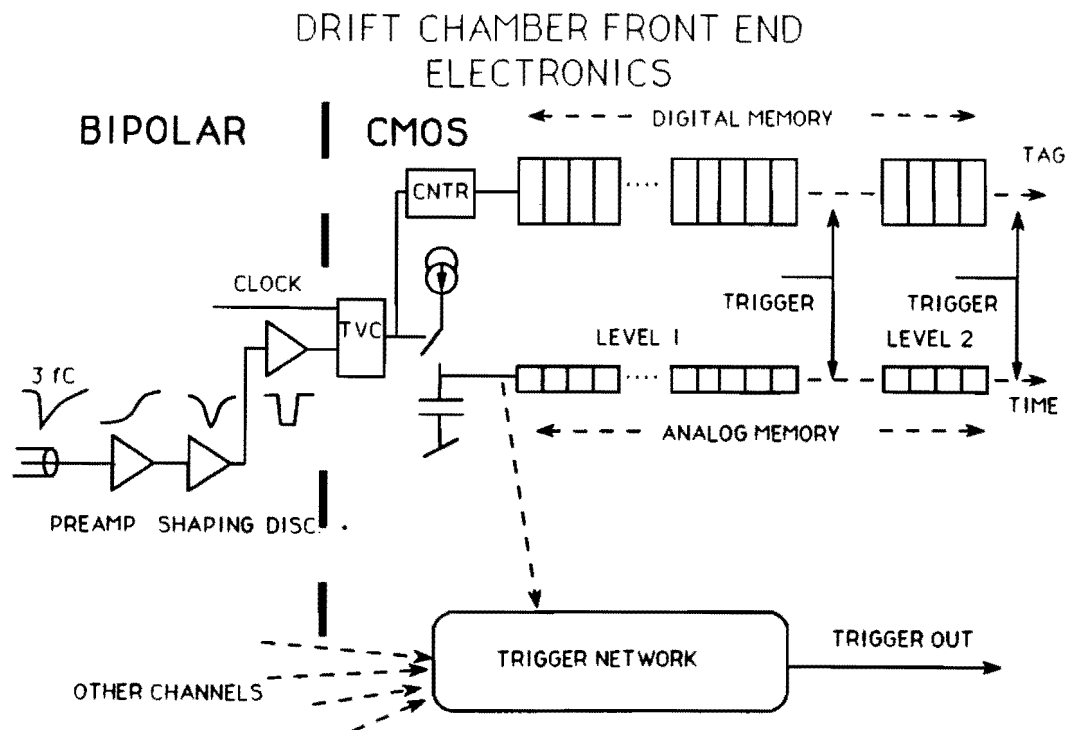


Figure 8: Block Diagram of the Bipolar/CMOS readout chip set for the straw-tubes.

the BVX chips may be used for these devices as well. However, the number of channels in the RICH counters and TRD is greater by at least an order of magnitude compared to the silicon vertex detector, so the major cost of electronics for the entire detector is likely that of the pad readout. Hence the pad readout may deserve a specifically optimized solution.

It should be possible to design pad-readout chips with rate capabilities significantly higher than those required at the Tevatron, but which could be suitable for the SSC. Very recently we have made contact with an electronics group at Rutherford Appleton Laboratory,^[7] who may be interested in a collaboration towards this end.

In any case, the low density, large channel count, and large physical size of the pad readout mandates a large R&D program addressing cost-effective methods of chip mounting and signal routing, in addition to the development of the readout chips themselves.

2.9.4 Electromagnetic Calorimeter

The calorimeter could use a readout system similar to that of the straw tubes in the sense that a Bipolar front end would feed a CMOS delay-and-encode section. However, the calorimeter requires charge measurement over a large dynamic range and may or may not require an accurate time measurement. Thus the Bipolar chip will necessarily require rather more power (for the dynamic range) and the CMOS chip will require more area for storage capacitors (high- and low-charge ranges).

In addition the calorimeter will serve as one of the primary triggering detectors and

must provide fast signals out of the detector to the central triggering system. These signals will require > 40 mW per output, but the trigger outputs will be sums of local channels so that the total power burden is not greatly increased. If a suitable clustering algorithm can be defined and tested, we could ship only cluster-position and -size information to the trigger system, greatly reducing the burden on and increasing the power of the trigger.

We estimate that the total power requirement per channel would be about 30 mW and the cost per channel would rise slightly to $< \$7$. Mounting and cooling is least restrictive in this region and we anticipate no major problems for the calorimeter system.

2.10 Data-Acquisition System

The overall signal-processing architecture for the Bottom Collider Detector has been introduced in section 2.7 and illustrated in fig. 5. The data-acquisition system incorporates three new technologies which require an R&D program:

- Fiber optics for digital-data transmission.
- Barrel-switch event builder.
- Industry-supported numeric processors for the second-level trigger.

The design goal for the data-acquisition system is an input of 10^5 events/sec containing about 5 gigabytes/sec of data, and an output of 1000 events/sec to archival storage. A design to meet this goal has been prepared by the group of Ed Barsotti at Fermilab as part of the present proposal.^[17,18]

2.10.1 Local Buffers and Transmitters

Figure 9 shows a portion of the data-acquisition system between the front-end electronics on the detector and the event-builder switch. The block labeled 'local buffer' resides on the CMOS data collection chips described in section 2.9.1. A fiber-optic link connects the local buffers to a smaller number of transmitters. The latter must organize the data from each event into units, called 'fragments,' whose format is suitable for processing by the event builder switch. A transmitter would receive data from the local buffers in parallel streams at a rate of 1 Mbyte/sec, and send out a serial data stream at a rate of 10 Mbyte/sec. About 512 transmitters will be required to accommodate the expected total data rate of 5 Gbyte/sec.

2.10.2 Barrel-Shifting Event-Builder Switch

The key section of the data path is the event-builder switch. This should organize the 512 event fragments from the transmitters into individual events at a rate of 10^5 events/sec (compared to 10/sec presently achieved in the CDF detector). This can be accomplished via the barrel-shifting technique used in the telephone industry.

A barrel-shifting event-builder switch is an N -input, N -output device with only N possible interconnects at any given moment (in contrast to a crossbar switch that has $N!$

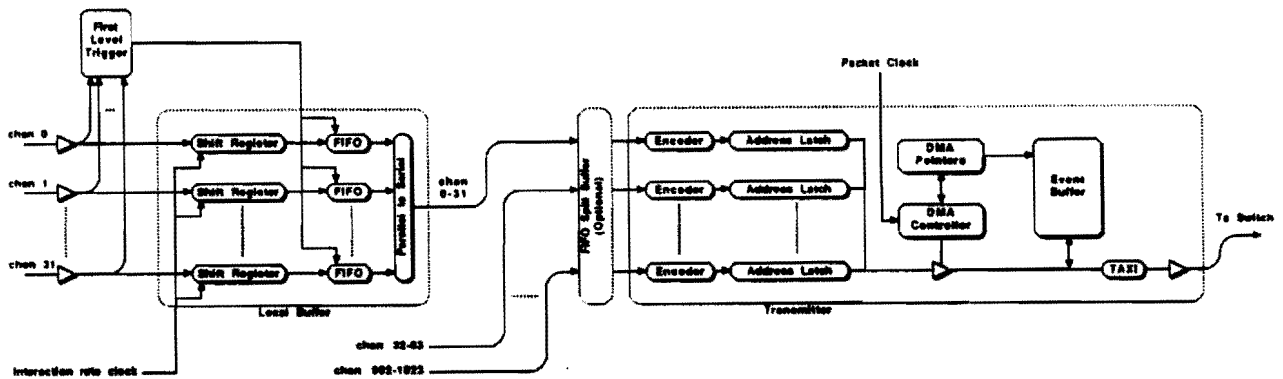


Figure 9: Block diagram of local buffers (data collection chips), 'event-fragment' transmitters, and their fiber-optic interconnections.

interconnections). The pattern of the N interconnections is altered at every cycle of a clock, so after N clock cycles all inputs have been connected to all outputs once. Since there are exactly as many interconnects as inputs, the switch can transmit the full input bandwidth.

To illustrate how the barrel switch organizes data fragments into whole events, consider a simple example in fig. 10. Fixed-length event fragments pass through the system with each input channel delayed by one clock cycle relative to the adjacent channel. With the switch-control word set to 00 (fig. 10a), the first fragment of event 1 (labeled 1A) passes directly through the switch along with three empty fragments. The switch-control word is incremented by one (fig. 10b) and the second fragment of the first event (1B) and the first fragment of the second event (2A) are transmitted; because the pattern of the interconnects has changed, fragment 1B now follows 1A. During the next cycle of the switch (fig. 10c), fragments 1C, 2B, and 3A are transmitted. After one full rotation of the switch control, the system reaches a steady-state condition, shown in figs. 10e and 10f. Parallel event fragments are converted to assembled event streams with no loss of bandwidth.

As a first step in the development of the barrel-shifter technique, a 16-channel demonstration system will be constructed, shown in fig. 11.

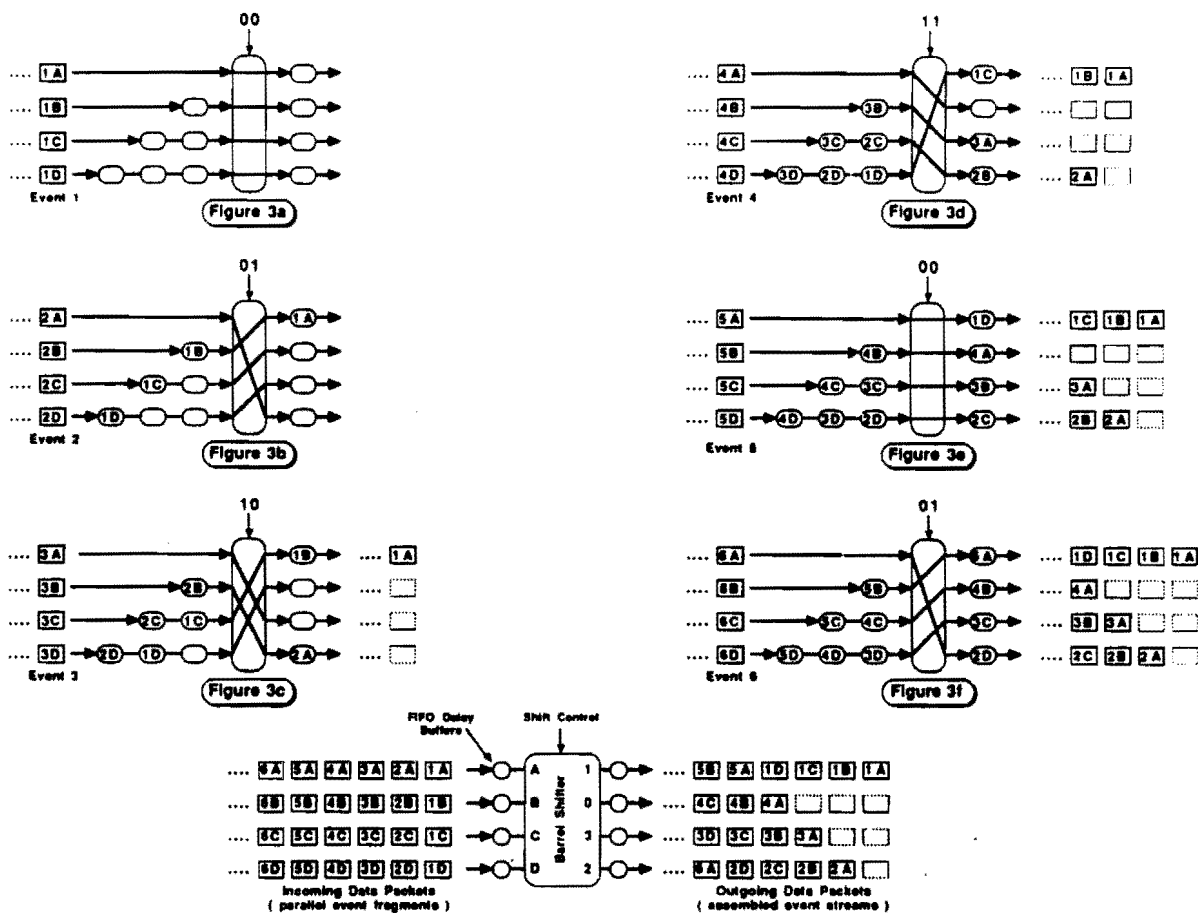


Figure 10: Principle of operation of a 4-input, 4-output barrel-shifting event-builder switch.

2.10.3 Numeric Processors and Archival Storage

The assembled events emerging from the event-builder switch are fed to a farm of numeric processors in which the level-2 trigger calculations are performed. No special-purpose numerical processors will be built; we propose to take maximum advantage of industry support of high-speed processors optimized for numerical calculations. Prototypes of 30-MIP processors will become available in Spring 1989, which we plan to incorporate them in the 16-channel demonstration system.

We anticipate the need for 5000-10000 processors in the eventual configuration of the Bottom Collider Detector. Then each processor would have about 0.1 second to make the level-2 trigger decision, with the goal of a factor of 100 reduction in the event rate.

The total archival data rate is expected to be 1000 events/sec, or 30 Mbyte/sec. This could be handled by an array of 120 Exabyte drives. Options for the use of fewer devices will emerge in the next few years. In 1989 the so-called 'digital paper' devices should become available from Creo.^[19] In this, one terabyte can be stored on a 2400' reel of write-only optical tape, with a data rate of 3 Mbyte/sec. A more virtual device is the Haystack drive, being developed for the radio-astronomy community, in which a magnetic drive with 100 heads should eventually be capable of writing 100 Mbytes/sec.

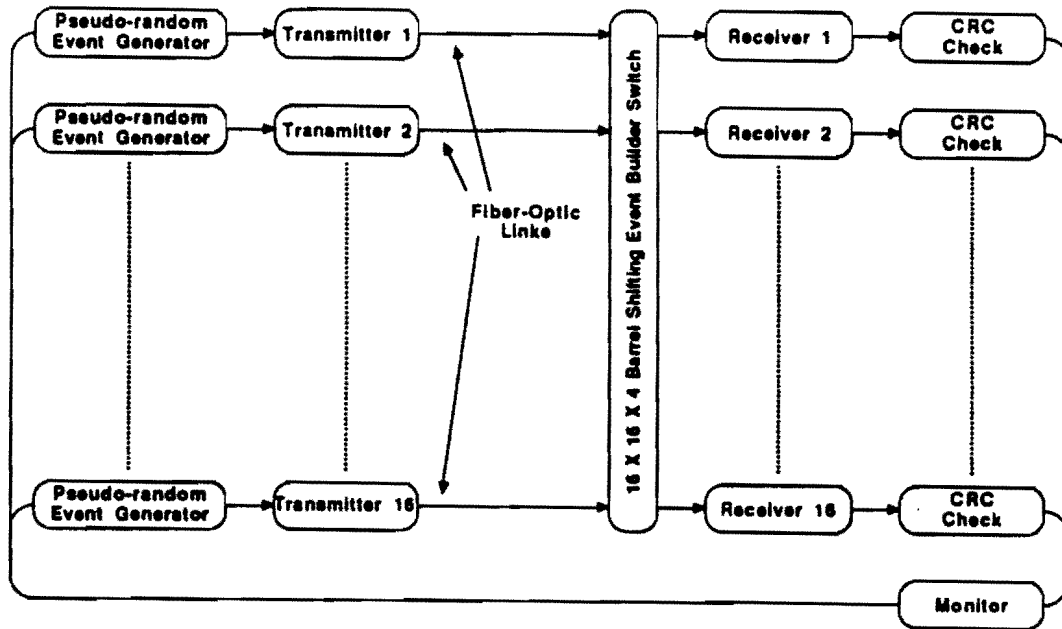


Figure 11: Proposed demonstration of a 16-channel barrel-shifting event-builder switch.

2.11 Accelerator Physics Issues

2.11.1 Luminosity

The window of opportunity for observation of CP violation in the B meson system at the Tevatron collider opens for luminosities above $10^{31} \text{ cm}^{-2}\text{sec}^{-1}$. We strongly support the Tevatron upgrade programs which would make this possible.

2.11.2 Beam Pipe

The resolution of a silicon vertex detector improves when the innermost detector is closer to the beam. We plan to use a beam pipe 1 inch in diameter with walls of 400- μm -thick beryllium.

2.11.3 Length of the Interaction Region

Most of the mechanical complexity of the silicon vertex detector arises because of the finite length of the interaction region which it must cover. We wish to explore the possibility of reducing the luminous region to a σ of 10 cm, down from the value of 35 cm in present running. Following discussions with Dave Finley, this might be accomplished in two ways:

- Reduce the β^* at the intersect with stronger quads. This might be possible because the 1-inch beam pipe would permit a smaller bore for the quads, and the experimental

configuration might permit the quads to be closer than 7.5 m from the intersect. Of course, a lower β^* is also useful in raising the luminosity.

- Add a higher-harmonic rf system to bunch the beams more tightly. This has the bad effect of increasing the intrabeam scattering, leading to a shorter luminosity lifetime. Calculations should be made to judge whether this option can produce a net gain in useful luminosity for a shorter interaction region.

2.11.4 Bunch Crossing Rate

The time between neighboring bunch crossing sets the time scale for all readout electronics. We now assume that this time will be 400 nsec, which is well matched to the stated goal of a luminosity of several times 10^{31} of the $p\text{-}\bar{p}$ upgrade program.

2.11.5 Beam Halo

Halo associated with the beams will contribute to the radiation exposure of the vertex detector and thereby shorten its lifetime. Present data indicate that the silicon detector can survive about 10^5 rads. It is clear that catastrophic beam loss must not occur near the detector. The beam-loss level for abort may need to be lowered compared to present operation.

2.11.6 Compensation for the Dipole Field

The presence of a spectrometer dipole in the Tevatron would alter the beam trajectory unless compensating measures are taken. The scheme that has been chosen for compensation uses two dogleg bends, one at each end of the straight section and each 20 feet from the center of the interaction region, just downstream of the low-beta quads. The two magnets are both of opposite polarity relative to the spectrometer dipole, and run in series with it (that is, the currents run up together). The spectrometer dipole and compensating magnets are energized only after coasting beam has been established. The beams at the crossing region then move laterally a few mm as the magnets are energized.

2.11.7 The Detector Hall and Support Facilities

The Detector Hall required for this facility will be comparable in size to that at D0. The detector itself will fill about one half the space available in a straight section at the Tevatron. The compensating dipoles are placed at the outer ends of the straight section. The need for electron detection, calorimetry and particle identification will require the use of special gasses and liquids. The detector may use ethane, TMAE, or TEA. Additional cryogenic support may be necessary to service the main dipole magnet. The detector will require a substantial signal-processing area. The Detector Building must also provide for a control room, office and technician space and shop support.

An initial design of a new collision hall is shown in fig. 12, as prepared by Nestander's Engineering Services Group.

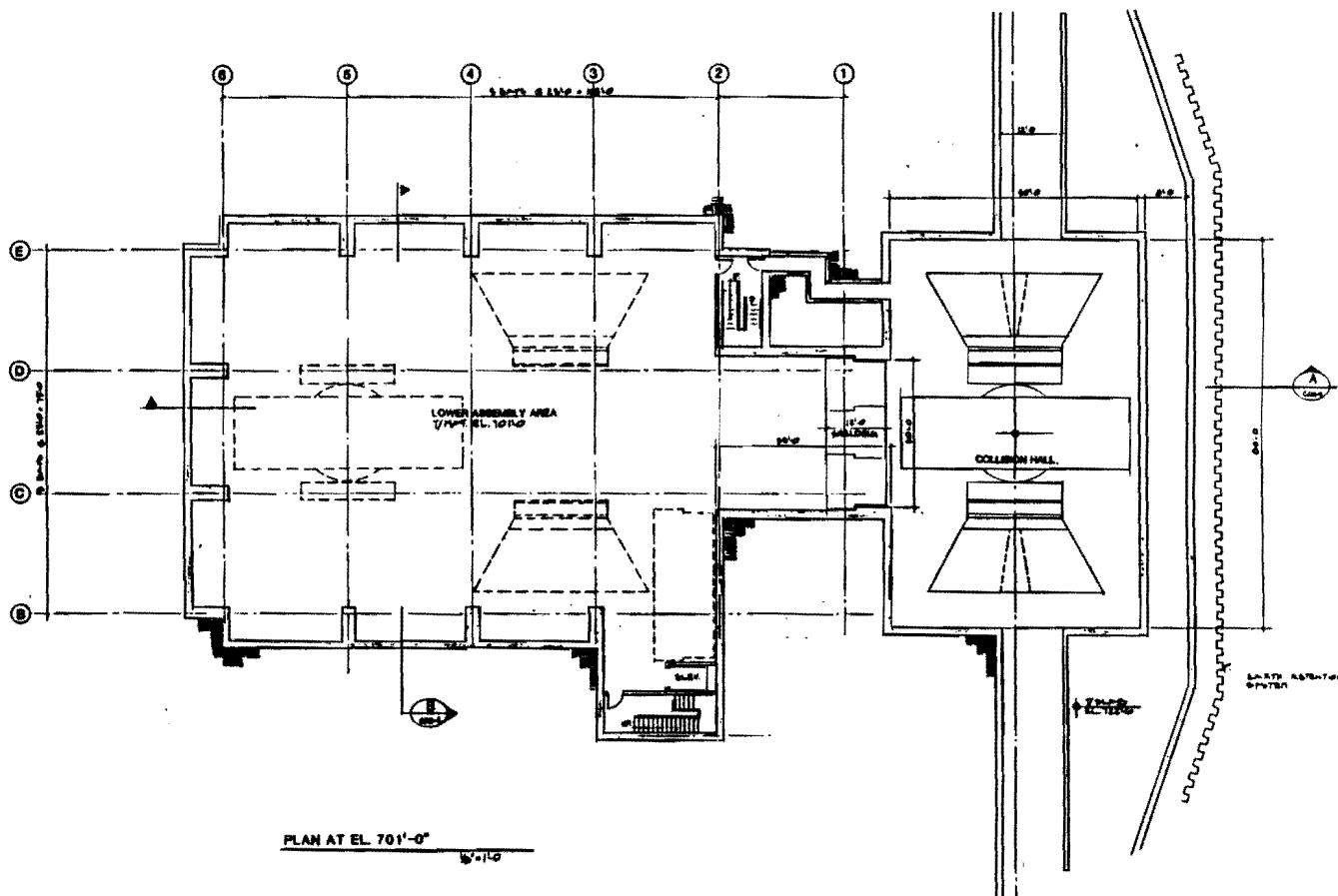


Figure 12: Layout of a new collision hall for the Bottom Collider Detector.

2.11.8 System Test at the C0 Intersect

We propose to test prototype versions of the silicon vertex detector, straw-tube chambers, and scintillating-fiber detector at the C0 intersect during the 1990-1991 collider run. This test will provide crucial evidence that secondary-decay vertices can be found at a hadron collider, and will also serve to focus the R&D efforts towards a timely measurement.

We can run at C0 in a parasitic mode in the sense that we would not require retuning of the beam for higher luminosity. But when we run, the electrostatic separators must be turned off so beams actually collide at C0.

In a run of 10^6 seconds at a luminosity of $10^{28} \text{ cm}^{-2}\text{sec}^{-1}$, about $100 K_S^0 \rightarrow \pi^+\pi^-$ decays would be observed (in the prototype apparatus) per each $100 \mu\text{m}$ of decay path. A study would then be made as to how close to the primary vertex the K -decay vertex can be reconstructed. This, of course, presumes the primary vertex can be located by the detector as well. A sample of about 50 decays $D^0 \rightarrow K^+\pi^-$ would also be observed in the

test run.

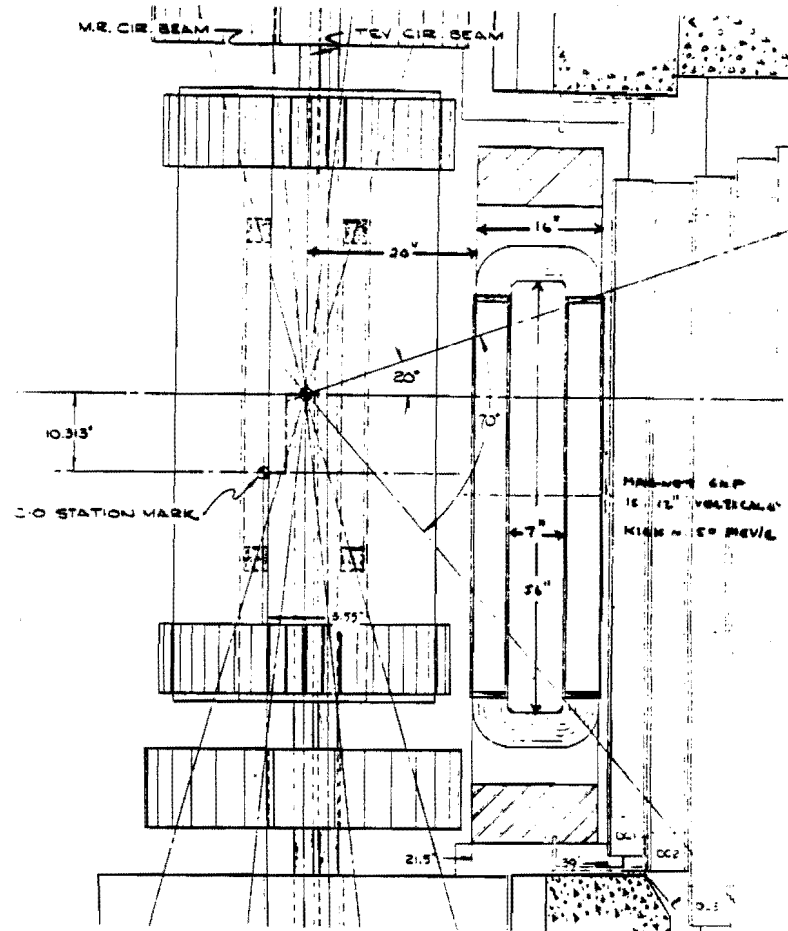


Figure 13: The existing layout of E-735 at the C0 intersect.

The existing configuration of E-735 in C0 is shown in fig. 13. We would need to replace the present central detector with our silicon vertex detector and straw tubes. A factor of about four in acceptance could be gained if the window-frame magnet were moved closer to the beams until it abuts the abort line of the 150-GeV ring. As mentioned in section 2.11.2, it is advantageous to have a small-diameter beam pipe for better resolution in the vertex reconstruction. The β^* is large in C0, so the pipe cannot be 1 inch in diameter. However, we would like the smallest pipe size compatible with the Tevatron beams.

3 Research & Development Program

The proposed research and development program for the Bottom Collider Detector is divided into three phases that overlap three fiscal years, 1989 through 1991.

- Phase I takes place in fiscal 1989 and consists of what might be called bench tests for each of the systems under consideration.
- Phase II takes place during fiscal 1990 and utilizes the fixed-target test beams available at the laboratory.
- Phase III takes place in fiscal 1991 and uses the C0 intersection region in a parasitic mode to perform system tests in the collider environment during the next collider run.

The three major systems addressed in this proposal are

1. The silicon vertex detector.
2. The tracking system.
3. The data-acquisition system.

The R&D issues for the silicon detector and straw-tube tracker are logically subdivided into mechanical and electrical parts, *i.e.*, construction and front-end electronics. The DAQ system includes everything after the front-end electronics including the fast trigger.

We outline below the R&D tasks and costs for each of the three systems, also breaking these down into the three phases.

3.1 Silicon Vertex Detector

3.1.1 Silicon: Mechanical & Electrical Tasks - Phase I

- Construct models of the silicon detector out of plastic and G-10 to explore assembly techniques.
- Continue modelling of the silicon cells and the supporting gutter structure using 'junk' (unprocessed) silicon and aluminum for the gutter. Survey various adhesives for resistance to creep, and for coefficients of thermal expansion matched to silicon. Add resistors to simulate the overall 2 kWatt heat load.
- Study the cable-plant issues with the silicon models. Develop techniques to cut slots in the silicon for cables (and cooling, possibly).
- Study the cooling requirements.
 - Can the device be cooled with a modest nitrogen gas flow?
 - Is liquid cooling an option?

- Is better electronic noise performance obtained at temperatures below ambient?
- Study alignment issues.
 - How accurately can the disks and barrels be assembled?
 - What is the long term stability?
 - How stable is the detector against thermal gradients?
 - Use the CORDAX (optical) measurement machine and proximity sensors for bench tests.
- Study the various techniques for bonding VLSI chips to silicon wafers now used by industry: bump bonding, tab bonding, and wire bonding.
 - Does the more robust procedure of tab bonding cause cracking of the silicon during heating?
 - Does the adhesive chemically damage the high-resistivity silicon near the bond?
- Test the performance of the double-sided silicon strip wafers. Obtain the a.c.-coupled detectors from Messerschmitt-Bölkow-Blohm GmbH, Munich and Senter for Industrieforskning, Oslo and test them.
- Design, build and test a VLSI readout chip set that permits a low cost, low power, and low noise readout system for the roughly 500,000 silicon strips.
 - Begin the front-end (BVX) chip design immediately.
 - * Define the specifications and overall architecture for the chips.
 - * Design the first chip in three parallel efforts: the amplifier/discriminator, the storage/delay array, and the digitization.
 - * The hardest part of the design is the amplifier and this will determine the schedule.
 - * Existing VLSI amplifier designs are excellent starting points.
 - * Goal is to have a first version sometime during the summer.
 - Start the collection-chip design in February.
 - * Specify the data-collection architecture for the whole detector, maintaining compatibility with the input formats for the data-acquisition system.
 - * The actual chip design will be relatively straightforward digital CMOS.
 - * Have first run back from MOSIS by summer 1989.

3.1.2 Silicon: Costs - Phase I

The mechanical costs and electrical costs are listed separately. An estimate of the salary costs are given for each category.

- Electronics: equipment/operating

- Chip-processing costs using MOSIS, 4 runs @ \$15k \$60k
- Test equipment \$30k
- Travel to conferences and workshops on VLSI \$10k
- Electronics: salaries
 - 1.5 FTE electrical engineer @ \$45k \$68k
 - 0.5 FTE electrical technician @ \$25k \$13k
- Mechanical: equipment/operating
 - Build gutter and alignment jigs using inside and outside shops \$10k
 - Use of outside companies to test bonding techniques, glueing, welding and cutting of silicon. Purchase of junk silicon for mechanical studies and of silicon strip detectors for bonding studies \$15k
 - Purchase power supplies and miscellaneous parts for thermal studies on junk-silicon model \$5k
 - Lab-D clean-room space for this work \$5k
- Mechanical: salaries
 - 0.5 FTE mechanical engineer @ \$45k \$23k

3.1.3 Silicon: Mechanical & Electrical Tasks - Phase II

This work will require the use of a test beam. Discussions with the laboratory are taking place on where (M-Test, M-Bottom or Lab-D) we could be located. We need a place where we can leave equipment set up over the period of the next fixed-target run. We require a low-intensity beam for single-track studies.

- Phase II of the silicon test involves the construction of two cells using junk silicon for alignment studies using the beam. This will require a support structure or jig that rotates and moves in such a way that alignment studies can be performed economically.
- We may need to build a partial beryllium support for the cells in order to study multiple-scattering effects.
- Some of the mechanical questions are:
 - How well is the silicon internally aligned?
 - How well is the silicon aligned with respect to the straws?
 - How large are the dead regions?
 - How robust are the bonds?

- We need to instrument (bond chips to and readout) about 10 double-sided wafers with 50- μ m pitch or roughly 5,000 channels. This will allow several studies of detector performance, as well as alignment. We hope to use an early version of the BVX chip for this work.
- Measure the resolution of the device as a function of momentum with and without the use of pulse-height information. Compare this to the Monte Carlo predictions.
- Perform signal-to-noise, efficiency and pulse-height-correlation studies using the double-sided detectors.
- Correlate tracks in the silicon and the straws.
- Study the issues associated with radiation damage. It is believed that a radiation-hard process can be specified once the desired electrical performance has been achieved in a possibly soft process.

3.1.4 Silicon: Costs - Phase II

- Electronics: equipment/operating
 - Purchase 10 doubled-sided silicon detectors @ \$1k each \$10k
- Electronics: salaries
 - 1.5 FTE electrical engineer @ \$45k \$68k
 - 1 FTE electrical technician \$25k
- Mechanical: equipment/operating
 - Glueing, cutting and bonding the chips to the wafers \$15k
 - Beryllium mechanical work \$8k
 - Miscellaneous supplies \$20k
- Mechanical: salaries
 - Mechanical engineer: 4 months @ \$45k \$15k
 - Mechanical technician: 1 year @ \$25k \$25k

3.1.5 Silicon: Mechanical & Electrical Tasks - Phase III

- Design and assemble a portion of a full 4π vertex detector, using about 20 wafers or roughly 5000 channels.
- Instrument this detector for operation at the C0 intersect.
- Readout every beam crossing (as a test of the data-acquisition system).

- Study the multi-track environment, including effects due to dipped tracks and closely spaced tracks.
- Determine impact-parameter resolution in 2 and 3 dimensions for both the disk and barrel configuration together and separately.
- Determine vertex resolution of the system in the multi-particle environment.
- Reconstruct a sample of $K_S \rightarrow \pi^+\pi^-$.

3.1.6 Silicon: Costs - Phase III

- Electronics: equipment/operating
 - 48 silicon detectors (2 cells) \$50k
 - BVX chips, data collection chips for above.....\$50k
- Electronics: salaries
 - 1 FTE electrical engineer\$45k
 - 2 FTE technician @ \$25k \$50k
- Mechanical: equipment/operating
 - Assembly of 2-cell prototype detector..... \$50k
 - Mounting of prototype in C0 intersect.....\$25k
 - Cooling, cabling for prototype detector.....\$25k
- Mechanical: salaries
 - Mechanical engineer: 4 months @ \$45k.....\$15k
 - Mechanical technician: 1 year @ \$25k \$25k

3.2 Tracking System

3.2.1 Tracking: Mechanical & Electrical Tasks - Phase I

The goal of this phase is build an instrumented superlayer of straw-tube chambers and perform a cosmic-ray test. In addition, we will start a program of R&D for a plastic scintillating fiber detector whose role would be to provide a fast measue of the z coordinate of the primary interaction vertex.

- Compare samples of straws from two vendors.
- Study different sizes of tubes. First try the 3-mm-diameter tube.
- Study both a short- and long-straw design, the latter with spacers inside the straw.

- Study the mechanical properties such as roundness, sag, and the adherence of the mylar to the aluminum as a function of temperature and pressure.
- Design and test the feedthroughs electrically and as gas seals.
- Make drift-velocity measurements as a function of high voltage, pressure, gas composition and magnetic field.
- Study the mechanical mounting and glueing techniques for assembling a superlayer.
- Measure the resolution as a function of all variables, including the orientation in the magnetic field.
- Study radiation damage.
- Study the feasibility of small pads on the straws as a means of obtaining fast z -coordinate information.
- Construct a sample of test straws.
- Design a readout system.
- Perform studies to see how well one can align and calibrate the system, and maintain optimal position resolution over time.
- Develop the readout chip set (3 chips):
 1. Bipolar amplifier/discriminator. Begin with the Penn-Louven design underway for SSC Generic R&D.
 2. CMOS time-to-voltage converter, analog storage/delay, and ADC.
 3. Data collection chip. Might be the same as for the silicon vertex detector.
 4. Study options for a fourth chip—for segment finding. This might be an analog processor implementing a neural-net algorithm, or a more conventional digital design.

Some of the group are interested in the development of plastic scintillating fibers. We are considering the application for both small-angle tracking and calorimetry. We discuss the need below as it pertains to the prompt trigger envisioned for the DAQ system. Because of the dipole field, the fast-tracking trigger needs the z coordinate within a few hundred nanoseconds after the collision.

- Develop a plastic scintillating fiber optic system that separates a beam-beam collision from a beam-gas collision. The system would subtend the rapidity range 4-6 units and is located several meters downstream and upstream of the collision point.
- Also use this system to determine the z -coordinate of the beam-beam interaction to 1-cm accuracy by tracing the low-angle tracks back to a common vertex.
- Design a fast readout system that can provide this information to the trigger.

3.2.2 Tracking: Costs - Phase I

- Electronics: equipment/operating
 - Chip development: 3 MOSIS runs @ \$15k \$45k
 - Studies of pad readout of straw tubes \$10k
- Electronics: salaries
 - 1.5 FTE electrical engineer @ \$45k \$68k
- Mechanical: equipment/operating
 - Purchase straws, travel to vendors \$10k
 - HV supply, wire, and gas system \$15k
 - Prototype feedthroughs \$5k
 - Test fixtures, cables, jigs and supplies \$40k
- Mechanical: salaries
 - 1 FTE mechanical engineer \$45k
 - 1 FTE technician for the mechanical straw work \$25k
 - 1 FTE technician for the gas studies \$25k
 - 1 FTE technician for alignment studies \$25k
- Fibers: equipment/operating
 - Scintillating fibers, and readout tubes \$50k
- Fibers: salaries
 - 1 FTE technician \$25k

3.2.3 Tracking: Mechanical & Electrical Tasks - Phase II

Phase II of the straw-tube development requires constructing a two-superlayer system to be tested in a test beam (M-Test, M-Bottom or Lab-D Test Beam). The scintillating-fiber detector will be tested in the beam also.

- Straw-tube studies
 - Perform pattern recognition and track fitting for tracks traversing several superlayers.
 - Measure the single-hit, single-track and two-track resolution.
 - Study the alignment issues associated with the assembly procedure of an octant of a 4π tracking system.

- Correlate tracks in the straw tubes with the tracks in the silicon.
- Study multiple-scattering effects.
- Test the readout system.
- Fiber studies
 - Build and test prototype fiber-array system.

3.2.4 Tracking: Costs - Phase II

- Electronics: equipment/operating
 - 6 MOSIS runs @ \$15k.....\$90k
 - Readout chips at \$7 per chip and 4 channels/chip \$13k
 - Test equipment such as digital scopes, and logic analysers \$50k
- Electronics: salaries
 - 2 FTE electrical engineer @ \$45k.....\$90k
- Mechanical: equipment/operating
 - Build 7000 straws with feedthroughs @ \$5 each.....\$35k
 - Cables, mounting boards, epoxies, and supplies \$20k
 - Bonding of readout chips to straws \$5k
- Mechanical: salaries
 - 1 FTE mechanical engineer @ \$45k.....\$45k
 - 2 FTE technicians @ \$25k.....\$50k
- Fibers: equipment/operating
 - Scintillating fibers.....\$20k
 - Test equipment \$30k
- Fibers: salaries
 - 1 FTE technician \$25k

3.2.5 Tracking: Production R&D - Phase III

A four superlayer straw-tube system would be used in the system test in C0 during Phase III, along with a prototype scintillating fiber detector.

A separate but parallel effort is needed to pursue the techniques for producing the very large number of straws that any major system will contain.

- Design overall layout for the C0 test.
- Reconstruct K_S 's in the straw-tube tracker.
- Devise tools and techniques for stringing the sense wires.
- Devise superlayer-alignment techniques.
- Design pressure-testing and voltage-testing devices and procedures.
- Design the assembly-line techniques in preparation for mass-production personnel.
- Design the overall electronics mounting scheme for the full system including the cooling.

3.2.6 Tracking: Costs - Phase III

- Electronics: equipment/operating
 - Test equipment such as digital scopes, and logic analysers \$50k
- Electronics: salaries
 - 1 FTE electrical engineer @ \$45k \$45k
- Mechanical: equipment/operating
 - Prototype fixtures for large-scale production \$100k
 - Mounting of prototype straw-tube system in C0 \$20k
- Mechanical: salaries
 - 1 FTE mechanical engineer @ \$45k \$45k
 - 3 FTE technicians @ \$25k \$75k
- Fibers: equipment/operating
 - Prototype detector for the C0 test \$50k
- Fibers: salaries
 - 1 FTE technician \$25k

3.3 Data-Acquisition System

3.3.1 Data Acquisition: Tasks - Phase I

- Specify in detail the overall architecture of the DAQ system including the interface between front-end electronics and the DAQ system.
- Build the following nine modules to test this architecture:
 - 2 transmitter boards
 - 2 receiver boards
 - 2 barrel-switch boards
 - 1 optical link
 - 2 boards with 4 numeric processors each

3.3.2 Data Acquisition: Costs - Phase I

- Development: equipment/operating
 - 9 prototype boards at roughly \$6k each \$54k
 - Terminals and workstations \$50k
- Development: salaries
 - 1.5 FTE electrical engineers @ \$45k \$68k
 - 1 FTE programmer \$45k

3.3.3 Data Acquisition: Tasks - Phase II

- Bring up system in test-beam area and connect to online system.
- Readout the silicon vertex detector through to the processors.
- Readout the straw-tube system.
- Develop the necessary performance and debugging tools for the system.

3.3.4 Data Acquisition: Costs - Phase II

- Development: equipment/operating
 - Simple clock system for readout in test beam \$10k
 - Alarms, crates, racks, power supplies \$100k
 - Host computer system for numeric processors \$30k
 - Terminals and workstations \$50k

- Development: salaries
 - 1 FTE electrical engineer\$45k
 - 1 FTE electrical technician\$25k
 - 1 FTE programmer \$45k
- Prototypes: equipment/operating
 - Board production\$300k
- Prototypes: salaries
 - 3 FTE electrical engineer @ \$45k.....\$135k
 - 3 FTE electrical technician @ \$25k.....\$75k
 - 1 FTE programmer \$45k

3.3.5 Data Acquisition: Tasks - Phase III

- Build up processor farm. Add racks and power supplies.
- Install hardware-protection system.
- Install network between racks and crates of processors.
- Develop downloading procedures for a large farm.

3.3.6 Data Acquisition: Costs - Phase III

- Development: equipment/operating
 - Terminals and workstations\$100k
- Prototypes: equipment/operating
 - 25 numeric processors\$400k
 - Racks, alarms\$50k
 - Exabyte tape drives (18) \$66k
- Prototypes: salaries
 - 3 FTE electrical engineers @ \$45k.....\$135k
 - 3 FTE technicians @ \$25k.....\$75k
 - 1 FTE programmer \$45k

4 Cost Summary

	FY89 Phase I (Bench Tests)		FY90 Phase II (Beam Tests)		FY91 Phase III (C0 System Test)	
	Equipment/ Operating	Salaries	Equipment/ Operating	Salaries	Equipment/ Operating	Salaries
Silicon Vertex Detector (FNAL)						
Electronics	\$100k	\$81k	\$10k	\$93k	\$100k	\$95k
Mechanical	35k	22k	43k	40k	100k	40k
	135k	103k	53k	133k	200k	135k
Tracking System (Universities)						
Electronics	55k	68k	153k	90k	50k	45k
Mechanical	70k	120k	60k	95k	120k	120k
Fibers	50k	25k	50k	25k	50k	25k
	175k	213k	263k	210k	220k	190k
Data-Acquisition System (FNAL)						
Development	104k	113k	190k	115k	100k	
Prototypes			300k	255k	516k	255k
	104k	113k	490k	370k	616k	255k
Total	414k	429k	806k	713k	1036k	580k

Table 2: Summary of costs of the proposed 3-year R&D program. Benefits, overhead, contingency, and escalation are not included.

5 References

- [1] H. Castro *et al.*, *Letter of Intent for the BCD, A Bottom Collider Detector for the Fermilab Tevatron*, October 7, 1988.
- [2] P.Nason, S. Dawson and R.K. Ellis, *The total cross section for the production of heavy quarks in hadronic collisions*, Fermilab 87-222-T; and private communication, Keith Ellis.
- [3] E. Berger, *Heavy Flavor Production*, ANL-HEP-PR 88-26.
- [4] N.S. Lockyer *et al.*, *Measurement of the Lifetime of Bottom Hadrons*, Phys. Rev. Lett. **51**, 1316 (1983); R. Ong, Ph.D thesis, Stanford Univ., SLAC-Report-320,1987; W.W. Ash *et al.*, Phys. Rev. Lett. **58**, 640 (1987); J. M. Brom *et al.*, Phys. Lett. **B195**, 301 (1987); D. Klem *et al.*, Phys. Rev. **D37**, 41 (1988).
- [5] See, for example, I. I. Bigi and A. I. Sanda, *CP Violation in Heavy Flavor Decays*, Nucl. Phys. **B281**, 41 (1987).
- [6] R. DeSalvo, *A Proposal for an SSC Central Tracking Detector*, Cornell University preprint CLNS87/52 (1987).
- [7] P. Sharp, private communication.
- [8] T. Ypsilantis, private communication.
- [9] T. Ludlam, *Summary of the Particle Identification Group*, Proceedings of the Workshop on High Sensitivity Beauty Physics at Fermilab, ed. by A.J. Slaughter, N.S. Lockyer and M. Schmidt (Nov. 1987) p. 447.
- [10] T. Åkesson *et al.*, *Estimate of a TRD's Performance as Part of an Electron Identification Scheme*, Proceedings of the LHC High Luminosity Study, ed. by J. Mulvey (1987).
- [11] G. Lutz *et al.*, *Low Noise Monolithic CMOS Front End Electronics*, Nucl. Instr. Meth. **A263**, 163 (1988).
- [12] W. Buttler *et al.*, *Noise Performance and Radiation Hardness of the CAMEX64 Analog Multiplexing Readout Chip*, Contribution to the XXIV International Conference on High Energy Physics (Munich, August, 1988).
- [13] S. Kleinfelder *et al.*, *A Flexible 128 Channel Silicon Strip Detector Instrumentation Integrated Circuit with Sparse Data Readout*, IEEE 1987 Nucl. Sci. Symposium, (San Francisco).
- [14] P.P. Allport, P. Seller and M. Tyndal, *A Low Power CMOS VLSI Multiplexed Amplifier for Silicon Strip Detectors*, London Conference on Position Sensitive Detectors (Sept., 1987).

- [15] L. Callewaert *et al.*, *Front End and Signal Processing Electronics for Detectors at High Luminosity Colliders*, U. Penn preprint UPR-162E, submitted to IEEE Trans. Nuc. Sci, 1988 Nuclear Science Symposium.
- [16] B. Denby, *Neural Networks and Cellular Automata in Experimental High Energy Physics*, Orsay preprint (Nov. 1987).
- [17] M. Bowden *et al.*, *A High-Throughput Data Acquisition Architecture Based on Serial Interconnects*, Fermilab preprint (Nov. 1988).
- [18] E. Barsotti *et al.*, *Proposal for Generic Detector R&D for the SSC*, (Nov. 1988).
- [19] K. Spencer, *The 60-second terabyte*, Can. Res. (June, 1988); M.S. Fisher, *Digital Paper Promises Cost, Storage Gains for Optical Media*, Datamation (May 15, 1988).